A fast, certified and "tuning free" two-field reduced basis method for the metamodelling of affinely-parametrised elasticity problems

K. C. Hoang[1], P. Kerfriden[1*], and S. P. A. Bordas[1,2]

[1]School of Engineering, Cardiff University, The Parade, CF24 3AA Cardiff, United Kingdom

[2]Faculté des Sciences, de la Technologie et de la Communication, University of Luxembourg, 6 rue Richard Coudenhove-Kalergi, L-1359 Luxembourg

Abstract

This paper proposes a new reduced basis algorithm for the metamodelling of parametrised elliptic problems. The developments rely on the Constitutive Relation Error (CRE), and the construction of separate reduced order models for the primal variable (displacement) and flux (stress) fields. A two-field greedy sampling strategy is proposed to construct these two fields simultaneously and in an efficient manner: at each iteration, one of the two fields is enriched by increasing the dimension of its reduced space in such a way that the CRE is minimised. This sampling strategy is then used as a basis to construct goal-oriented reduced order modelling. The resulting algorithm is certified and "tuning-free": the only requirement from the engineer is the level of accuracy that is desired for each of the outputs of the surrogate. It is also shown to be significantly more efficient in terms of computational expense than competing methodologies.

Keywords: two-field reduced basis method (TF-RBM); model order reduction; constitutive relation error; goal-oriented greedy sampling; *a posteriori* error estimation

1 Introduction

Model order reduction is an increasingly popular family of metamodelling techniques for parametrised boundary value problems (BVP) solved using numerical methods. As opposed to response surface methodologies, the output of the computation is not interpolated directly over the parameter domain. Instead, one constructs an approximation of the BVP that can be solved efficiently, and from which the quantities of interest can be post-processed. The applicability of reduced order modelling requires a certain smoothness of the solution to the original BVP over the parameter domain.

Reduced order modelling (ROM) can be performed in various ways (*e.g. a priori* reduction approach [1], Proper Generalised Decomposition [2, 3, 4], operator interpolation in attractive manifolds [5], machine-learning-based interpolations in attractive manifolds [6], classical mode synthesis, ...), but we will focus our discussion on the popular case of projection-based ROM (*e.g.* [7, 8, 9]). In this context, the reduced model is obtained by the projection of the original boundary value problem in a space of small dimension. Three ingredients are required for the metamodel to be efficient: (i) a reliable way to construct the projection space, (ii) an efficient (if possible optimum) projection of the solution to the BVP in this space and (iii) a method to decompose the numerical complexity of tasks (i) and (ii) in an "offline/online" manner. The latter point means that the expensive operations should be

*Contact: pierre.kerfriden@gmail.com

performed in advanced ("offline"), whilst the solution of the reduced model itself ("online") should remain computationally inexpensive.

The most popular way to extract the projection subspace is probably the Proper Orthogonal Decomposition (POD) [10, 11, 12]. The idea is to solve a finite number of realisations of the parametrised BVP to be reduced, and perform a spectral analysis of the space spanned by the corresponding solutions (*i.e.* the "snapshot"). This procedure delivers a hierarchy of subspaces in which the snapshots are best approximated in an average sense (*i.e.* an average of the distance between the original snapshot vectors and an optimal representation of these vectors in the reduced space is minimised). The BVP in then projected into one of these subspaces using a Galerkin [7, 8, 13, 14], Petrov-Galerkin [15] or residual minimising formulation [16, 17]. This projected BVP can be solved "online" at reduced numerical costs. The success of this approach lies in the fact that it is very general with regard to the nature of the original BVP. In particular, it remains the main candidate for the projection-based ROM of nonlinear problems [15, 16, 18, 19, 20]. However, it suffers from two drawbacks: (i) it is a priori difficult to choose the location of the snapshots, although some authors have recently addressed this issue, and (ii) the optimality of this procedure is established on the average over the parameter domain, and consequently its accuracy may be sensitive to outliers.

The reduced basis method (RBM) [21] is a powerful alternative to POD-based methodologies. It overcomes the two limitations mentioned previously by construction. The main idea is to construct the reduced spaces in such a way that the maximum error of projection of the solution over the entire parameter domain is minimised. As this problem is not solvable using direct algebraic tools, its solution is approximated by means of a greedy algorithm [22, 23]. Typically, one-dimensional enrichments of the reduced space are looked for by identifying the point of the parameter domain that displays the largest projection error. The solution corresponding to this point is computed and its projection error is reduced by adding some of its components to the reduced basis. The main difficulty of the approach is to evaluate the projection error in an affordable and efficient manner over the entire parameter domain. This can be done efficiently in the case of affinely parametrised linear elliptic or parabolic problems, as reliable and inexpensive error bounds are available. This is the setting in which the RBM has been the most successful so far, but extensions to linear hyperbolic problems or more complex settings have been proposed, for instance using direct search [24, 25], global optimisation [26] or gradient-based optimisation [27].

In the context of affinely parametrised elliptic PDEs [21, 28], the reduced basis method proceeds as follows. Given a certain projection subspace, one evaluates an upper bound of the projection error (measured in "energy norm") over an exhaustive sampling of the parameter domain. The solution of the BVP is computed at this point and added to the basis of the previous reduced space after an orthonormalisation. Efficient upper bounds have been developed over the years, and the most widely used is probably the *residual-based* a posteriori error bounds based on the Successive Constraint Method (SCM) [29, 30]. Once the projection subspace is sufficiently large (*i.e.* the maximum error of projection over the parameter domain is sufficiently small), this "offline" greedy algorithm is stopped. The metamodel can then be used online by performing a simple Galerkin projection of the original BVP in the reduced space.

In this paper, we propose an alternative to this procedure, based on our previous work on the Constitutive Relation Error (CRE) [14] and goal-oriented reduced basis sampling [24]. The first idea is to create two separate ROMs: one for the primal field of the elliptic BVP and an other one for the flux field. The primal ROM is required to deliver continuous solutions that satisfy the Dirichlet boundary conditions, whilst the flux ROM satisfies the balance equation of the flux and the Neumann boundary conditions. In this context, the Prager-Synge theorem gives us a relationship between the projection errors of the two fields and a certain distance between the primal and flux reduced solutions (*i.e.* the CRE [31]). A remarkable fact is that this distance can be computed in an inexpensive manner, and gives us (a) a joint indication of the accuracy of the two ROMs (b) an upper bound for the projection error in terms of primal variable and (c) an upper bound for the projection error in terms of flux. In view of remark (b), the CRE could be used as an alternative to a *residual-based* a posteriori error

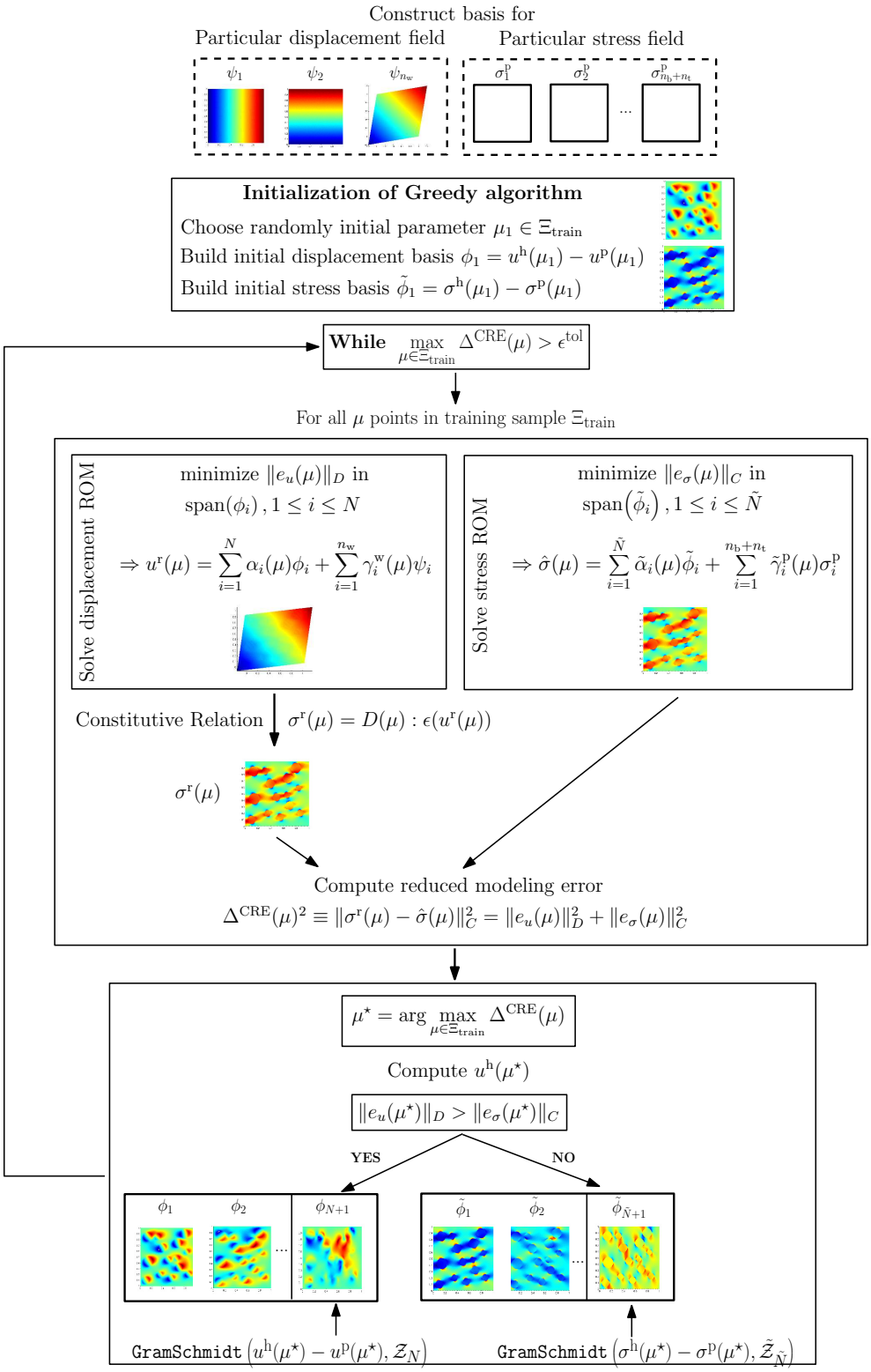

Figure 1: Schematic representation of the TF-RBM method based on the Constitutive Relation Error.

bound in the traditional RBM algorithm, as argued in the perspectives of our previous work [14]. However, we will propose a different, more elegant approach, the two-field reduced basis (TF-RBM) (see fig. 1). The CRE will be used as an indication of accuracy of the two ROMs over the entire parameter domain, following remark (a). The training phase of the proposed reduced basis method is a greedy algorithm, whereby we enrich either one of the two ROMs, depending on which one of these operations yields the largest decrease in the CRE. The practical advantage of this procedure, compared to the residual-based RBM, is that we do not need to train and compute an upper bound for the projection error of the primal field. The training stage is a single "for" loop, simple to implement, that only requires operations related to the solution of the two ROMs. Numerically, we observe that (i) the convergence rate of the training stage, as a function of the dimension of the projection space, is similar to the one obtained when using the residual-based approach and (ii) the online computational costs are reduced by up to one order of magnitude.

In order to be fully operational, this strategy is integrated in a goal-oriented setting, whereby the reduced spaces are constructed in such a way that the uncertainty in the outputs of the metamodel are minimised, as opposed to an arbitrary measure of the projection error of the primal field [32, 8, 27, 33, 24]. In this context, we need to construct additional two-field reduced models for the adjoint problems related to each of the outputs. The greedy sampling is then performed as follows. One first identifies which of the quantity of interest displays the largest level of uncertainty, and the corresponding point of the parameter domain. Then, either of the corresponding four ROMs are enriched, depending on which of these operations reduces this uncertainty most. The goal-oriented greedy algorithm is stopped whenever all the outputs of interest are approximated with a sufficient level of accuracy over the whole parameter domain.

Though the combination of the CRE-based greedy approach and goal-oriented setting, the proposed goal-oriented TF-RBM is certified and "tuning-free": the only input of the algorithm is the level of accuracy that is required for each of the quantities of interest. Moreover, it inherits the properties of the TF-RBM: it is simple to implement and exhibits similar convergence rates of the quantities of interest than what can be expected from an residual-based procedure, for significantly reduced online costs. All the developments and examples will be formally dedicated to linear elasticity, but they can be extended in a straightforward manner to any affinely parametrised linear elliptic BVP (steady temperature diffusion, electro-statics or magnetics, ...). Extensions to linear parabolic problems should be possible, as the CRE has successfully been applied to certify proper generalised decomposition in this context [34]. Some recent investigations on the use of CRE to estimate reduced modelling errors in nonlinear problems can also be found in [35]. The proposed strategy also offers an interesting framework to quantify the interaction between reduced modelling error and discretisation error (as suggested for instance in [34]). However, we focus here on the control of the former quantity only.

The paper is organised as follows. In section 2, we introduce necessary definitions and notations and state the exact parametrised elasticity BVP and its finite element approximation. In section 3, we describe our reduced order modelling approximations of displacement and stress fields. We emphasise that the description of these two ROMs is presented in a completely parallel manner. Section 4 is devoted to the constitutive relation error and the proposed TF-RBM. Goal-oriented error bounds, and the extension of the TF-RBM to the goal-oriented sampling setting are presented in section 5. We verify the performance of all the proposed algorithms by investigating a 2D material homogenisation problem in section 6. Finally, we provide some concluding remarks in section 7.

2 Parametrised problem of linear elasticity

2.1 Exact formulation

We consider a domain $\Omega \in \mathbb{R}^d$ ($d = 1, 2$ or 3) with Lipschitz continuous boundary $\partial\Omega$. We look for a displacement field $u \in \mathcal{U}(\Omega) = H^1(\Omega)$ that satisfies (nonhomogeneous) Dirichlet boundary conditions $u = w$ on the part $\partial\Omega^{\mathrm{w}}$ of the boundary $\partial\Omega$. (Here, $H^1(\Omega) = \left\{v \,|\, v \in L^2(\Omega), \nabla v \in (L^2(\Omega))^d\right\}$ is a

Hilbert space and $L^2(\Omega)$ is the space of square integrable functions over Ω.) Any displacement field that satisfies the conditions of regularity and Dirichlet boundary conditions is said to be kinematically admissible and belongs to space $\mathcal{U}^{\mathrm{Ad}}(\Omega) \subset \mathcal{U}(\Omega)$. We introduce the Cauchy stress tensor field σ, which belongs to a space $\mathcal{S}(\Omega)$ of sufficiently regular second-order tensor fields. A density of surface tractions t is applied on the boundary part $\partial\Omega^{\mathrm{t}} = \partial\Omega \backslash \partial\Omega^{\mathrm{w}}$ of the domain; and a density of body forces b is applied over Ω.

We define a set of input parameters $\mathcal{D} \subset \mathbb{R}^P$, a typical point of which is denoted by $\mu \equiv (\mu_1, \ldots, \mu_P)$. In particular, the force densities b and t, the Dirichlet boundary conditions w and the material properties of the structure may be functions of parameter μ. We assume that Ω and $\partial\Omega^{\mathrm{w}}$ do not undergo any parametric changes.

For a given parameter μ, a kinematically admissible displacement field will be sought in $\mathcal{U}^{\mathrm{Ad}}(\Omega;\mu) = \big\{v \in \mathcal{U}(\Omega) \,|\, v_{|\partial\Omega^{\mathrm{w}}} = w(\mu)\big\}$. Similarly, a statically admissible stress field $\sigma(\mu) \in \mathcal{S}^{\mathrm{Ad}}(\Omega;\mu)$ will satisfy the parametrised principle of virtual work:

$$-\int_\Omega \sigma(\mu) : \epsilon(v)\, d\Omega + \int_\Omega b(\mu)\cdot v\, d\Omega + \int_{\partial\Omega^{\mathrm{t}}} t(\mu)\cdot v\, d\Gamma = 0, \quad \forall v \in \mathcal{U}^{\mathrm{Ad},0}(\Omega). \tag{1}$$

Here, $\mathcal{U}^{\mathrm{Ad},0}(\Omega) = \big\{v \in \mathcal{U}(\Omega) \,|\, v_{|\partial\Omega^{\mathrm{w}}} = 0\big\}$; and $\epsilon(v) = \frac{1}{2}(\nabla v + \nabla v^T)$ is the symmetric part of the displacement gradient (*i.e.* the strain field). The solution to the parametrised problem of elasticity is an admissible pair $\Big(u(\mu), \sigma(\mu)\Big) \in \mathcal{U}^{\mathrm{Ad}}(\Omega;\mu) \times \mathcal{S}^{\mathrm{Ad}}(\Omega;\mu)$ that verifies the isotropic linear constitutive law

$$\sigma(\mu) = \lambda(\mu)\,\mathrm{Tr}\big(\epsilon\,(u(\mu))\,\big) I_d + 2G(\mu)\,\epsilon(u(\mu)) =: D(\mu) : \epsilon(u(\mu)), \tag{2}$$

where $\lambda(\mu)$ and $G(\mu)$ are the Lamé constants. $D(\mu)$ is the fourth-order Hooke's elasticity tensor and I_d is the second-order identity tensor. The inverse of this constitutive law reads

$$\epsilon(u(\mu)) = \frac{1+\nu(\mu)}{E(\mu)}\,\mathrm{Tr}\big(\sigma(\mu)\big) I_d - \frac{\nu}{E(\mu)}\,\sigma(\mu) =: C(\mu) : \sigma(\mu), \tag{3}$$

with E and ν the Young's modulus and Poisson's ratio, respectively, which are linked to the Lamé constants by the relationships $\lambda = \frac{E\nu}{(1+\nu)(1-2\nu)}$ and $G = \frac{E}{2(1+\nu)}$, and $C(\mu) = D(\mu)^{-1}$ the compliance tensor.

By substituting (2) into (1), the parametric problem of elasticity can be written in the following primal variational form: for any $\mu \in \mathcal{D}$, find the displacement field $u(\mu) \in \mathcal{U}(\Omega)$ such that

$$a\,(u(\mu), v; \mu) = f\,(v;\mu)\,, \qquad \forall v \in \mathcal{U}^{\mathrm{Ad},0}(\Omega), \tag{4}$$

In the above equations, the parametrised bilinear and linear forms associated with the problem of elasticity are defined as

$$a\,(u, v; \mu) = \int_\Omega \epsilon(u) : D(\mu) : \epsilon(v)\, d\Omega, \tag{5a}$$

$$f\,(v;\mu) = \int_\Omega b(\mu)\cdot v\, d\Omega + \int_{\partial\Omega^{\mathrm{t}}} t(\mu)\cdot v\, d\Gamma, \tag{5b}$$

respectively. We recall that $a : \mathcal{U}^{\mathrm{Ad},0}(\Omega) \times \mathcal{U}^{\mathrm{Ad},0}(\Omega) \times \mathcal{D}$ is a symmetric, continuous and coercive parametrised bilinear form; and we assume that $f : \mathcal{U}^{\mathrm{Ad},0}(\Omega) \times \mathcal{D}$ is a continuous, bounded linear form. Under these conditions, there exists a unique "weak" solution $u(\mu) \in \mathcal{U}(\Omega)$ to equation (4).

Multiple quantities of interest (QoI) can be extracted from $u(\mu)$ as

$$Q_i(\mu) = \ell_i\,(u(\mu))\,, \qquad 1 \le i \le n_{\mathrm{Q}}. \tag{6}$$

with $\ell_i : \mathcal{U}^{\mathrm{Ad},0}(\Omega) \times \mathcal{D}, 1 \leq i \leq n_{\mathrm{Q}}$ continuous, bounded linear forms. Outputs $\ell_i, 1 \leq i \leq n_{\mathrm{Q}}$ may be compliant or noncompliant linear functionals.

A crucial assumption to efficiently deal with parametrised problems is the *affine decomposition* property of the operators that governs our problem. In particular, $\forall u, v \in \mathcal{U}^{\mathrm{Ad},0}(\Omega)$, $\mu \in \mathcal{D}$, we require that

$$a\left(u, v; \mu\right) = \sum_{q=1}^{Q_a} \Theta_a^q(\mu) a^q(u, v), \tag{7a}$$

$$f\left(v; \mu\right) = \sum_{q=1}^{Q_f} \Theta_f^q(\mu) f^q(v), \tag{7b}$$

$$\ell_i\left(v; \mu\right) = \sum_{q=1}^{Q_{\ell_i}} \Theta_{\ell_i}^q(\mu) \ell_i^q(v), \qquad 1 \leq i \leq n_{\mathrm{Q}}, \tag{7c}$$

for some (preferably) small integers Q_{a,f,ℓ_i}. Here, the smooth functions $\Theta_{a,f,\ell_i}^q(\mu) : \mathcal{D} \to \mathbb{R}$ depend on μ, but the bilinear and linear forms a^q, f^q and ℓ_i^q do *not* depend on the parameter. In particular, such a *affine decomposition* is at hand if the parametrised data are originally given in the form of separate variables, namely

$$D(x, \mu) = \sum_{i=1}^{n_{\mathrm{d}}} \gamma_i^{\mathrm{d}}(\mu)\, \bar{D}_i(x), \qquad \forall \mu \in \mathcal{D}, x \in \Omega, \tag{8a}$$

$$t(x, \mu) = \sum_{i=1}^{n_{\mathrm{t}}} \gamma_i^{\mathrm{t}}(\mu)\, \bar{t}_i(x), \qquad \forall \mu \in \mathcal{D}, x \in \partial\Omega^{\mathrm{t}}, \tag{8b}$$

$$b(x, \mu) = \sum_{i=1}^{n_{\mathrm{b}}} \gamma_i^{\mathrm{b}}(\mu)\, \bar{b}_i(x), \qquad \forall \mu \in \mathcal{D}, x \in \Omega, \tag{8c}$$

$$w(x, \mu) = \sum_{i=1}^{n_{\mathrm{w}}} \gamma_i^{\mathrm{w}}(\mu)\, \bar{w}_i(x), \qquad \forall \mu \in \mathcal{D}, x \in \partial\Omega^{\mathrm{w}}. \tag{8d}$$

Here $\gamma_i^{\mathrm{d,t,b,w}}(\mu) : \mathcal{D} \to \mathbb{R}$ are explicitly known functions of the parameter μ, whilst $\bar{D}_i(x)$, $\bar{t}_i(x)$, $\bar{b}_i(x)$, $\bar{w}_i(x)$ are operators/functions that do not depend on μ.

2.2 Finite element discretization

We approximate the solutions of exact problem (4) by using the classical finite element method. We introduce the finite element space $\mathcal{U}^{\mathrm{h}}(\Omega) \subset \mathcal{U}(\Omega)$. Since we assume that the domain Ω does not depend on the parameter μ, we can construct a unique finite element space for all the realisations of problem (4). The finite element space is defined as

$$\mathcal{U}^{\mathrm{h}}(\Omega) = \Big\{ v \in \mathcal{U}(\Omega) \,|\, \forall j \in \{1, \ldots, d\}, v_j \in \mathrm{span}\big\{\hat{N}_i, 1 \leq i \leq n_{\mathrm{n}}\big\} \Big\}, \tag{9}$$

where v_j denotes the j^{th} component of the vector field v and functions $\hat{N}_i, 1 \leq i \leq n_{\mathrm{n}}$ are compactly supported finite element shape functions belonging to $\mathcal{U}(\Omega)$; n_{n} is the number of nodes in the finite element mesh; and $\mathcal{N}$ denotes the dimension of the finite element space, respectively.

Let $\mathcal{U}^{\mathrm{h},0}(\Omega) = \mathcal{U}^{\mathrm{h}}(\Omega) \cap \mathcal{U}^{\mathrm{Ad},0}(\Omega)$ be the space of finite element fields that vanish on $\partial\Omega^{\mathrm{w}}$, and let $u^{\mathrm{p}}(\mu)$ be a particular field of $\mathcal{U}^{\mathrm{Ad}}(\Omega; \mu)$, for any $\mu \in \mathcal{D}$. The finite element approximation $u^{\mathrm{h}}(\mu)$ of $u(\mu)$ is the solution to the following variational problem [36]: find $u^{\mathrm{h}}(\mu) \in \mathcal{U}^{\mathrm{h},0}(\Omega) + \{u^{\mathrm{p}}(\mu)\}$ such that

$$a\left(u^{\mathrm{h}}(\mu), v; \mu\right) = f\left(v; \mu\right), \qquad \forall v \in \mathcal{U}^{\mathrm{h},0}(\Omega). \tag{10}$$

We will assume in this paper that the parametrised Dirichlet boundary conditions conform to the finite element space, which means that $\mathcal{U}^{\mathrm{h,Ad}}(\Omega;\mu) = \mathcal{U}^{\mathrm{h}}(\Omega) \cap \mathcal{U}^{\mathrm{Ad}}(\Omega;\mu) \neq \{\}$. In this context, $u^{\mathrm{p}}(\mu)$ can always be chosen in the finite element space $\mathcal{U}^{\mathrm{h}}(\Omega)$.

Now, the variational problem (10) can be recast in the following form:

$$a\left(u^{\mathrm{h},0}(\mu), v; \mu\right) = f\left(v; \mu\right) - a\left(u^{\mathrm{p}}(\mu), v; \mu\right), \qquad \forall v \in \mathcal{U}^{\mathrm{h},0}(\Omega). \tag{11}$$

As $u^{\mathrm{p}}(\mu)$ is known, let us denote $\hat{f}\left(v; \mu\right) = f\left(v; \mu\right) - a\left(u^{\mathrm{p}}(\mu), v; \mu\right)$ then the final variational form will be: for a given $\mu \in \mathcal{D}$, find $u^{\mathrm{h},0}(\mu) \in \mathcal{U}^{\mathrm{h},0}(\Omega)$ such that

$$a\left(u^{\mathrm{h},0}(\mu), v; \mu\right) = \hat{f}\left(v; \mu\right), \qquad \forall v \in \mathcal{U}^{\mathrm{h},0}(\Omega), \tag{12}$$

and the finite element solution is obtained by using the lifting identity $u^{\mathrm{h}}(\mu) = u^{\mathrm{h},0}(\mu) + u^{\mathrm{p}}(\mu)$. Under standard assumptions, linear system (12) possesses a unique solution. The FE quantities of interest (QoI) can then be evaluated as

$$Q_i^{\mathrm{h}}(\mu) = \ell_i\left(u^{\mathrm{h}}(\mu)\right), \qquad 1 \leq i \leq n_{\mathrm{Q}}. \tag{13}$$

In the following, we assume that the finite element space is sufficiently fine so that any relevant measure of the finite element error $e^{\mathrm{h}}(\mu) = u(\mu) - u^{\mathrm{h}}(\mu)$ is very small for all $\mu \in \mathcal{D}$. In this context, we can assume that the FE output quantities are the ones that should be reproduced with a sufficient level of accuracy when using the metamodelling technique described in the next sections.

3 Reduced basis approximations for displacement and stress fields

The basic idea of projection-based reduced order modelling relies on the fact that the solutions of the parametrised boundary value problem reside on a smooth and low-dimensional parametrically induced manifold. The governing equations can then be projected in this manifold, leading to a reduced system of equations that can be solved inexpensively for any parameter set.

We assume in this section that the relevant projection subspaces have been identified, and we show how to perform the optimal projections. The novelty of our approach is that it relies on the reduced order modelling of both the displacement and stress fields. For the displacement, an optimal projection (in the sense of the energy norm) is classically obtained by the Galerkin formulation of the governing equation in a reduced space of kinematically admissible functions. For the stress, we can proceed in the same way, by minimising the projection error in a space of functions that satisfies the weak equilibrium *a priori*. This leads to a dual formulation, as shown in [14].

In this section, we emphasise the symmetry between displacement and stress optimal projections. We also show that the stress ROM can be solved efficiently by using an "offline/online" decomposition, which was claimed but not fully implemented in our previous work. This decomposition of the numerical complexity, restricted to the case of affine parameter dependencies, is key to ensuring that solving both reduced order models remain inexpensive (*i.e.* independent of the dimension of the underlying fine finite element space).

3.1 Reduced order model for the displacement field

3.1.1 Homogeneous/non-homogeneous separation of the displacement field

In order to apply the reduced basis method for general nonhomogeneous Dirichlet boundary condition problems, we first perform a lifting of the finite element solution over the parameter domain

$$u^{\mathrm{h}}(\mu) = u^{\mathrm{h},0}(\mu) + u^{\mathrm{h},\mathrm{p}}(\mu), \qquad \forall \mu \in \mathcal{D}. \tag{14}$$

In equation (14), $u^{\mathrm{h},0}(\mu) \in \mathcal{U}^{\mathrm{h},0}(\Omega)$, which means that the displacement fields $u^{\mathrm{h},0}(\mu)$ vanishes on $\partial\Omega^{\mathrm{w}}$ for any $\mu \in \mathcal{D}$, whilst $u^{\mathrm{h},\mathrm{p}}(\mu) \in \mathcal{U}^{\mathrm{h}}(\Omega)$ satisfies the nonhomogeneous Dirichlet boundary conditions. This equation is to be understood as follows: given a valid lifting $u^{\mathrm{h},\mathrm{p}}(\mu)$, the complementary part $u^{\mathrm{h},0}(\mu)$ can be formally calculated from the knowledge of $u^{\mathrm{h}}(\mu)$.

We will approximate $u^{\mathrm{h},0}(\mu)$ by its projection in a reduced vector space, as explained later on, whilst the lifting $u^{\mathrm{h},\mathrm{p}}(\mu)$ will be an explicit function of the parameters, as described in the next section.

3.1.2 Nonhomogeneous Dirichlet boundary conditions in reduced order modeling

We use a global lifting technique as described in [14]. The technique makes use of the assumed affine form of the prescribed displacements (8d). In the offline stage of the method, we compute a set of n_{w} finite element displacement fields $\psi_i \in \mathcal{U}^{\mathrm{h}}(\Omega), 1 \leq i \leq n_{\mathrm{w}}$ that satisfy

$$\begin{cases} a(\psi_i, v; \mu_0) = 0, \quad \forall v \in \mathcal{U}^{\mathrm{h},0}(\Omega), \\ \psi_i(x) = \bar{w}_i(x), \quad \forall x \in \partial\Omega^{\mathrm{w}}, \end{cases} \qquad 1 \leq i \leq n_{\mathrm{w}}. \tag{15}$$

This set of fields is obtained by solving n_{w} standard finite element problems with nonhomogeneous boundary conditions. The choice of $\mu_0 \in \mathcal{D}$ is arbitrary.

The finite element lifting function $u^{\mathrm{h},\mathrm{p}}(\mu)$, which satisfies exactly the nonhomogeneous Dirichlet boundary conditions for any $\mu \in \mathcal{D}$, can now be defined by the affine expansion

$$u^{\mathrm{h},\mathrm{p}}(\mu) = \sum_{i=1}^{n_{\mathrm{w}}} \gamma_i^{\mathrm{w}}(\mu)\, \psi_i, \qquad \forall \mu \in \mathcal{D}. \tag{16}$$

3.1.3 Displacement reduced basis surrogate

We assume the availability of nested parameter sets $S_N = \{\mu_1 \in \mathcal{D}, \ldots, \mu_N \in \mathcal{D}\}, 1 \leq N \leq N_{\max}$, and associated nested Lagrange RB spaces $\mathcal{U}_N^{\mathrm{r},0}(\Omega) = \mathrm{span}\,\{\phi_n, 1 \leq n \leq N\}, 1 \leq N \leq N_{\max}$, where $\phi_n \in \mathcal{U}_N^{\mathrm{r},0}(\Omega), 1 \leq n \leq N_{\max}$ are mutually orthonormal RB basis functions with respect to a particular norm using a Gram-Schmidt process. The procedure to construct efficiently the sets S_N and $\mathcal{U}_N^{\mathrm{r},0}(\Omega)$ will be discussed in section 4.2.2 afterwards.

For any $\mu \in \mathcal{D}$, we look for an approximation $u^{\mathrm{r}}(\mu)$ to $u^{\mathrm{h}}(\mu)$ in the form

$$u^{\mathrm{h}}(\mu) \approx u^{\mathrm{r}}(\mu) = u^{\mathrm{r},0}(\mu) + u^{\mathrm{h},\mathrm{p}}(\mu), \qquad \text{where} \qquad u^{\mathrm{r},0}(\mu) = \sum_{n=1}^{N} \alpha_n(\mu)\, \phi_n, \tag{17}$$

and $\alpha_n(\mu)$ are interpolation weights, called "reduced variables". Our RB approximation $u^{\mathrm{r},0}(\mu)$ to $u^{\mathrm{h},0}(\mu)$ is optimally (in the sense of the energy norm, see Céa Lemma) obtained by a standard Galerkin projection: given $\mu \in \mathcal{D}$, we look for $u^{\mathrm{r},0}(\mu)$ that satisfies

$$a(u^{\mathrm{r},0}(\mu), v; \mu) = \hat{f}(v; \mu), \qquad \forall v \in \mathcal{U}_N^{\mathrm{r},0}(\Omega),\ \mu \in \mathcal{D}. \tag{18}$$

This typically very small system of linear equations can be solved on demand, for any parameter set of interest.

The RB quantities of interest can then be evaluated from the reduced solution as

$$Q_i^{\mathrm{r}}(\mu) = \ell_i\left(u^{\mathrm{r}}(\mu)\right), \qquad 1 \leq i \leq n_{\mathrm{Q}}. \tag{19}$$

3.1.4 Offline-Online computational procedures for the reduced variables

In this section, we recall the usual offine-online computational procedures for the Galerkin ROM, which is necessary in order to fully exploit the dimensional reduction of the problem [22, 37, 24].

Inserting (17) and $v = \phi_n, 1 \le n \le N$ into (18) and recalling the definition (11) of $\hat{f}(v;\mu)$, we obtain the following small system of N coupled equations in the reduced variables $\alpha_n(\mu), 1 \le n \le N$

$$\sum_{m=1}^{N} a\left(\phi_m, \phi_n; \mu\right) \alpha_m(\mu) = f(\phi_n;\mu) - a\left(u^{\mathrm{h,p}}(\mu), \phi_n; \mu\right), \qquad 1 \le n \le N. \tag{20}$$

The RB quantities of interest are then evaluated by inserting (17) into (19) as

$$Q_i^{\mathrm{r}}(\mu) = \ell_i\left(\sum_{n=1}^{N} \alpha_n(\mu)\phi_n + u^{\mathrm{h,p}}(\mu)\right), \qquad 1 \le i \le n_{\mathrm{Q}}. \tag{21}$$

Finally, invoking the affine decomposition (7), (8), equations (20) and (21) can be expressed explicitly as

$$\begin{aligned}\sum_{m=1}^{N}\left(\sum_{q=1}^{Q_a} \Theta_a^q(\mu)\boldsymbol{a^q(\phi_m,\phi_n)}\right)\alpha_m(\mu) = &\sum_{q=1}^{Q_f} \Theta_f^q(\mu)\boldsymbol{f^q(\phi_n)} \\ &- \sum_{q=1}^{Q_a}\sum_{i=1}^{n_{\mathrm{w}}} \Theta_a^q(\mu)\gamma_i^{\mathrm{w}}(\mu)\,\boldsymbol{a^q\left(\psi_i,\phi_n\right)}, \qquad 1 \le n \le N,\end{aligned} \tag{22}$$

and

$$Q_i^{\mathrm{r}}(\mu) = \sum_{n=1}^{N}\sum_{q=1}^{Q_{\ell_i}} \Theta_{\ell_i}^q(\mu)\alpha_n(\mu)\boldsymbol{\ell_i^q\left(\phi_n\right)} + \sum_{j=1}^{n_{\mathrm{w}}}\sum_{q=1}^{Q_{\ell_i}} \gamma_j^{\mathrm{w}}(\mu)\Theta_{\ell_i}^q(\mu)\boldsymbol{\ell_i^q\left(\psi_j\right)}, \qquad 1 \le i \le n_{\mathrm{Q}}, \tag{23}$$

respectively.

The parameter-independent quantities (in bold typeface) are rewritten as follows

$$(\mathbf{A}_N^q)_{mn} = a^q(\phi_m,\phi_n), \qquad 1 \le m,n \le N,\ 1 \le q \le Q_a; \tag{24}$$

$$(\mathbf{F}_N^q)_n = f^q(\phi_n), \qquad 1 \le n \le N,\ 1 \le q \le Q_f; \tag{25}$$

$$(\mathbf{F}_{N,i}^{\mathrm{p},q})_n = a^q(\psi_i,\phi_n), \qquad 1 \le n \le N,\ 1 \le i \le n_{\mathrm{w}},\ 1 \le q \le Q_a; \tag{26}$$

$$\mathbf{Q}_{q,n}^i = \ell_i^q(\phi_n), \qquad 1 \le n \le N,\ 1 \le q \le Q_{\ell_i},\ 1 \le i \le n_{\mathrm{Q}}; \tag{27}$$

$$\mathbf{Q}_{q,j}^{\mathrm{p},i} = \ell_i^q(\psi_j), \qquad 1 \le j \le n_{\mathrm{w}},\ 1 \le q \le Q_{\ell_i},\ 1 \le i \le n_{\mathrm{Q}}. \tag{28}$$

Here, $\mathbf{A}_N^q \in \mathbb{R}^{N\times N}$ are the RB "stiffness" matrices (which are also symmetric positive definite following, for instance, the proof in Proposition 5.1 page 136 of [38]), $\mathbf{F}_N^q \in \mathbb{R}^N$ are the RB "load" vectors due to body forces and surface tractions, $\mathbf{F}_{N,i}^{\mathrm{p},q} \in \mathbb{R}^N$ are the RB "load" vectors due to nonhomogeneous Dirichlet boundary conditions, $\mathbf{Q}_{q,n}^i$ is the output component due to RB basis functions' contribution and $\mathbf{Q}_{q,j}^{\mathrm{p},i}$ is the output component due to nonhomogeneous Dirichlet boundary conditions' contribution, respectively.

From the above analysis, the computational procedures are now clear: an expensive μ-independent Offline stage performed only once and a cheap Online stage for any chosen parameter value $\mu \in \mathcal{D}$. In the Offline stage, the terms $\{\psi_i, 1 \le i \le n_{\mathrm{w}}\}$ and the RB basis functions $\mathcal{Z}_N = \{\phi_n, 1 \le n \le N\}, 1 \le N \le N_{\max}$ are computed first; then all the terms in (24)–(28) are computed and stored. In the Online

stage, for any given μ, all the coefficients $\Theta_{a,f,\ell_i}(\mu)$ and $\gamma^{\mathrm{w,d}}(\mu)$ are evaluated, and the linear system (22) is assembled and solved to find the RB coefficients $\alpha_n(\mu), 1 \leq n \leq N$. Then, the RB QoI are obtained through the simple scalar products (23). Although being dense (rather than sparse as in the FE case), the system matrix is very small, with a size $(N \times N)$ completely independent of the FE space dimension $\mathcal{N}$.

The Online operation count is $O\left(Q_a N^2\right)$ to assemble the system and $O\left(N^3\right)$ to invert the reduced operator in (22). The RB QoI is then evaluated with the cost of $O\left(N\right)$ from (23). Therefore, the Online operation count to evaluate $\mu \rightarrow Q_i^{\mathrm{r}}(\mu), 1 \leq i \leq n_{\mathrm{Q}}$ is completely independent of $\mathcal{N}$.

3.2 Reduced order model for the stress field

3.2.1 Homogeneous/non-homogeneous separation of the stress field

The principles underlying the construction of the stress surrogate are parallel to those employed for the construction of the displacement surrogate [14].

We first recall that the "exact" finite element stress field $\sigma^{\mathrm{h}}(\mu) := D(\mu) : \epsilon(u^{\mathrm{h}}(\mu))$, satisfies the equilibrium in the finite element sense, namely, it verifies

$$-\int_\Omega \sigma^{\mathrm{h}}(\mu) : \epsilon(v)\, d\Omega + \int_\Omega b(\mu) \cdot v\, d\Omega + \int_{\partial\Omega^{\mathrm{t}}} t(\mu) \cdot v\, d\Gamma = 0, \quad \forall v \in \mathcal{U}^{\mathrm{h},0}(\Omega). \tag{29}$$

We will denote by $\mathcal{S}^{\mathrm{h,Ad}}(\Omega;\mu)$ the space of stresses satisfying the parametrised equilibrium in the finite element sense (29).

The construction of the stress surrogate relies on the separation of the finite element stress field into two parts:

$$\sigma^{\mathrm{h}}(\mu) = \sigma^{\mathrm{h,0}}(\mu) + \sigma^{\mathrm{h,p}}(\mu), \qquad \forall \mu \in \mathcal{D}. \tag{30}$$

The first part $\sigma^{\mathrm{h,0}}(\mu)$ belongs to the space $\mathcal{S}^{\mathrm{h,0}}(\Omega)$ of stress fields satisfying the following homogeneous equilibrium conditions

$$\int_\Omega \sigma^{\mathrm{h,0}}(\mu) : \epsilon(v)\, d\Omega = 0, \qquad \forall v \in \mathcal{U}^{\mathrm{h,0}}(\Omega),\ \mu \in \mathcal{D}. \tag{31}$$

whilst the second part belongs to $\mathcal{S}^{\mathrm{h,Ad}}(\Omega;\mu)$ and therefore satisfies the equation

$$-\int_\Omega \sigma^{\mathrm{h,p}}(\mu) : \epsilon(v)\, d\Omega + \int_\Omega b(\mu) \cdot v\, d\Omega + \int_{\partial\Omega^{\mathrm{t}}} t(\mu) \cdot v\, d\Gamma = 0, \quad \forall v \in \mathcal{U}^{\mathrm{h,0}}(\Omega). \tag{32}$$

Equation (30) is to be understood as follows: given a valid equilibrated stress $\sigma^{\mathrm{h,p}}(\mu)$, then the complementary part $\sigma^{\mathrm{h,0}}(\mu)$ can be formally calculated from the knowledge of the exact finite element stress $\sigma^{\mathrm{h}}(\mu)$.

The stress field $\sigma^{\mathrm{h,p}}(\mu) \in \mathcal{S}^{\mathrm{h,Ad}}(\Omega;\mu)$ will be explicitly defined as a function of the parametrised body forces and surface tractions, which is detailed in the next section. The complementary part $\sigma^{\mathrm{h,0}}(\mu)$ will be approximated by its projection in a reduced vector space.

3.2.2 Treatment of body forces and surface tractions

This section is to compute the particular stress field $\sigma^{\mathrm{h,p}}(\mu)$ for any given parameter $\mu \in \mathcal{D}$.

We showed in [14] that $\sigma^{\mathrm{h,p}}(\mu)$ could be constructed as

$$\sigma^{\mathrm{h,p}}(\mu) = D(\mu_0) : \epsilon\left(\tilde{u}^{\mathrm{h,p}}(\mu)\right), \tag{33}$$

where $\tilde{u}^{\mathrm{h,p}}(\mu) \in \mathcal{U}^{\mathrm{h,0}}(\Omega)$ is the dual representation of the finite element stress with respect to the fixed bilinear form $a(\cdot,\cdot;\mu_0)$. This representation satisfies

$$a\left(\tilde{u}^{\mathrm{h,p}}(\mu), v; \mu_0\right) = \sum_{i=1}^{n_\mathrm{b}} \gamma_i^\mathrm{b}(\mu) \int_\Omega \bar{b}_i(x) \cdot v \, d\Omega + \sum_{i=1}^{n_\mathrm{t}} \gamma_i^\mathrm{t}(\mu) \int_{\partial\Omega^\mathrm{t}} \bar{t}_i(x) \cdot v \, d\Gamma, \qquad \forall v \in \mathcal{U}^{\mathrm{h},0}(\Omega), \tag{34}$$

and it can be obtained by solving the following "offline" set of subproblems

$$a\left(\tilde{\psi}_i^\mathrm{b}, v; \mu_0\right) = \int_\Omega \bar{b}_i(x) \cdot v \, d\Omega, \qquad \forall v \in \mathcal{U}^{\mathrm{h},0}(\Omega),\ 1 \le i \le n_\mathrm{b}, \tag{35a}$$

$$a\left(\tilde{\psi}_i^\mathrm{t}, v; \mu_0\right) = \int_{\partial\Omega^\mathrm{t}} \bar{t}_i(x) \cdot v \, d\Gamma, \qquad \forall v \in \mathcal{U}^{\mathrm{h},0}(\Omega),\ 1 \le i \le n_\mathrm{t}, \tag{35b}$$

where homogeneous Dirichlet boundary conditions are systematically applied over $\partial\Omega^\mathrm{w}$. Finally, $\tilde{u}^{\mathrm{h,p}}(\mu)$ and $\sigma^{\mathrm{h,p}}(\mu)$ are obtained as the simple linear combinations

$$\tilde{u}^{\mathrm{h,p}}(\mu) = \sum_{i=1}^{n_\mathrm{b}} \gamma_i^\mathrm{b}(\mu)\, \tilde{\psi}_i^\mathrm{b} + \sum_{i=1}^{n_\mathrm{t}} \gamma_i^\mathrm{t}(\mu)\, \tilde{\psi}_i^\mathrm{t}, \tag{36a}$$

$$\sigma^{\mathrm{h,p}}(\mu) = D(\mu_0) : \epsilon\left(\tilde{u}^{\mathrm{h,p}}(\mu)\right) = D(\mu_0) : \epsilon\left(\sum_{i=1}^{n_\mathrm{b}} \gamma_i^\mathrm{b}(\mu)\, \tilde{\psi}_i^\mathrm{b} + \sum_{i=1}^{n_\mathrm{t}} \gamma_i^\mathrm{t}(\mu)\, \tilde{\psi}_i^\mathrm{t}\right), \tag{36b}$$

respectively.

Based on (36b) we can define the affine form of $\sigma^{\mathrm{h,p}}(\mu)$ as follows

$$\sigma^{\mathrm{h,p}}(\mu) = \sum_{i=1}^{\tilde{n}_\mathrm{p}} \tilde{\gamma}_i^\mathrm{p}(\mu)\, \sigma_i^\mathrm{p}, \tag{37}$$

where $\tilde{n}_\mathrm{p} = n_\mathrm{b} + n_\mathrm{t}$;

$$\tilde{\gamma}_i^\mathrm{p}(\mu) = \begin{cases} \gamma_i^\mathrm{b}(\mu), & 1 \le i \le n_\mathrm{b}, \\ \gamma_{i-n_\mathrm{b}}^\mathrm{t}(\mu), & n_\mathrm{b}+1 \le i \le n_\mathrm{b}+n_\mathrm{t}; \end{cases} \tag{38}$$

and

$$\sigma_i^\mathrm{p} = \begin{cases} D(\mu_0) : \epsilon\left(\tilde{\psi}_i^\mathrm{b}\right), & 1 \le i \le n_\mathrm{b}, \\ D(\mu_0) : \epsilon\left(\tilde{\psi}_{i-n_\mathrm{b}}^\mathrm{t}\right), & n_\mathrm{b}+1 \le i \le n_\mathrm{b}+n_\mathrm{t}. \end{cases} \tag{39}$$

3.2.3 Stress reduced basis surrogate

We introduce the nested parameter sets $\tilde{S}_{\tilde{N}} = \{\tilde{\mu}_1 \in \mathcal{D}, \ldots, \tilde{\mu}_{\tilde{N}} \in \mathcal{D}\}, 1 \le \tilde{N} \le \tilde{N}_{\max}$, and associated nested Lagrange RB spaces $\mathcal{S}_{\tilde{N}}^{\mathrm{r},0}(\Omega) = \operatorname{span}\left\{\tilde{\phi}_m, 1 \le m \le \tilde{N}\right\}, 1 \le \tilde{N} \le \tilde{N}_{\max}$, where $\tilde{\phi}_m \in \mathcal{S}_{\tilde{N}}^{\mathrm{r},0}(\Omega), 1 \le m \le \tilde{N}_{\max}$ are mutually orthonormal RB basis functions with respect to a particular norm using a Gram-Schmidt process. Details on how to construct efficiently the sets $\tilde{S}_{\tilde{N}}$ and $\mathcal{S}_{\tilde{N}}^{\mathrm{r},0}(\Omega)$ will be discussed in section 4.2.2 later.

As mentioned in section 3.2.1, we will construct the surrogate stress field $\hat{\sigma}(\mu)$ as

$$\sigma^\mathrm{h}(\mu) \approx \hat{\sigma}(\mu) = \sigma^{\mathrm{r},0}(\mu) + \sigma^{\mathrm{h,p}}(\mu), \qquad \forall \mu \in \mathcal{D}, \quad \text{where} \quad \sigma^{\mathrm{r},0}(\mu) = \sum_{i=1}^{\tilde{N}} \tilde{\alpha}_i(\mu)\, \tilde{\phi}_i \tag{40}$$

where $\tilde{\alpha}(\mu) \in \mathbb{R}^{\tilde{N}}$ are (unknown) generalised coefficients to be obtained by the projection.

More precisely, the generalised coefficients are required to satisfy the optimum property:

$$\hat{\sigma}(\mu) = \arg \min_{\sigma^\star \in \mathcal{S}^{\mathrm{r}}(\Omega;\mu)} \left\| \sigma^\star - \sigma^{\mathrm{h}}(\mu) \right\|_{C(\mu)}, \tag{41}$$

where the admissible space for reduced stress field is defined by $\mathcal{S}^{\mathrm{r}}(\Omega;\mu) = \{\sigma^\star \in \mathcal{S}(\Omega) \,|\, \sigma^\star = \sum_{i=1}^{\tilde{N}} \alpha_i^\star \, \tilde{\phi}_i + \sigma^{\mathrm{h,p}}(\mu),\ \forall \alpha^\star \in \mathbb{R}^{\tilde{N}}\}$; $\| \cdot \|_{C(\mu)}$ is the so-called energy norm for the stress fields and is defined in Proposition 4.1.

Using the constitutive relation (2), the optimisation problem (41) can be recast in the following variational form: find $\hat{\sigma}(\mu) \in \mathcal{S}^{\mathrm{r}}(\Omega;\mu)$ such that

$$-\int_\Omega \hat{\sigma}(\mu) : C(\mu) : \sigma^\star \, d\Omega + \int_\Omega \epsilon\left(u^{\mathrm{h}}(\mu)\right) : \sigma^\star \, d\Omega = 0, \qquad \forall \sigma^\star \in \mathcal{S}^{\mathrm{r},0}(\Omega), \tag{42}$$

where the space $\mathcal{S}^{\mathrm{r},0}(\Omega)$ is defined as $\mathcal{S}^{\mathrm{r},0}(\Omega) = \{\sigma^\star \in \mathcal{S}(\Omega) \,|\, \sigma^\star = \sum_{i=1}^{\tilde{N}} \alpha_i^\star \, \tilde{\phi}_i,\ \forall \alpha^\star \in \mathbb{R}^{\tilde{N}}\}$. Now, substituting equations (40) and (14) into (42) and noting (31), we obtain the variational form that we will use to compute the stress field $\sigma^{\mathrm{r},0}(\mu)$:

$$\int_\Omega \sigma^{\mathrm{r},0}(\mu) : C(\mu) : \sigma^\star \, d\Omega = \int_\Omega \epsilon\left(u^{\mathrm{h,p}}(\mu)\right) : \sigma^\star \, d\Omega - \int_\Omega \sigma^{\mathrm{h,p}}(\mu) : C(\mu) : \sigma^\star \, d\Omega, \qquad \forall \sigma^\star \in \mathcal{S}^{\mathrm{r},0}(\Omega). \tag{43}$$

Finally, inserting the expression of $\sigma^{\mathrm{r},0}(\mu)$ (in (40)) and $\sigma^\star = \tilde{\phi}_j$ into (43), we obtain the following small linear system of $\tilde{N}$ coupled equations in the reduced variables $\tilde{\alpha}_i(\mu), 1 \le i \le \tilde{N}$

$$\sum_{i=1}^{\tilde{N}} \left(\int_\Omega \tilde{\phi}_i : C(\mu) : \tilde{\phi}_j \, d\Omega \right) \tilde{\alpha}_i(\mu) = \int_\Omega \epsilon\left(u^{\mathrm{h,p}}(\mu)\right) : \tilde{\phi}_j \, d\Omega - \int_\Omega \sigma^{\mathrm{h,p}}(\mu) : C(\mu) : \tilde{\phi}_j \, d\Omega, \qquad 1 \le j \le \tilde{N}. \tag{44}$$

3.2.4 Offline-Online computational procedures for the dual ROM

Thanks to the *affine* properties of $u^{\mathrm{h,p}}(\mu)$ eq. (16) and $\sigma^{\mathrm{h,p}}(\mu)$ eq. (37), we see that equation (44) can also be decomposed into Offline-Online computational procedures if the operator $C(\mu)$ is also *affine*, which we will assume:

$$C(x,\mu) = \sum_{i=1}^{n_{\mathrm{c}}} \gamma_i^{\mathrm{c}}(\mu) \, \bar{C}_i(x), \qquad \forall \mu \in \mathcal{D}, x \in \Omega. \tag{45}$$

Invoking (16), (37) and (45), equation (44) can then be written as

$$\begin{aligned} \sum_{i=1}^{\tilde{N}} \sum_{k=1}^{n_{\mathrm{c}}} \gamma_k^{\mathrm{c}}(\mu) \left(\int_{\boldsymbol{\Omega}} \tilde{\boldsymbol{\phi}}_{\boldsymbol{i}} : \bar{\boldsymbol{C}}_{\boldsymbol{k}} : \tilde{\boldsymbol{\phi}}_{\boldsymbol{j}} \, \boldsymbol{d\Omega} \right) \tilde{\alpha}_i(\mu) &= \sum_{k=1}^{n_{\mathrm{w}}} \gamma_k^{\mathrm{w}}(\mu) \left(\int_{\boldsymbol{\Omega}} \boldsymbol{\epsilon}(\boldsymbol{\psi}_{\boldsymbol{k}}) : \tilde{\boldsymbol{\phi}}_{\boldsymbol{j}} \, \boldsymbol{d\Omega} \right) \\ &\quad - \sum_{k=1}^{\tilde{n}_{\mathrm{p}}} \sum_{l=1}^{n_{\mathrm{c}}} \tilde{\gamma}_k^{\mathrm{p}}(\mu) \, \gamma_l^{\mathrm{c}}(\mu) \left(\int_{\boldsymbol{\Omega}} \boldsymbol{\sigma}_{\boldsymbol{k}}^{\mathbf{p}} : \bar{\boldsymbol{C}}_{\boldsymbol{l}} : \tilde{\boldsymbol{\phi}}_{\boldsymbol{j}} \, \boldsymbol{d\Omega} \right), \qquad 1 \le j \le \tilde{N}, \end{aligned} \tag{46}$$

The parameter-independent terms (in bold typeface) from the above equation are

$$(\tilde{\mathbf{A}}^{k}_{\tilde{N}})_{ij} = \int_\Omega \tilde{\phi}_i : \bar{C}_k : \tilde{\phi}_j \, d\Omega, \qquad 1 \le i,j \le \tilde{N},\ 1 \le k \le n_{\mathrm{c}}; \tag{47}$$

$$(\tilde{\mathbf{F}}^{\mathrm{p},k}_{\tilde{N}})_j = \int_\Omega \epsilon(\psi_k) : \tilde{\phi}_j \, d\Omega, \qquad 1 \le j \le \tilde{N},\ 1 \le k \le n_{\mathrm{w}}; \tag{48}$$

$$(\tilde{\mathbf{F}}^{k,l}_{\tilde{N}})_j = \int_\Omega \sigma^{\mathrm{p}}_k : \bar{C}_l : \tilde{\phi}_j \, d\Omega, \qquad 1 \le j \le \tilde{N},\ 1 \le k \le \tilde{n}_{\mathrm{p}}, 1 \ \le l \le n_{\mathrm{c}}. \tag{49}$$

Here, $\tilde{\mathbf{A}}^{k}_{\tilde{N}} \in \mathbb{R}^{\tilde{N}\times\tilde{N}}$ are the RB stress matrices, $\tilde{\mathbf{F}}^{\mathrm{p},k}_{\tilde{N}} \in \mathbb{R}^{\tilde{N}}$ are the RB stress vectors due to nonhomogeneous Dirichlet boundary conditions, and $\tilde{\mathbf{F}}^{k,l}_{\tilde{N}} \in \mathbb{R}^{\tilde{N}}$ are the RB stress vectors due to body force and surface traction, respectively.

From the above analysis, the computational procedures are now clear: an expensive μ-independent Offline stage performed only once and a cheap Online stage for any chosen parameter value $\mu \in \mathcal{D}$. In the Offline stage, the terms $\{\psi_i, 1 \le i \le n_{\mathrm{w}}\}$, $\{\sigma^{\mathrm{p}}_k, 1 \le k \le \tilde{n}_{\mathrm{p}}\}$ and the RB stress basis functions $\tilde{\mathcal{Z}}_{\tilde{N}} = \{\tilde{\phi}_n, 1 \le n \le \tilde{N}\}, 1 \le \tilde{N} \le \tilde{N}_{\max}$ are computed first; then all the terms in (47)–(49) are computed and stored. In the Online stage, for any given μ, all the coefficients $\gamma^{\mathrm{c}}(\mu)$, $\gamma^{\mathrm{w}}(\mu)$ and $\tilde{\gamma}^{\mathrm{p}}(\mu)$ are evaluated, and the linear system (46) is assembled and solved, in order to obtain the RB coefficients $\tilde{\alpha}_n(\mu), 1 \le n \le \tilde{N}$. The system matrix is very small, with a size $(\tilde{N} \times \tilde{N})$ completely independent of the FE space dimension $\mathcal{N}$ (More precisely, $\mathcal{N}$ here should be the dimension of the FE stress field – not that of the FE displacement field. We avoid using further symbols for simplicity.) The Online operation count is $O\left(n_{\mathrm{c}}\tilde{N}^2\right)$ to assemble the system and $O\left(\tilde{N}^3\right)$ to invert the matrix in (46). Therefore, the Online operation count to evaluate $\mu \to \tilde{\alpha}(\mu)$ is also independent of $\mathcal{N}$.

4 Constitutive relation error and two-field greedy sampling strategy (TF-RBM)

We have presented the construction of separate reduced order models for the displacement and stress fields. Now, we will propose a new algorithm to find efficient projection spaces for both fields, based on the CRE. We recall the principle of the CRE in the context of projection-based ROM [14] in section 4.1, and then provide a detailed methodology for our new greedy sampling algorithm in section 4.2.

4.1 Constitutive relation error (CRE)

4.1.1 Formulation

We consider a realisation of the parametrised problem of elasticity corresponding to an arbitrary parameter $\mu \in \mathcal{D}$, which is solved approximately using the two reduced basis surrogates described in section 3. The displacement reduced order model delivers a kinematically admissible displacement field, whilst the stress reduced order model delivers an approximated solution that satisfies the equilibrium in the FE sense. In this context, we have the following remarkable property:

Proposition 4.1. *Let $e_u(\mu) = u^{\mathrm{h}}(\mu) - u^{\mathrm{r}}(\mu)$ and $e_\sigma(\mu) = \sigma^{\mathrm{h}}(\mu) - \hat{\sigma}(\mu)$ be the RB errors for the displacement and stress fields, respectively; $\|\sigma^\star\|_{C(\mu)} = \left(\int_\Omega \sigma^\star : C(\mu) : \sigma^\star \, d\Omega\right)^{1/2}$ be the energy norm associated to an arbitrary stress field $\sigma^\star \in \mathcal{S}(\Omega)$ and $\|v\|_{D(\mu)} = \left(\int_\Omega \epsilon(v) : D(\mu) : \epsilon(v) \, d\Omega\right)^{1/2}$ be the energy norm associated to an arbitrary displacement field $v \in \mathcal{U}^{\mathrm{h},0}(\Omega)$.*

Then, the square of the distance $\Delta^{\mathrm{CRE}}(\mu)$ between the RB stress field $\sigma^{\mathrm{r}}(\mu) \in \mathcal{S}(\Omega)$ and the surrogate stress field $\hat{\sigma}(\mu) \in \mathcal{S}^{\mathrm{h,Ad}}(\Omega;\mu)$, measured in energy norm, will be equal exactly to the sum of square of energy norms of the RB errors of the displacement and stress fields as follows

$$\Delta^{\mathrm{CRE}}(\mu)^2 := \|\sigma^{\mathrm{r}}(\mu) - \hat{\sigma}(\mu)\|^2_{C(\mu)} = \|e_u(\mu)\|^2_{D(\mu)} + \|e_\sigma(\mu)\|^2_{C(\mu)}\,. \tag{50}$$

The proof is given in appendix A. It is important to understand from (50) that the RB errors $\|e_u(\mu)\|_{D(\mu)}$ and $\|e_\sigma(\mu)\|_{C(\mu)}$ are individually uncomputable, but the sum of their squares is computable in an *a posteriori* manner. In the next subsection, we show that its computation is in fact very efficient within the context of Offline-Online computational procedures. From another point of view, $\Delta^{\mathrm{CRE}}(\mu)$ can also be considered as an upper bound for the RB errors in both displacement field and stress field, that is,

$$\Delta^{\mathrm{CRE}}(\mu) \geq \|e_u(\mu)\|_{D(\mu)} \geq 0, \qquad \text{and} \qquad \Delta^{\mathrm{CRE}}(\mu) \geq \|e_\sigma(\mu)\|_{C(\mu)} \geq 0, \tag{51}$$

respectively.

We define the effectivities of CRE error bound for both displacement and stress fields as follows

$$\eta_u^{\mathrm{CRE}}(\mu) = \frac{\Delta^{\mathrm{CRE}}(\mu)}{\|u^{\mathrm{h}}(\mu) - u^{\mathrm{r}}(\mu)\|_{D(\mu)}}, \quad \text{and} \quad \eta_\sigma^{\mathrm{CRE}}(\mu) = \frac{\Delta^{\mathrm{CRE}}(\mu)}{\|\sigma^{\mathrm{h}}(\mu) - \hat{\sigma}(\mu)\|_{C(\mu)}}\,, \tag{52}$$

respectively.

4.1.2 Offline-Online computational procedures for $\Delta^{\mathrm{CRE}}(\mu)$

Similar to the well-known residual-based SCM (or coercivity) error bound [22, 28], the *a posteriori* CRE defined in (50) can also be computed very efficiently by an Offline-Online strategy. For the clarity of the paper, we leave the details of this procedure in appendix B and discuss its computational cost in the following.

In the Offline stage, the terms $\{\psi_i, 1 \leq i \leq n_{\mathrm{w}}\}$, $\{\sigma_k^{\mathrm{p}}, 1 \leq k \leq \tilde{n}_{\mathrm{p}}\}$ and the RB basis functions $\mathcal{Z}_N = \{\phi_n, 1 \leq n \leq N\}, 1 \leq N \leq N_{\max}$, $\tilde{\mathcal{Z}}_{\tilde{N}} = \{\tilde{\phi}_m, 1 \leq m \leq \tilde{N}\}, 1 \leq \tilde{N} \leq \tilde{N}_{\max}$ are computed first; then all the offline terms in (76)–(83) are computed and stored. In the Online stage, for any given μ, we first solve (22) to get $\alpha_n(\mu), 1 \leq n \leq N$; then solve (46) to get $\tilde{\alpha}_m(\mu), 1 \leq m \leq \tilde{N}$; and finally assemble all the remaining terms to compute $\Delta^{\mathrm{CRE}}_{N,\tilde{N}}(\mu)$ from (73).

For any given μ, the Online operation count at this stage includes (excluding the Online counts described in section 3.1.4 and section 3.2.4): $O\left(Q_a(N^2 + N n_{\mathrm{w}} + n_{\mathrm{w}}^2)\right)$ operations to assemble and compute $\mathbf{RR}(\mu)$ in (76), $O\left(\tilde{N}^2 n_{\mathrm{c}} + \tilde{N}\tilde{n}_{\mathrm{p}} + \tilde{n}_{\mathrm{p}}^2 n_{\mathrm{c}}\right)$ operations to assemble and compute $\mathbf{HH}(\mu)$ in (80), and $O\left(N\tilde{N} + N\tilde{n}_{\mathrm{p}} + \tilde{N} n_{\mathrm{w}} + n_{\mathrm{w}}\tilde{n}_{\mathrm{p}}\right)$ operations to assemble and compute $\mathbf{RH}(\mu)$ in (82)*. Therefore, the Online operation count to evaluate $\mu \to \Delta^{\mathrm{CRE}}_{N,\tilde{N}}(\mu)$ is also independent of $\mathcal{N}$.

Remark 4.2. *In summary, from (73) and (76)–(83), the computation of $\Delta^{\mathrm{CRE}}(\mu)$ can be performed very efficiently through Offline-Online procedures. In fact, several offline terms were already computed in the offline stages of RB displacement and stress fields: the offline terms of $\boldsymbol{RRss}(\mu)$ (77), $\boldsymbol{RRst}(\mu)$ (78), $\boldsymbol{HHss}(\mu)$, $\boldsymbol{HHst}(\mu)$ (81), and $\boldsymbol{RHts}(\mu)$ (83) were already computed from (24), (26), (47), (49) and (48), respectively. Therefore, for a very general problem with nonhomogeneous Dirichlet boundary conditions together with nonzero body force and surface traction, there are totally 5 remaining terms need to be computed and stored: $\boldsymbol{RRtt}(\mu)$; $\boldsymbol{HHtt}(\mu)$; and $\boldsymbol{RHss}(\mu)$, $\boldsymbol{RHst}(\mu)$, $\boldsymbol{RHtt}(\mu)$, respectively.*

*For all model problems considered in section 6, usually $N, \tilde{N} \gg Q_a, n_{\mathrm{w}}, n_{\mathrm{c}}, \tilde{n}_{\mathrm{p}}$ the online computational cost thus depends mostly on the terms which have N and $\tilde{N}$.

4.2 Two-field, CRE-based greedy sampling

4.2.1 Principle

In view of our previous exposition of the Constitutive Relation Error in the context of reduced modelling, the main ideas underlying the construction of our projection subspaces are very simple. Equation (50) shows that the accuracy of both stress and displacement ROMs is controlled by the CRE. Therefore, it is natural to set the minimisation of the maximum CRE over the parameter domain as our target for the construction of the projection spaces.

Of course, such a minimisation problem is not directly solvable, and we will make use of a greedy algorithm, as proposed in the original RBM. The method proceeds iteratively by assuming the existence of projection subspaces for both displacement and stress and performing a rank-one correction in such a way that the maximum of the CRE over the parameter domain is approximately minimised. As the CRE is a bound for both RB displacement and stress errors, the algorithm can be stopped whenever the CRE is sufficiently low over the entire parameter domain.

The rank-one update is performed as follows. First, we identify the point of the parameter domain where the CRE is at its largest. Then, we compute the corresponding exact displacement and stress fields, taking care of subtracting their respective nonhomogeneous parts. Finally, we enrich either the displacement or the stress ROM by adding the corresponding solution (after orthonormalisation), to the corresponding existing reduced basis. The choice of the field to enrich is simply based on testing which one of the enrichments would result in the largest decrease in the CRE at this particular point of the parameter domain.

4.2.2 TF-RBM algorithm: two-field greedy sampling procedure

Algorithm 1: Two-field greedy sampling strategy.

INPUT: Ξ_{train}, ϵ^{tol} (or $N_{\max}$)
OUTPUT: $\mathcal{Z}_N = \{\phi_n, 1 \le n \le N\}$; $\tilde{\mathcal{Z}}_{\tilde{N}} = \{\tilde{\phi}_m, 1 \le m \le \tilde{N}\}$

1: $\phi_1 = \dfrac{u^{\text{h},0}(\mu_1)}{\|u^{\text{h},0}(\mu_1)\|_{D(\mu_0)}}$; $\mathcal{Z}_1 = \{\phi_1\}$; $N = 1$;
2: $\tilde{\phi}_1 = \dfrac{\sigma^{\text{h},0}(\tilde{\mu}_1)}{\|\sigma^{\text{h},0}(\tilde{\mu}_1)\|_{C(\mu_0)}}$; $\tilde{\mathcal{Z}}_1 = \{\tilde{\phi}_1\}$; $\tilde{N} = 1$;
3: **while** $\Delta^{\text{CRE,max}} > \epsilon^{\text{tol}}$ **do**
4: • Compute $\alpha_N(\mu)$, $\tilde{\alpha}_{\tilde{N}}(\mu)$ and $\Delta^{\text{CRE}}_{N,\tilde{N}}(\mu)$, $\forall \mu \in \Xi_{\text{train}}$ from (73);
5: • Set: $\Delta^{\text{CRE,max}} = \max_{\mu \in \Xi_{\text{train}}} \Delta^{\text{CRE}}_{N,\tilde{N}}(\mu)$; $\mu^\star = \arg\max_{\mu \in \Xi_{\text{train}}} \Delta^{\text{CRE}}_{N,\tilde{N}}(\mu)$;
6: • Compute $\begin{cases} u^{\text{h}}(\mu^\star) \;\Rightarrow\; \|e_u(\mu^\star)\|_{D(\mu^\star)} \left(=: \Delta^{\text{CRE}}_{N,\tilde{N}+1}(\mu^\star)\right); \\ \sigma^{\text{h}}(\mu^\star) \;\Rightarrow\; \|e_\sigma(\mu^\star)\|_{C(\mu^\star)} \left(=: \Delta^{\text{CRE}}_{N+1,\tilde{N}}(\mu^\star)\right); \end{cases}$
7: **if** $\|e_u(\mu^\star)\|_{D(\mu^\star)} > \|e_\sigma(\mu^\star)\|_{C(\mu^\star)}$ **then**
8: $\phi_{N+1} = \texttt{GSdisp}\left(u^{\text{h}}(\mu^\star) - u^{\text{h,p}}(\mu^\star), \mathcal{Z}_N\right)$;
9: $\mathcal{Z}_{N+1} \leftarrow \mathcal{Z}_N \cup \phi_{N+1}$; $N \leftarrow N+1$;
10: **else**
11: $\tilde{\phi}_{N+1} = \texttt{GSstress}\left(\sigma^{\text{h}}(\mu^\star) - \sigma^{\text{h,p}}(\mu^\star), \tilde{\mathcal{Z}}_{\tilde{N}}\right)$;
12: $\tilde{\mathcal{Z}}_{\tilde{N}+1} \leftarrow \tilde{\mathcal{Z}}_{\tilde{N}} \cup \tilde{\phi}_{\tilde{N}+1}$; $\tilde{N} \leftarrow \tilde{N}+1$;
13: **end if**
14: **end while**

$$\texttt{GSdisp}: \; \phi_{N+1} \leftarrow u^{\text{h},0}(\mu^\star) - \sum_{n=1}^{N} \left(u^{\text{h},0}(\mu^\star), \phi_n\right)_{D(\mu_0)} \phi_n; \qquad \phi_{N+1} \leftarrow \frac{\phi_{N+1}}{\|\phi_{N+1}\|_{D(\mu_0)}};$$

$$\texttt{GSstress}: \; \tilde{\phi}_{\tilde{N}+1} \leftarrow \sigma^{\text{h},0}(\mu^\star) - \sum_{m=1}^{\tilde{N}} \left(\sigma^{\text{h},0}(\mu^\star), \tilde{\phi}_m\right)_{C(\mu_0)} \tilde{\phi}_m; \qquad \tilde{\phi}_{\tilde{N}+1} \leftarrow \frac{\tilde{\phi}_{\tilde{N}+1}}{\|\tilde{\phi}_{\tilde{N}+1}\|_{C(\mu_0)}};$$

We are given ϵ^{tol}, which can be set either directly or through a maximum RB dimension $N_{\max}$; and a training sample $\Xi_{\text{train}} \subset \mathcal{D}$, which is a discrete set representing a very fine sample of $n_{\text{train}} = |\Xi_{\text{train}}|$ points in the parameter domain. The two-field greedy sampling algorithm is presented in Algorithm 1.

As observed from Algorithm 1, there are two sets of RB basis functions to be built: the RB displacement set ($\mathcal{Z}_N$) and the RB stress set ($\tilde{\mathcal{Z}}_{\tilde{N}}$). The two-field greedy algorithm starts with arbitrarily chosen parameters $\mu_1, \tilde{\mu}_1 \in \Xi_{\text{train}}$ to construct $\mathcal{Z}_1 = \{\phi_1\}$ and $\tilde{\mathcal{Z}}_1 = \{\tilde{\phi}_1\}$, respectively (lines 1–2). We now analyse each greedy iteration in detail as follows. We compute the CRE error indicators $\Delta^{\text{CRE}}_{N,\tilde{N}}(\mu), \forall \mu \in \Xi_{\text{train}}$ based on the current RB displacement and stress spaces, i.e., $\mathcal{U}^{\text{r},0}_N(\Omega) = \text{span}\{\phi_n, 1 \le n \le N\}$ and $\mathcal{S}^{\text{r},0}_{\tilde{N}}(\Omega) = \text{span}\{\tilde{\phi}_m, 1 \le m \le \tilde{N}\}$ (line 4). The "worst" parameter

point $\mu^\star$ which induces the maximum error indicator thus can be found (line 5). We then perform two following tests by applying equation (50) at $\mu^\star$. First, we compute the exact displacement error $\|e_u(\mu^\star)\|_{D(\mu^\star)}$ via the FE displacement $u^{\mathrm{h}}(\mu^\star)$. Note that this exact error will equal exactly the CRE error indicator $\Delta^{\mathrm{CRE}}_{N,\tilde{N}+1}(\mu^\star)$ which is evaluated (at $\mu^\star$) after enriching the current RB stress space with $\tilde{\phi}(\mu^\star)$. Second, we compute the exact stress error $\|e_\sigma(\mu^\star)\|_{C(\mu^\star)}$ via the FE stress $\sigma^{\mathrm{h}}(\mu^\star)$. Note also that this exact error will equal exactly the CRE error indicator $\Delta^{\mathrm{CRE}}_{N+1,\tilde{N}}(\mu^\star)$ which is evaluated (at $\mu^\star$) after enriching the current RB displacement space with $\phi(\mu^\star)$ (line 6). These two exact errors are then compared with each other, and the actual enrichment is decided based on this comparison. If $\Delta^{\mathrm{CRE}}_{N,\tilde{N}+1}(\mu^\star) > \Delta^{\mathrm{CRE}}_{N+1,\tilde{N}}(\mu^\star)$, this implies that the "testing" displacement enrichment helps to decrease the CRE error indicator at $\mu^\star$ more than the "testing" stress enrichment does; and hence "actual" displacement enrichment will be performed (lines 8–9). In a completely opposite way, the fact $\Delta^{\mathrm{CRE}}_{N,\tilde{N}+1}(\mu^\star) \leq \Delta^{\mathrm{CRE}}_{N+1,\tilde{N}}(\mu^\star)$ implies that the "testing" stress enrichment reduces the CRE error indicator at $\mu^\star$ more than the "testing" displacement enrichment does; and hence "actual" stress enrichment will be performed (lines 11–12). The algorithm is iterated and stopped when the stopping criteria satisfies (line 3). Lastly, `GSdisp` and `GSstress` are two functions which construct next RB basis functions for displacement and stress fields using Gram-Schmidt orthogonalisation process, respectively.

The basic idea of this proposed algorithm is that we use only one single greedy loop to build simultaneously two RB spaces ($\mathcal{U}^{\mathrm{r},0}_N(\Omega)$ and $\mathcal{S}^{\mathrm{r},0}_{\tilde{N}}(\Omega)$) in an optimal way. At one greedy iteration, the particular set of RB basis functions will be chosen for "actual" enrichment depending on the performance of its "testing" enrichment set on $\mu^\star$: which "testing" set decreases $\Delta^{\mathrm{CRE}}(\mu^\star)$ the most will be chosen. Here, we also mention the inner products and norms used in the Gram-Schmidt process for the displacement field as

$$\begin{aligned}(u,v)_{D(\mu_0)} &= \int_\Omega \epsilon(u) : D(\mu_0) : \epsilon(v)\, d\Omega, \qquad \forall u, v \in \mathcal{U}^{\mathrm{h},0}(\Omega),\\ \|v\|_{D(\mu_0)} &= (v,v)^{1/2}_{D(\mu_0)},\end{aligned} \tag{53}$$

and for the stress field

$$\begin{aligned}(\sigma_1,\sigma_2)_{C(\mu_0)} &= \int_\Omega \sigma_1 : C(\mu_0) : \sigma_2\, d\Omega, \qquad \forall \sigma_1, \sigma_2 \in \mathcal{S}^{\mathrm{h},0}(\Omega),\\ \|\sigma\|_{C(\mu_0)} &= (\sigma,\sigma)^{1/2}_{C(\mu_0)},\end{aligned} \tag{54}$$

where μ_0 is a prescribed parameter chosen as in (15) and (33).

Finally, the efficient offline-online computational procedures for the TF-greeedy sampling algorithm are detailed as follows. We consider one TF-greedy iteration in more details. With the reduced spaces $\mathcal{Z}_N$, $\tilde{\mathcal{Z}}_{\tilde{N}}$ and associated offline terms available from the previous iteration, we can perform an exhaustive search over the training sample Ξ_{train} to compute $\Delta^{\mathrm{CRE}}_{N,\tilde{N}}(\mu)$ from equation (73) (line 4, Algorithm 1); from which, the "worst" parameter point $\mu^\star$ can be extracted (line 5, Algorithm 1). At $\mu^\star$, we solve the full order equations (14) and (2) to compute $\|e_u(\mu^\star)\|_{D(\mu^\star)}$ (*i.e.* $\Delta^{\mathrm{CRE}}_{N,\tilde{N}+1}(\mu^\star)$) and $\|e_\sigma(\mu^\star)\|_{C(\mu^\star)}$ (*i.e.* $\Delta^{\mathrm{CRE}}_{N+1,\tilde{N}}(\mu^\star)$) (line 6, Algorithm 1). The comparison of these two error measures tells us which field should be enriched. If the displacement field is enriched, $u^{\mathrm{h},0}(\mu^\star)$ will be added to the set $\mathcal{Z}_N$, a Gram-Schmidt orthogonalisation will be performed and N will be updated (lines 8–9, Algorithm 1). Correspondingly, all the offline terms that are associated with the RB displacement basis functions (*i.e.* ϕ) in (24)–(27) and the CRE in (76)–(83) are all computed/updated and stored. In the other case, if the stress field is enriched, $\sigma^{\mathrm{h},0}(\mu^\star)$ will be added to the set $\tilde{\mathcal{Z}}_{\tilde{N}}$, a Gram-Schmidt process will also be realised and $\tilde{N}$ will be updated accordingly (lines 11–12, Algorithm 1). At last, all the offline terms which associate with the RB stress basis functions (*i.e.* $\tilde{\phi}$) in (47)–(49) and the CRE error in (76)–(83) are all updated and stored.

5 Goal-oriented TF-RBM: "tuning-free" sampling strategy

Several authors have shown the advantage of devising goal-oriented sampling strategies to construct the projection spaces used in reduced order modelling [8, 24]. Instead of aiming at minimising the maximum over the parameter domain of an arbitrary measure of the error, one aims at minimising the error in the quantity or quantities of interest. This type of approach has been shown to lead to faster convergence rates of the greedy algorithm in terms input-output maps.

There is an other advantage of using such approaches. They permit to devise construction algorithms that are "tuning-free": algorithms that do not require any hidden calibration from the user. Ideally, the only input of a reduced basis algorithm should be the error that the engineer is willing to accept on the accuracy of the output(s) of the ROM. This is the point of view that we are going to follow in this section.

We first show that the errors in quantities of interest can be written in terms of errors measured in energy norms, using standard adjoint techniques [39, 40, 41, 42, 22, 43, 44]. In turn, computable bounds can be obtained by substituting these exact error measures by the CRE. From there, it is relatively easy to derive a goal-oriented variant of the greedy sampling strategy exposed in the previous section. One simply locates the point of the parameter domain that yields the largest error in quantity of interest. Next, a (sub-)optimal rank-one update of the projection subspaces is defined by enriching one, and only one of the bases, displacement/stress of the primal or displacement/stress of one of the adjoint problems, by its corresponding exact solution. Again, the choice of which of the ROMs to enrich will be guided by the minimisation of the errors in quantities of interest.

5.1 Upper and lower bounds engineering quantities of interest (QoI)

This section introduces standard tools required to bound engineering QoIs from the results of approximate computations [39, 40], as well as our notations for multi-objective problems. Readers that are familiar with this topic should only scan through this section to identify the notations used throughout the remainder of this paper.

For each one of the QoIs, we define the finite element dual (or adjoint) problem as follows

$$a\left(z_i^{\mathrm{h},0}(\mu), v; \mu\right) = \ell_i\left(v; \mu\right), \qquad \forall v \in \mathcal{U}^{\mathrm{h},0}(\Omega), \quad 1 \leq i \leq n_{\mathrm{Q}}, \tag{55}$$

where $z_i^{\mathrm{h},0}(\mu) \in \mathcal{U}^{\mathrm{h},0}, 1 \leq i \leq n_{\mathrm{Q}}$ is the FE dual displacement field corresponding to output functional ℓ_i, which is required to satisfy homogeneous Dirichlet boundary conditions.

We solve this problem approximately by projection-based ROM, which is obtained by the reduced Galerkin formulation: find $z_i^{\mathrm{r},0}(\mu) \in \mathcal{U}^{\mathrm{h},0}(\Omega)$ such that

$$a\left(z_i^{\mathrm{r},0}(\mu), v; \mu\right) = \ell_i\left(v; \mu\right), \qquad \forall v \in \mathcal{U}_{z,i}^{\mathrm{r},0}(\Omega), \quad 1 \leq i \leq n_{\mathrm{Q}}, \tag{56}$$

where $\mathcal{U}_{z,i}^{\mathrm{r},0}(\Omega) \subset \mathcal{U}^{\mathrm{h},0}(\Omega)$ is the reduced basis space for the dual displacement field associated with output functional ℓ_i; and generally $\mathcal{U}_{z,i}^{\mathrm{r},0}(\Omega) \neq \mathcal{U}_N^{\mathrm{r},0}(\Omega)$, $1 \leq i \leq n_{\mathrm{Q}}$. For consistency, we also define the sets of RB basis functions for dual displacements $\mathcal{Z}_{N^{\mathrm{du}_i}}^{\mathrm{du}_i} = \{\phi_n^{\mathrm{du}_i}, 1 \leq n \leq N^{\mathrm{du}_i}\}$, and that for dual stresses $\tilde{\mathcal{Z}}_{\tilde{N}^{\mathrm{du}_i}}^{\mathrm{du}_i} = \{\tilde{\phi}_m^{\mathrm{du}_i}, 1 \leq m \leq \tilde{N}^{\mathrm{du}_i}\}$, $1 \leq i \leq n_{\mathrm{Q}}$ for the i-th QoI, respectively.

Now, the following expression is classically obtained to link the error in quantity of interest as a function of the error in energy norm:

$$Q_i^{\mathrm{h}}(\mu) - Q_i^{\mathrm{r}}(\mu) = a\left(e_{z,i}(\mu), e_u(\mu); \mu\right) + R\left(z_i^{\mathrm{r},0}(\mu); \mu\right), \qquad 1 \leq i \leq n_{\mathrm{Q}}, \tag{57}$$

where $e_{z,i}(\mu) := z_i^{\mathrm{h}}(\mu) - z_i^{\mathrm{r}}(\mu)$ and $R : \mathcal{U}^{\mathrm{h},0}(\Omega) \times \mathcal{D} \to \mathbb{R}$ is the residual form of (18) defined as

$$R(v; \mu) = \hat{f}(v; \mu) - a(u^{\mathrm{r},0}(\mu), v; \mu), \qquad \forall v \in \mathcal{U}^{\mathrm{h},0}(\Omega), \forall\, \mu \in \mathcal{D}. \tag{58}$$

Applying the Cauchy-Schwarz inequality to separate the errors in primal and dual problems, and substituting the CRE as a computable bound for exact errors in energy norm, we obtain

$$Q_i^{\mathrm{r},-}(\mu) \leq Q_i^{\mathrm{h}}(\mu) \leq Q_i^{\mathrm{r},+}(\mu), \tag{59}$$

$$\text{where} \quad \begin{cases} Q_i^{\mathrm{r},-}(\mu) = Q_i^{\mathrm{r}}(\mu) + R\left(z_i^{\mathrm{r},0}(\mu);\mu\right) - \Delta^{\mathrm{CRE}}(\mu)\,\Delta_{z,i}^{\mathrm{CRE}}(\mu) \\ Q_i^{\mathrm{r},+}(\mu) = Q_i^{\mathrm{r}}(\mu) + R\left(z_i^{\mathrm{r},0}(\mu);\mu\right) + \Delta^{\mathrm{CRE}}(\mu)\,\Delta_{z,i}^{\mathrm{CRE}}(\mu) \end{cases}, \quad 1 \leq i \leq n_{\mathrm{Q}}.$$

Equation (59) is fundamental to our sampling strategy. It provides an interval in which the exact output, which is not computable, is guaranteed to be found. We will call this interval "uncertainty gap", and our aim will be to control and minimise its length through our sampling algorithm. In fact, we will use a relative measure of this gap defined as

$$\mathtt{gap}_i(\mu) = \frac{\left|Q_i^{\mathrm{r},+}(\mu) - Q_i^{\mathrm{r},-}(\mu)\right|}{1/2\left(\left|Q_i^{\mathrm{r},+}(\mu)\right| + \left|Q_i^{\mathrm{r},-}(\mu)\right|\right)}, \qquad \forall \mu \in \mathcal{D}, \quad 1 \leq i \leq n_{\mathrm{Q}}, \tag{60}$$

for the i-th QoI.

Remark 5.1. *For the special case of a compliant output, dual and primal solutions coincide to a multiplicative constant. In this case, we naturally choose to use a unique two-field ROM for both primal and dual problems. Inequality (59) can therefore be sharpened as*

$$Q^{\mathrm{r}}(\mu) \leq Q^{\mathrm{h}}(\mu) \leq Q^{\mathrm{r}}(\mu) + \Delta^{\mathrm{CRE}}(\mu)^2. \tag{61}$$

5.2 Goal-oriented greedy sampling strategy

Algorithm 2: The goal-oriented greedy sampling strategy.

INPUT: Ξ_{train}, $\epsilon^{\text{gap,tol}}$ (or $N^{\text{pr}}_{\max}$)
OUTPUT: $\mathcal{Z}^{\text{pr}}_{N^{\text{pr}}} = \{\phi^{\text{pr}}_n, 1 \le n \le N^{\text{pr}}\}$; $\tilde{\mathcal{Z}}^{\text{pr}}_{\tilde{N}^{\text{pr}}} = \{\tilde{\phi}^{\text{pr}}_m, 1 \le m \le \tilde{N}^{\text{pr}}\}$;
$\mathcal{Z}^{\text{du}_i}_{N^{\text{du}_i}} = \{\phi^{\text{du}_i}_n, 1 \le n \le N^{\text{du}_i}\}$; $\tilde{\mathcal{Z}}^{\text{du}_i}_{\tilde{N}^{\text{du}_i}} = \{\tilde{\phi}^{\text{du}_i}_m, 1 \le m \le \tilde{N}^{\text{du}_i}\}$; $1 \le i \le n_{\text{Q}}$.

$\phi^{\text{pr}}_1 = \dfrac{u^{\text{h},0}(\mu^{\text{pr}}_1)}{\|u^{\text{h},0}(\mu^{\text{pr}}_1)\|_{D(\mu_0)}}$; $\mathcal{Z}^{\text{pr}}_1 = \{\phi^{\text{pr}}_1\}$; $N^{\text{pr}} = 1$;

$\tilde{\phi}^{\text{pr}}_1 = \dfrac{\sigma^{\text{h},0}(\tilde{\mu}^{\text{pr}}_1)}{\|\sigma^{\text{h},0}(\tilde{\mu}^{\text{pr}}_1)\|_{C(\mu_0)}}$; $\tilde{\mathcal{Z}}^{\text{pr}}_1 = \{\tilde{\phi}^{\text{pr}}_1\}$; $\tilde{N}^{\text{pr}} = 1$;

$\phi^{\text{du}_i}_1 = \dfrac{z^{\text{h},0}_i(\mu^{\text{du}_i}_1)}{\|z^{\text{h},0}_i(\mu^{\text{du}_i}_1)\|_{D(\mu_0)}}$; $\mathcal{Z}^{\text{du}_i}_1 = \{\phi^{\text{du}_i}_1\}$; $N^{\text{du}_i} = 1$;

$\tilde{\phi}^{\text{du}_i}_1 = \dfrac{\sigma^{\text{h},0}_{z,i}(\tilde{\mu}^{\text{du}_i}_1)}{\|\sigma^{\text{h},0}_{z,i}(\tilde{\mu}^{\text{du}_i}_1)\|_{C(\mu_0)}}$; $\tilde{\mathcal{Z}}^{\text{du}_i}_1 = \{\tilde{\phi}^{\text{du}_i}_1\}$; $\tilde{N}^{\text{du}_i} = 1$;

while $\texttt{gap}^{\max} > \epsilon^{\text{gap,tol}}$ **do**

- Compute $\alpha^{\text{pr}}_{N^{\text{pr}}}(\mu)$, $\tilde{\alpha}^{\text{pr}}_{\tilde{N}^{\text{pr}}}(\mu)$, $\alpha^{\text{du}_i}_{N^{\text{du}_i}}(\mu)$, $\tilde{\alpha}^{\text{du}_i}_{\tilde{N}^{\text{du}_i}}(\mu)$; and $\Delta^{\text{CRE}}_{N^{\text{pr}},\tilde{N}^{\text{pr}}}(\mu)$, $\Delta^{\text{CRE},z}_{N^{\text{du}_i},\tilde{N}^{\text{du}_i}}(\mu)$;
  $\Rightarrow \texttt{gap}_i(\mu)$, $\forall \mu \in \Xi_{\text{train}}, 1 \le i \le n_{\text{Q}}$ from (60);
- Set: $\texttt{gap}^{\max} = \max\limits_{\mu \in \Xi_{\text{train}}, 1 \le i \le n_{\text{Q}}} \texttt{gap}_i(\mu)$; $(\mu^\star, I) = \arg \max\limits_{\mu \in \Xi_{\text{train}}, 1 \le i \le n_{\text{Q}}} \texttt{gap}_i(\mu)$;
- `ComputeExactErrors`; (see Algorithm 3)

  if $\delta_1 = \min\{\delta_j, 1 \le j \le 4\}$ **then**
    $\tilde{\phi}^{\text{pr}}_{\tilde{N}^{\text{pr}}+1} = \texttt{GSstress}\left(\sigma^{\text{h}}(\mu^\star) - \sigma^{\text{h,p}}(\mu^\star), \tilde{\mathcal{Z}}^{\text{pr}}_{\tilde{N}^{\text{pr}}}\right)$;
    $\tilde{\mathcal{Z}}^{\text{pr}}_{\tilde{N}^{\text{pr}}+1} \leftarrow \tilde{\mathcal{Z}}^{\text{pr}}_{\tilde{N}^{\text{pr}}} \cup \tilde{\phi}^{\text{pr}}_{\tilde{N}^{\text{pr}}+1}$; $\tilde{N}^{\text{pr}} \leftarrow \tilde{N}^{\text{pr}} + 1$;
  else if $\delta_2 = \min\{\delta_j, 1 \le j \le 4\}$ **then**
    $\phi^{\text{pr}}_{N^{\text{pr}}+1} = \texttt{GSdisp}\left(u^{\text{h}}(\mu^\star) - u^{\text{h,p}}(\mu^\star), \mathcal{Z}^{\text{pr}}_{N^{\text{pr}}}\right)$;
    $\mathcal{Z}^{\text{pr}}_{N^{\text{pr}}+1} \leftarrow \mathcal{Z}^{\text{pr}}_{N^{\text{pr}}} \cup \phi^{\text{pr}}_{N^{\text{pr}}+1}$; $N^{\text{pr}} \leftarrow N^{\text{pr}} + 1$;
  else if $\delta_3 = \min\{\delta_j, 1 \le j \le 4\}$ **then**
    $\tilde{\phi}^{\text{du}_I}_{\tilde{N}^{\text{du}_I}+1} = \texttt{GSstressdu}\left(\sigma^{\text{h}}_{z,I}(\mu^\star) - \sigma^{\text{h,p}}_{z,I}(\mu^\star), \tilde{\mathcal{Z}}^{\text{du}_I}_{\tilde{N}^{\text{du}_I}}\right)$;
    $\tilde{\mathcal{Z}}^{\text{du}_I}_{\tilde{N}^{\text{du}_I}+1} \leftarrow \tilde{\mathcal{Z}}^{\text{du}_I}_{\tilde{N}^{\text{du}_I}} \cup \tilde{\phi}^{\text{du}_I}_{\tilde{N}^{\text{du}_I}+1}$; $\tilde{N}^{\text{du}_I} \leftarrow \tilde{N}^{\text{du}_I} + 1$;
  else if $\delta_4 = \min\{\delta_j, 1 \le j \le 4\}$ **then**
    $\phi^{\text{du}_I}_{N^{\text{du}_I}+1} = \texttt{GSdispdu}\left(z^{\text{h}}_I(\mu^\star) - z^{\text{h,p}}_I(\mu^\star), \mathcal{Z}^{\text{du}_I}_{N^{\text{du}_I}}\right)$;
    $\mathcal{Z}^{\text{du}_I}_{N^{\text{du}_I}+1} \leftarrow \mathcal{Z}^{\text{du}_I}_{N^{\text{du}_I}} \cup \phi^{\text{du}_I}_{N^{\text{du}_I}+1}$; $N^{\text{du}_I} \leftarrow N^{\text{du}_I} + 1$;
  end if

end while

Algorithm 3: `ComputeExactErrors`

1: ∘ Compute $u^{\mathrm{h}}(\mu^\star) \Rightarrow \|e_u^{\mathrm{pr}}(\mu^\star)\|_{D(\mu^\star)}$ $\left(=: \Delta^{\mathrm{CRE}}_{N^{\mathrm{pr}},\tilde{N}^{\mathrm{pr}}+1}(\mu^\star)\right)$;

2: then recompute $\Delta^{\mathrm{CRE}}_{N^{\mathrm{pr}},\tilde{N}^{\mathrm{pr}}+1}(\mu^\star)\Delta^{\mathrm{CRE},z}_{N^{\mathrm{du}_I},\tilde{N}^{\mathrm{du}_I}}(\mu^\star) \to \delta_1$;

3: ∘ Compute $\sigma^{\mathrm{h}}(\mu^\star) \Rightarrow \|e_\sigma^{\mathrm{pr}}(\mu^\star)\|_{C(\mu^\star)}$ $\left(=: \Delta^{\mathrm{CRE}}_{N^{\mathrm{pr}}+1,\tilde{N}^{\mathrm{pr}}}(\mu^\star)\right)$;

4: then recompute $\Delta^{\mathrm{CRE}}_{N^{\mathrm{pr}}+1,\tilde{N}^{\mathrm{pr}}}(\mu^\star)\Delta^{\mathrm{CRE},z}_{N^{\mathrm{du}_I},\tilde{N}^{\mathrm{du}_I}}(\mu^\star) \to \delta_2$;

5: ∘ Compute $z_I^{\mathrm{h}}(\mu^\star) \Rightarrow \|e_z^{\mathrm{du}_I}(\mu^\star)\|_{D(\mu^\star)}$ $\left(=: \Delta^{\mathrm{CRE},z}_{N^{\mathrm{du}_I},\tilde{N}^{\mathrm{du}_I}+1}(\mu^\star)\right)$;

6: then recompute $\Delta^{\mathrm{CRE}}_{N^{\mathrm{pr}},\tilde{N}^{\mathrm{pr}}}(\mu^\star)\Delta^{\mathrm{CRE},z}_{N^{\mathrm{du}_I},\tilde{N}^{\mathrm{du}_I}+1}(\mu^\star) \to \delta_3$;

7: ∘ Compute $\sigma^{\mathrm{h}}_{z,I}(\mu^\star) \Rightarrow \|e_\sigma^{\mathrm{du}_I}(\mu^\star)\|_{C(\mu^\star)}$ $\left(=: \Delta^{\mathrm{CRE},z}_{N^{\mathrm{du}_I}+1,\tilde{N}^{\mathrm{du}_I}}(\mu^\star)\right)$;

8: then recompute $\Delta^{\mathrm{CRE}}_{N^{\mathrm{pr}},\tilde{N}^{\mathrm{pr}}}(\mu^\star)\Delta^{\mathrm{CRE},z}_{N^{\mathrm{du}_I}+1,\tilde{N}^{\mathrm{du}_I}}(\mu^\star) \to \delta_4$;

$$\texttt{GSdispdu:}\quad \phi^{\mathrm{du}_i}_{N^{\mathrm{du}_i}+1} \leftarrow z_i^{\mathrm{h},0}(\mu^\star) - \sum_{n=1}^{N^{\mathrm{du}_i}} \left(z_i^{\mathrm{h},0}(\mu^\star), \phi_n^{\mathrm{du}_i}\right)_{D(\mu_0)} \phi_n^{\mathrm{du}_i};$$

$$\phi^{\mathrm{du}_i}_{N^{\mathrm{du}_i}+1} \leftarrow \frac{\phi^{\mathrm{du}_i}_{N^{\mathrm{du}_i}+1}}{\|\phi_{N+1}\|_{D(\mu_0)}};$$

$$\texttt{GSstressdu:}\quad \tilde{\phi}^{\mathrm{du}_i}_{\tilde{N}^{\mathrm{du}_i}+1} \leftarrow \sigma_i^{\mathrm{h},0}(\mu^\star) - \sum_{m=1}^{\tilde{N}^{\mathrm{du}_i}} \left(\sigma_{z,i}^{\mathrm{h},0}(\mu^\star), \tilde{\phi}_m^{\mathrm{du}_i}\right)_{C(\mu_0)} \tilde{\phi}_m^{\mathrm{du}_i};$$

$$\tilde{\phi}^{\mathrm{du}_i}_{\tilde{N}^{\mathrm{du}_i}+1} \leftarrow \frac{\tilde{\phi}^{\mathrm{du}_i}_{\tilde{N}^{\mathrm{du}_i}+1}}{\|\tilde{\phi}^{\mathrm{du}_i}_{\tilde{N}^{\mathrm{du}_i}+1}\|_{C(\mu_0)}};$$

We are given $\epsilon^{\mathrm{gap,tol}}$, which can be set either directly or through a maximum RB primal dimension $N^{\mathrm{pr}}_{\max}$; and a training sample Ξ_{train} which contains $n_{\mathrm{train}} = |\Xi_{\mathrm{train}}|$ discrete points in the parameter domain. The goal-oriented greedy strategy aims to build the sets of RB basis functions such that the "uncertainty gaps" of n_{Q} QoI are minimised by using one single greedy loop. For an i-th general noncompliant QoI, there are 4 sets of RB basis functions to be built: the RB primal displacement set ($\mathcal{Z}^{\mathrm{pr}}_{N^{\mathrm{pr}}}$), RB primal stress set ($\tilde{\mathcal{Z}}^{\mathrm{pr}}_{\tilde{N}^{\mathrm{pr}}}$), RB dual displacement set ($\mathcal{Z}^{\mathrm{du}_i}_{N^{\mathrm{du}_i}}$) and RB dual stress set ($\tilde{\mathcal{Z}}^{\mathrm{du}_i}_{\tilde{N}^{\mathrm{du}_i}}$). The greedy loop will manipulate simultaneously these 4 sets, as presented in Algorithm 2.

The goal-oriented greedy algorithm starts with arbitrarily chosen parameters μ^{pr}_1, $\tilde{\mu}^{\mathrm{pr}}_1$, $\mu^{\mathrm{du}_i}_1$, $\tilde{\mu}^{\mathrm{du}_i}_1 \in \Xi_{\mathrm{train}}$ to construct $\mathcal{Z}^{\mathrm{pr}}_1 = \{\phi^{\mathrm{pr}}_1\}$, $\tilde{\mathcal{Z}}^{\mathrm{pr}}_1 = \{\tilde{\phi}^{\mathrm{pr}}_1\}$, $\mathcal{Z}^{\mathrm{du}_i}_1 = \{\phi^{\mathrm{du}_i}_1\}$ and $\tilde{\mathcal{Z}}^{\mathrm{du}_i}_1 = \{\tilde{\phi}^{\mathrm{du}_i}_1\}$, $1 \le i \le n_{\mathrm{Q}}$ (Algorithm 2, lines 1–4). Then, at each greedy iteration, we will compute the QoI gaps $\texttt{gap}_i(\mu)$, $\forall \mu \in \Xi_{\mathrm{train}}, 1 \le i \le n_{\mathrm{Q}}$ eq. (60), based on the current RB primal/dual displacement/stress spaces which have dimensions N^{pr}, $\tilde{N}^{\mathrm{pr}}$, N^{du_i} and $\tilde{N}^{\mathrm{du}_i}$ (Algorithm 2, lines 6–7). The "worst" parameter point $\mu^\star$ and QoI index I which induce the maximum gap thus can be found (Algorithm 2, line 8). With $\mu^\star$ and I at hand, we will compute the exact errors at $\mu^\star$ as described in Algorithm 3. In particular, the energy norms at $\mu^\star$ of exact errors of primal displacement, primal stress, I-th dual displacement and I-th dual stress are computed in turn; and note that these values essentially are primal/dual CRE errors which are evaluated at $\mu^\star$ after enriching RB primal stress, RB primal displacement, RB I-th dual stress and RB I-th dual displacement, respectively. Next, we recompute correspondingly the product $\Delta^{\mathrm{CRE}}(\mu^\star)\Delta^{\mathrm{CRE},z}(\mu^\star)$ for each of the 4 computations above since the numerator of $\texttt{gap}_i(\mu)$ (eq. (60)) is proportional to this product. These 4 resulting values are then compared to each other, and the actual enrichment will be decided based on this comparison: which "testing" set decreases this product the most will be chosen for the "actual" enrichment (Algorithm 2, lines 10–22). For instance, if $\delta_3 = \min\{\delta_j, 1 \le j \le 4\}$, this implies that the I-th dual stress enrichment would reduce the product

$\Delta^{\text{CRE}}(\mu^\star)\Delta^{\text{CRE},z}(\mu^\star)$ the most among 4 "testing" enrichments; and hence "actual" I-th dual stress enrichment will be performed (Algorithm 2, lines 17–18). The algorithm will iterate and stop when the stopping criteria is satisfied (line 5).

We observe that even for multiple QoI, at each greedy iteration we only "test" 4 sets of RB basis functions which are associated with the I-th QoI; and then enrich only one of these four sets. This is due to the contributions of $\mathcal{Z}^{\text{pr}}_{N^{\text{pr}}}$ and $\tilde{\mathcal{Z}}^{\text{pr}}_{\tilde{N}^{\text{pr}}}$ to $\Delta^{\text{CRE}}(\mu^\star)$, and that of $\mathcal{Z}^{\text{du}_I}_{N^{\text{du}_I}}$ and $\tilde{\mathcal{Z}}^{\text{du}_I}_{\tilde{N}^{\text{du}_I}}$ to $\Delta^{\text{CRE},z}_I(\mu^\star)$; and these ultimately contribute to $\texttt{gap}_I(\mu^\star)$. This property makes the algorithm very efficient and attractive for multiple-QoI problems.

In comparison with the two-field greedy algorithm, the goal-oriented greedy strategy has three main differences which are the objective function, the total number of RB sets to be built and the number of RB sets tested at each greedy iteration. First, we try to minimise the "uncertainty gap" $\texttt{gap}_i(\mu), 1 \le i \le n_{\text{Q}}$ rather than the CRE error $\Delta^{\text{CRE}}(\mu)$. Second, we need to build all RB spaces for displacement/stress fields which are associated with n_{Q} QoI. Finally, at each greedy iteration, we need to consider simultaneously 4 RB sets instead of 2 RB sets as in the two-field greedy algorithm. However, the principle to choose and enrich RB sets is completely similar to that of the two-field greedy algorithm. Namely, the particular RB set will be chosen depending on the performance of its new "testing" set on $\mu^\star$: which "testing" set decreases $\texttt{gap}_I(\mu^\star)$ the most will be selected for the "actual" enrichment.

6 Numerical examples

In this section, we will apply the TF-RBM algorithm to the metamodelling of computational models of elastic heterogeneous materials, under 2D plane strain assumption. The heterogeneous material of interest is made of two isotropic linear elastic phases possessing distinct elastic properties: circular/ellipsoid inclusions and surrounding matrix. The positions and diameters of the inclusions are distributed randomly. The aim is to determine the so-called "overall" (or "effective") elasticity tensor as a function of some characteristics $\mu^{\text{m}} \in \mathcal{D}^{\text{m}}$ of the material heterogeneities. In other words, we want to build a virtual chart of the overall homogenised properties of the class of composite materials under investigation.

6.1 A one-parameter example

6.1.1 Finite element discretisation

We consider a 2D statistical volume element (SVE) model under plane strain assumption in fig. 3 [45, 46]. The domain Ω is a unit square which is defined by $\Omega = [0,1] \times [0,1]$. The model is composed of two distinct material phases: the circular inclusions characterised by Young's modulus E^{inc} and the surrounding matrix characterised by Young's modulus E^{mat}. Both phases are assumed to have elastic and isotropic behaviour. The random distribution of positions and diameters of the inclusions is performed via the package [47, 48]. There are no body force nor surface traction – the only load applying to the model is via parametrised Dirichlet boundary conditions.

The SVE boundary value problem is parametrised by the material parameters μ^{m} and the load parameters μ^{l} as: $\mu = \left(\mu^{\text{m}}, \mu^{\text{l}}\right) \equiv \left(\mu^{\text{m}}, \mu^{\text{l}}_1, \mu^{\text{l}}_2, \mu^{\text{l}}_3\right) \equiv (\mu_1, \mu_2, \mu_3, \mu_4)$. We assume in this example that the material heterogeneities are only parametrised by the elastic contrast $\mu^{\text{m}} \equiv \mu_1 = \frac{E^{\text{inc}}}{E^{\text{mat}}}$. The load parameters μ^{l} are constituted by the independent components of the effective strain tensor ϵ^{M}, where $\epsilon^{\text{M}} \in \mathbb{R}^2 \times \mathbb{R}^2$ and $\epsilon^{\text{M}} = \epsilon^{\text{M}^T}$. More precisely, we define $\mu^{\text{l}}_1 \equiv \mu_2 = \epsilon^{\text{M}}_{11}$, $\mu^{\text{l}}_2 \equiv \mu_3 = \epsilon^{\text{M}}_{22}$ and $\mu^{\text{l}}_3 \equiv \mu_4 = \epsilon^{\text{M}}_{12}$. The affine representation of the Dirichlet boundary conditions is thus defined as

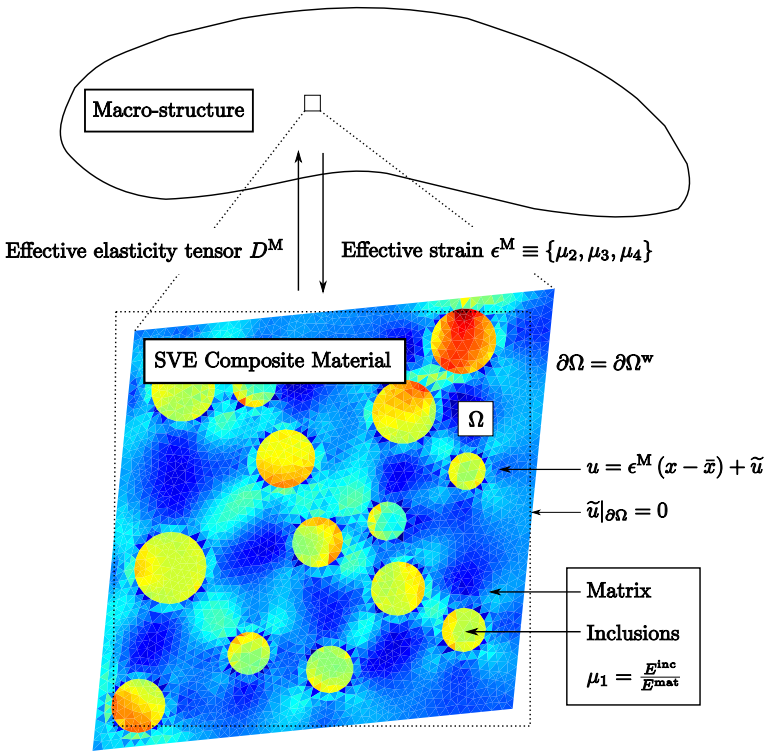

Figure 2: Schematic representation of the computational homogenisation framework for composite materials. The elastic contrast of the particulate composite is parametrised.

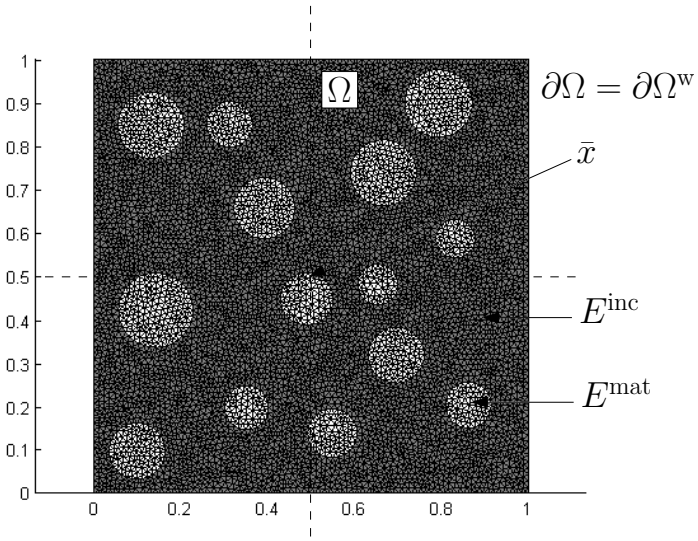

Figure 3: The finite element discretisation of the parametrised SVE.

$$
\begin{aligned}
w(x,\mu) &= \epsilon^{\mathrm{M}}(\mu^{\mathrm{l}})(x-\bar{x}) \\
&= \left(\begin{pmatrix} 1 & 0 \\ 0 & 0 \end{pmatrix} \mu_2 + \begin{pmatrix} 0 & 0 \\ 0 & 1 \end{pmatrix} \mu_3 + \begin{pmatrix} 0 & 1 \\ 1 & 0 \end{pmatrix} \mu_4 \right) (x-\bar{x}), \quad \forall \mu \in \mathcal{D}, x \in \partial\Omega^{\mathrm{w}},
\end{aligned} \tag{62}
$$

with $\bar{x}$ the barycenter of Ω (i.e., $\int_\Omega (x-\bar{x}) d\Omega = 0$).
The "truth" finite element SVE problem reads: find $u^{\mathrm{h},0}(\mu) \in \mathcal{U}^{\mathrm{h},0}(\Omega)$ such that

$$
\begin{aligned}
\int_\Omega \epsilon\left(u^{\mathrm{h},0}(\mu)\right) : D(\mu) : \epsilon(v)\, d\Omega &= -\int_\Omega \epsilon\left(u^{\mathrm{h,p}}(\mu)\right) : D(\mu) : \epsilon(v)\, d\Omega, \\
&= \hat{f}(v), \qquad \forall v \in \mathcal{U}^{\mathrm{h},0}(\Omega),
\end{aligned} \tag{63}
$$

where $u^{\mathrm{h,p}}(x,\mu) = w(x,\mu), \forall \mu \in \mathcal{D}, x \in \partial\Omega^{\mathrm{w}}$ is a known displacement field as described above, and $u^{\mathrm{h},0}(\mu)$ is the unknown displacement field which will be approximated using RB method. The "truth" effective Lamé constants $G^{\mathrm{M,h}}(\mu^{\mathrm{m}}) \equiv G^{\mathrm{h}}(\mu)$ and $\lambda^{\mathrm{M,h}}(\mu^{\mathrm{m}}) \equiv \lambda^{\mathrm{h}}(\mu)$ are computed as (see Chapter 7 of [45])

$$
G^{\mathrm{h}}(\mu) = \ell^G\left(u^{\mathrm{h}}(\mu)\right) = \frac{1}{|\Omega|}\int_\Omega \Sigma_G : D(\mu) : \epsilon(u^{\mathrm{h}}(\mu))\, d\Omega, \tag{64a}
$$

$$
\lambda^{\mathrm{h}}(\mu) = \ell^\lambda\left(u^{\mathrm{h}}(\mu)\right) = \frac{1}{|\Omega|}\int_\Omega \Sigma_\lambda : D(\mu) : \epsilon(u^{\mathrm{h}}(\mu))\, d\Omega, \tag{64b}
$$

where Σ_G and Σ_λ are field extractors such that $\ell^G(v) = -\frac{1}{|\Omega|}\hat{f}(v)$ and $\ell^\lambda(v) \neq \hat{f}(v)$. Hence, $G^{\mathrm{h}}(\mu)$ and $\lambda^{\mathrm{h}}(\mu)$ are compliant and noncompliant outputs, respectively.

The elastic contrast μ^{m} ranges from 0.1 (soft inclusions) to 10 (hard inclusions). The Poisson's ratios of both phases are set to $\nu = 0.3$. In this context, the affine representation of the Hooke's elasticity tensor over the parameter domain reads:

$$
D(x,\mu) = D^{\mathrm{mat}} + (\mu_1 - 1) H^{\mathrm{inc}}(x) D^{\mathrm{mat}}, \qquad \forall \mu \in \mathcal{D}, x \in \Omega. \tag{65}
$$

In equation (65) above, the function H^{inc} is the indicator function of the inclusion phase. Namely, it is equal to 1 for a point located in an inclusion and 0 elsewhere. The elasticity tensor of the matrix phase D^{mat} is defined by equation (2), with $E^{\mathrm{mat}} = 1$ and $\nu^{\mathrm{mat}} = 0.3$. The affine representation of the compliance tensor over the parameter domain becomes

$$
C(x,\mu) = C^{\mathrm{mat}} + \left(\frac{1}{\mu_1} - 1\right) H^{\mathrm{inc}}(x) C^{\mathrm{mat}}, \qquad \forall \mu \in \mathcal{D}, x \in \Omega, \tag{66}
$$

where C^{mat} is the compliance tensor of the matrix phase.

We now note that by solving {(63), (64)}, setting $\mu \equiv \mu^G = \left(\mu_1, 0, 0, \frac{1}{2}\right)$, $\Sigma_G = \begin{pmatrix} 0 & \frac{1}{2} \\ \frac{1}{2} & 0 \end{pmatrix}$ will render $G^{\mathrm{h}}(\mu)$; while setting $\mu \equiv \mu^\lambda = \left(\mu_1, 1, 0, \frac{1}{\sqrt{2}}\right)$, $\Sigma_\lambda = \begin{pmatrix} 1 & -\frac{1}{\sqrt{2}} \\ -\frac{1}{\sqrt{2}} & 0 \end{pmatrix}$ will render $\lambda^{\mathrm{h}}(\mu)$, respectively. Therefore, the only "actual" parameter of this problem is $\mu_1 = \frac{E^{\mathrm{inc}}}{E^{\mathrm{mat}}} \in \mathcal{D} \equiv [0.1, 10]$; and note that each μ_1 provides correspondingly one μ^G and one μ^λ as described above. The (very fine) finite element mesh consists of 7728 nodes and 15184 linear triangular elements as shown in fig. 3. The FE space to approximate the 2D homogenisation problem is of dimension $\mathcal{N} = 14916$. The reference parameter used in this work is chosen as $\mu_0 = (1, 0, 0, 0)$; $Q_a = 2$, $n_{\mathrm{w}} = 3$, $n_{\mathrm{c}} = 2$, and $\tilde{n}_{\mathrm{p}} = 0$ as there is no body force nor surface traction applied to the model. (Note that the dual problem will have $\tilde{n}_{\mathrm{p}} \neq 0$ as there is an applied body force which comes from the primal output $\ell^\lambda(v)$.) The entire work

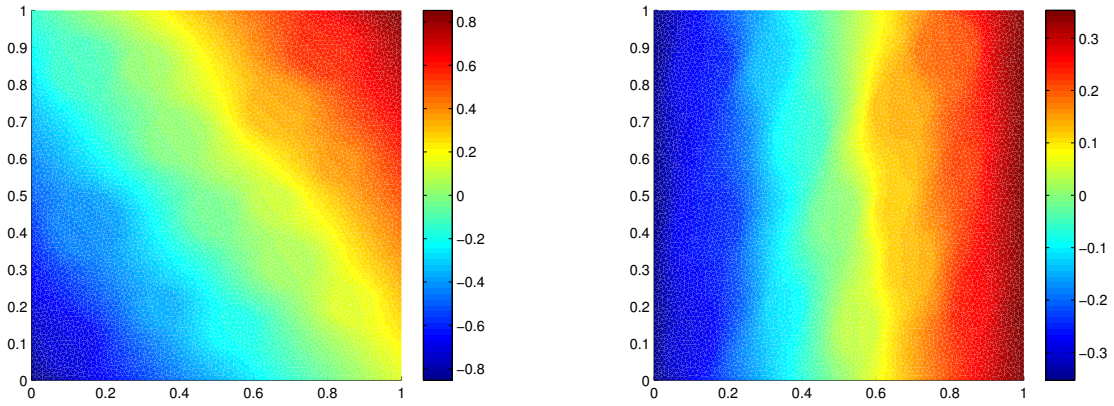

(a) (b)

Figure 4: FE displacement field in x-direction (a), and y-direction (b), with $\mu^{\text{test}} \equiv \mu^{\lambda} = \left(5, 1, 0, \frac{1}{\sqrt{2}}\right)$.

is implemented using the software Matlab R2012b. We show the FE displacement field in fig. 4 and the corresponding FE stress field in fig. 5 with $\mu^{\text{test}} \equiv \mu^{\lambda} = \left(5, 1, 0, \frac{1}{\sqrt{2}}\right)$, respectively.

In order to implement the sampling strategies which were described in section 4.2.2 and section 5.2, we first create the training sample set Ξ_{train}. In particular, the range $\mathcal{D} \equiv [0.1, 10]$ is divided by a logarithmically equidistant distribution with 500 sample points μ^{m}; and each μ^{m} provides correspondingly one μ^{G} and one μ^{λ}. Hence, the training sample set Ξ_{train} contains a total of 1000 sample parameter values which are 500 pairs (μ^{G}, μ^{λ}) logarithmically equidistant distributed.

6.1.2 Two-field greedy algorithm

We first test our implementation of the TF-greedy (two-field greedy) algorithm described in section 4.2.2. In fig. 6, we present the convergence of the algorithm for the parametrised SVE problem. In fig. 6(a), we show the value of the maximum of CRE error $\Delta^{\text{CRE,max}} = \max_{\mu \in \Xi_{\text{train}}} \Delta^{\text{CRE}}(\mu)$, the displacement error $\varepsilon_u^{\text{max}} = \max_{\mu \in \Xi_{\text{train}}} \|e_u\|_{D(\mu)}$ and stress error $\varepsilon_\sigma^{\text{max}} = \max_{\mu \in \Xi_{\text{train}}} \|e_\sigma\|_{C(\mu)}$ over Ξ_{train} as a function of the greedy iteration number. In fig. 6(b), we report the displacement and stress effectivities at $\mu^{\star}$: $\eta_u^{\text{CRE}}(\mu^{\star})$ and $\eta_\sigma^{\text{CRE}}(\mu^{\star})$ as a function of the greedy iterations, while in fig. 6(c), we show the evolution of the displacement and stress reduced basis, $\mathcal{Z}_N$ and $\tilde{\mathcal{Z}}_{\tilde{N}}$ respectively.

a) From fig. 6(a), we see that the TF-RBM converges both in stress and displacement, as it is designed to converge in the CRE error measure, which is a combination of the exact error in these two fields. The "stair" shape of the convergence curves of the stress and displacement errors is easily explained: we have chosen to correct only one of the surrogates at each greedy iteration.

   For comparison purpose, we also show the behaviour of the RB method using the well-known SCM upper error bound[†] [29, 22, 28] in fig. 7 (The SCM algorithm and all associated parameters used for this comparison are described in details in section 10 of [22]; we use the open source "rbMIT" software [49] that implements this version of the SCM. We also use the same training set Ξ_{train}

[†]For convenience, we will call the RB greedy procedure which uses residual-based error estimation with coercivity constant bounding via SCM as "SCM-greedy procedure" or "SCM-based procedure" onwards. This procedure is presented briefly in appendix C for reference.

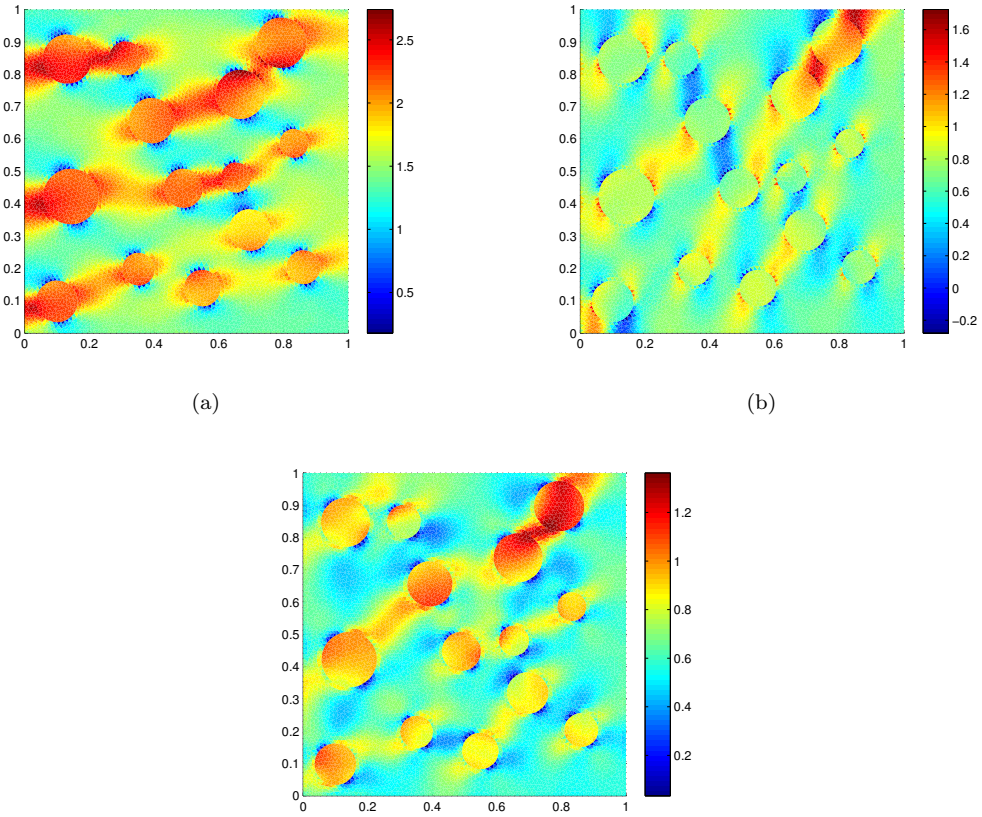

(a) (b)

(c)

Figure 5: FE stress field σ_{xx} (a), σ_{yy} (b), and σ_{xy} (c), with $\mu^{\text{test}} \equiv \mu^{\lambda} = \left(5, 1, 0, \frac{1}{\sqrt{2}}\right)$.

for the offline stage of the SCM algorithm.) Comparing fig. 6(a) and fig. 7(a), we see that the convergent rate of our proposed TF-greedy strategy is similar to that of the SCM-based greedy strategy. This statement is made on the basis that the dimension of each of the TF-RBM surrogate is approximately equal to the number of greedy iterations divided by two. Therefore, if we consider the displacement surrogate as "master" surrogate in the TF-RBM, whilst the "stress" surrogate is considered as a tool for certification purposes, then the displacement convergence rate of the two methods as a function of the dimension of the corresponding reduced basis is similar. We acknowledge the fact that comparing the convergence of the two methods in such a way is arguable as they are conceptually different. However, it does show that the TF-RBM extracts attractive subspaces at a speed that is at least comparable to that of the SCM-based RBM.

b) The effectivites of the TF-RBM bounds of the stress and displacement errors automatically "balance themselves" out. When the stress error is larger than the displacement error, the algorithm increases the dimension of the stress surrogate at the next greedy iteration, thereby increasing the effectivity of the displacement error bound, while the effectivity of the stress error bound is left free to degrade. This property appears more clearly in fig. 6(b)). We see that the two curves $\eta_u^{\text{CRE}}(\mu^\star)$ and $\eta_\sigma^{\text{CRE}}(\mu^\star)$ develop in opposite directions from one greedy iteration to the next one: when $\eta_u^{\text{CRE}}(\mu^\star)$ increases, $\eta_\sigma^{\text{CRE}}(\mu^\star)$ decreases and vice versa.

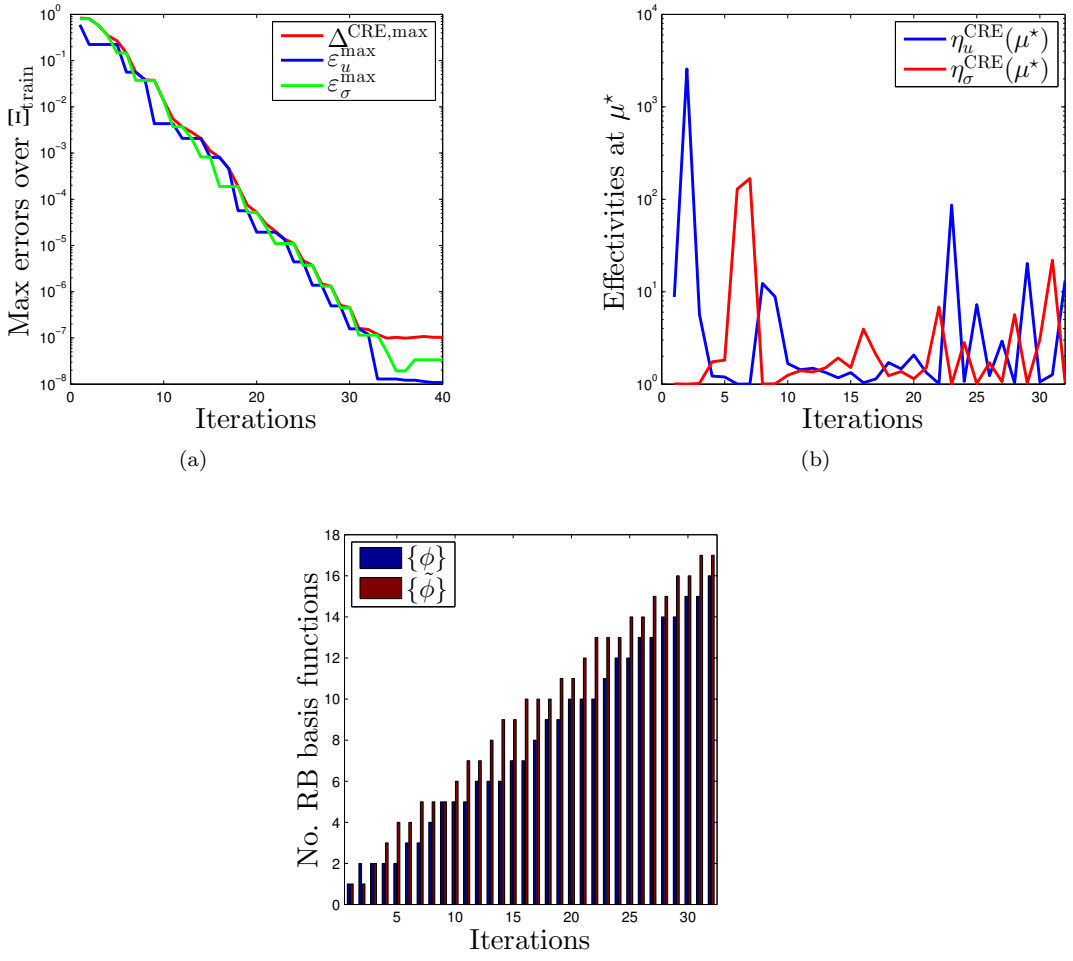

Figure 6: (a) Maximum of CRE error $\Delta^{\text{CRE,max}}$, displacement RB error $\varepsilon_u^{\max}$ and stress RB error $\varepsilon_\sigma^{\max}$ over Ξ_{train}, (b) displacement and stress effectivities at $\mu^\star$, and (c) sizes of the sets $\mathcal{Z}_N$ and $\tilde{\mathcal{Z}}_{\tilde{N}}$ as functions of greedy iterations (only first 32 iterations are shown in fig. 6(b) and fig. 6(c)).

This is in contrast to the the SCM-based RBM, which, by design, requires a uniformly sharp effectivity for the displacement error bound (see figure fig. 7). This sharp error bound needs to be trained in advance during the offline stage, while the error bounds of the TF-RBM "train themselves" during the greedy iterations. In facts, the error bounds of the TF-RBM are an outcome of the training process, and not a requirement for the training to be performed, which is what makes this method appealing and easy to implement.

c) We now present some results in terms of "online" and "offline" computational time for the SVE problem. All computations were performed on a desktop Intel(R) Core(TM) i7-3930K CPU @3.20GHz 3.20GHz, RAM 32GB, 64-bit Windows 7 Operating System.

We first report the "online" CPU time of the computation $\mu \to \Delta^{\text{X}}(\mu)$ where either X=CRE or X=SCM in fig. 8(a), which involves solving the reduced order model(s) and computing the

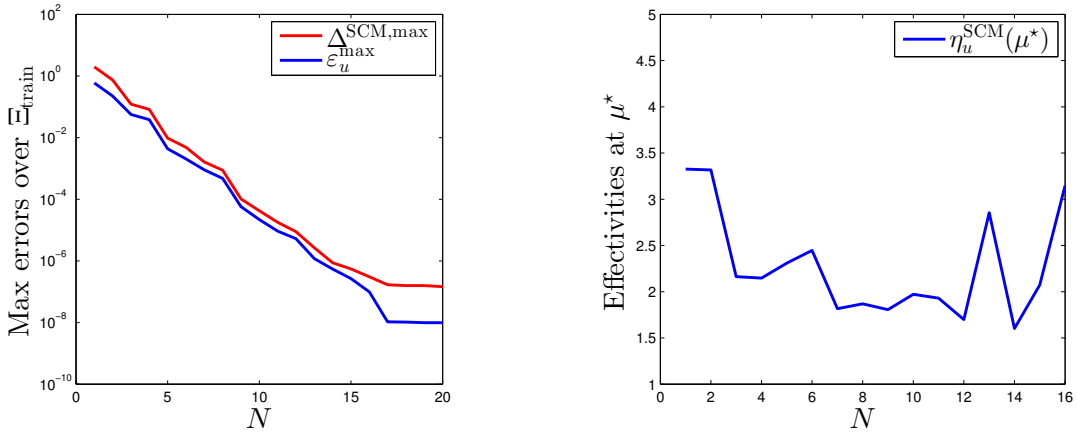

(a) (b)

Figure 7: (a) Maximum of SCM upper error bound $\Delta^{\text{SCM,max}}$ and displacement RB error $\varepsilon_u^{\text{max}}$ over Ξ_{train}, and (b) displacement effectivity at $\mu^\star$ as functions of N (only first 16 iterations are shown in fig. 7(b)).

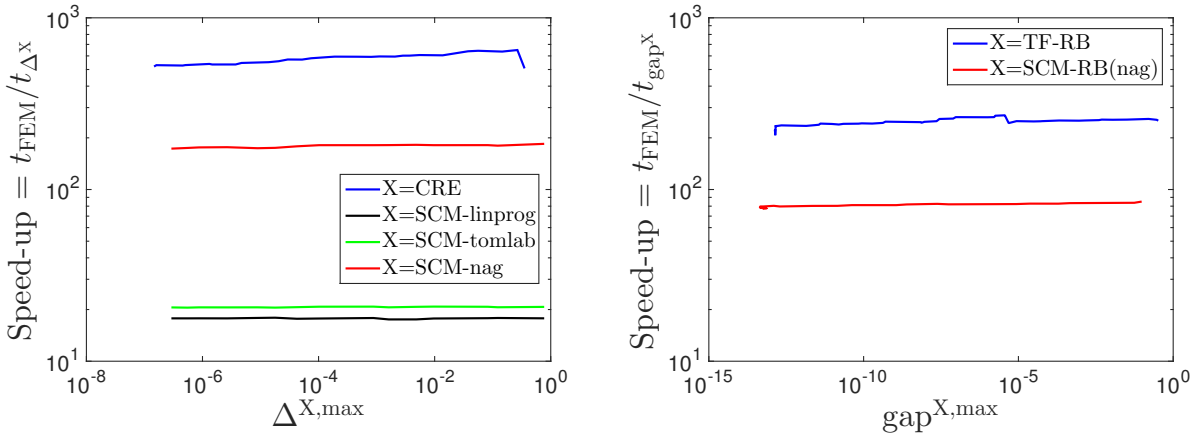

(a) (b)

Figure 8: Speed-up as functions of max error indicators for Δ^{max} (a), and for $\mathtt{gap}^{\text{max}}$ (b) ($t_{\text{FEM}} = 0.0918$ sec).

error indicator. In order to do this, we choose a test parameter point $\mu^{\text{test}} \equiv \mu^\lambda = \left(5, 1, 0, \frac{1}{\sqrt{2}}\right)$. Then, for each order of reduced basis surrogates obtained by the TF-RBM and SCM-based greedy processes, we compute $\mu^{\text{test}} \to \Delta^{\text{CRE}}(\mu^{\text{test}})$ and $\mu^{\text{test}} \to \Delta^{\text{SCM}}(\mu^{\text{test}})$ and measure the corresponding computational time. These operations are performed repeatedly 1000 times and we report the average cost in terms of CPU time. In fig. 8(a) this recorded time (normalised by t_{FEM}) is plotted as a function of the measures of accuracy $\Delta^{\text{CRE,max}}$ and $\Delta^{\text{SCM,max}}$, respectively. Regarding the computation of $\Delta^{\text{SCM}}(\mu)$, we observed that the evaluation of the coercivity constant $\alpha_{\text{LB}}^{\mathcal{N}}(\mu)$ is the

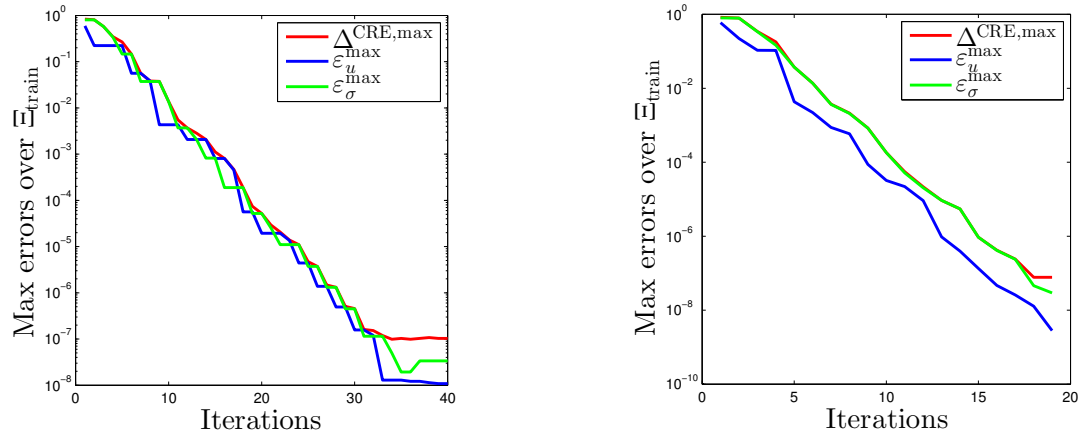

Figure 9: Maximum of relative errors using: (a) our proposed TF-greedy algorithm and (b) TF-greedy algorithm enriching both fields simultaneously at one iteration.

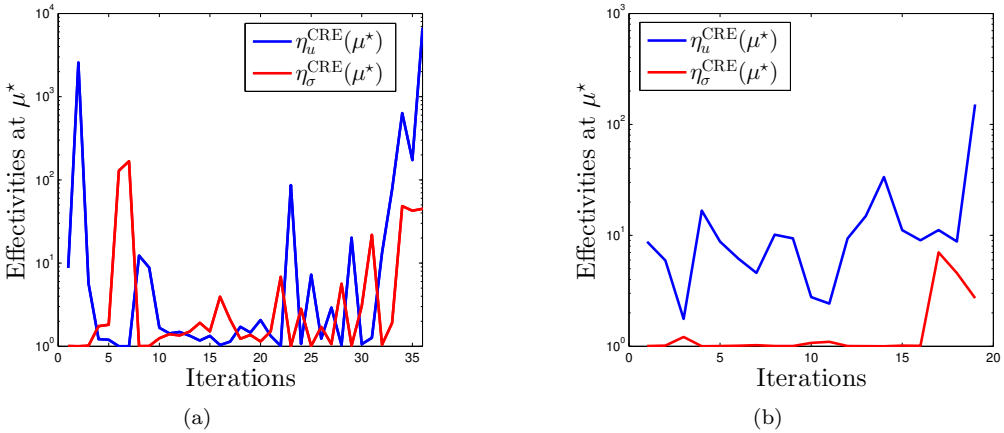

Figure 10: Displacement and stress effectivities at $\mu^\star$ using: (a) the proposed TF-greedy algorithm and (b) TF-greedy algorithm enriching both fields simultaneously.

most time-consuming operation. As this operation involves solving a linear programming problem, we have tried various stat-of-the-art optimisation packages for the calculation of this constant. We have reported the results obtained with the Matlab built-in "linprog" [50], and with the TOMLAB [51] and NAG packages [52] (all these packages are commercial softwares that are interfaced with Matlab).

From the observation of fig. 8(a), we see that the speed-up of $\Delta^{\text{CRE}}(\mu)$ is larger than that of $\Delta^{\text{SCM}}(\mu)$. The difference is up to one order of magnitude. This is intuitively explainable: the SCM-based approach requires solving an optimisation problem to compute $\Delta^{\text{SCM}}(\mu)$ (via the SCM coercivity coefficient $\alpha_{\text{LB}}^{\mathcal{N}}(\mu)$), which takes more computing resources than inverting the $(\tilde{N} \times \tilde{N})$ matrix required to obtain $\Delta^{\text{CRE}}(\mu)$. In short, when "online" certification of the reduced basis

approach is required, we can conclude that the TF-RBM is faster than the SCM-based approach. Again, we acknowledge that this conclusion may be problem- and implementation-dependent. In particular, the efficiency of optimisation algorithms is sensitive to the properties of the problem to solve and to the input parameters of these algorithms (*i.e.* tolerance, relaxation parameters, ...). The crucial point here is that the TF-RBM does not need to solve any linear programming at all.

This speed-up statement should be further mitigated. Indeed, the requirement for certification is arguable. Firstly, if the training set samples the parameter domain in a sufficiently fine way, then we can trust that the online error for an arbitrary set of parameters will be smaller than the maximum error over the training set. Secondly, the usefulness of certification depends on the ability of the engineer to increase the accuracy of the reduced model after it has been constructed, which is highly application-dependant. However, this "online" speed-up may have a significant impact in applications where high-dimensional parameter domains are considered, as fine training sets may be out of reach. An other particularly interesting case is the family of "on-the-fly" model order reduction (*e.g.* [1, 18] or [53, 54] in optimisation), where "offline/online" decomposition of the computational effort is irrelevant. In this case, the training is performed "online", for instance directly on the trajectory of a gradient-based optimisation algorithm or during the iterations of a Monte-Carlo algorithm [55].

In terms of "offline" CPU time, the cost of the construction of the TF-RBM surrogate is similar to the cost of the SCM-based RBM. This is due to the fact that the mass of the computational resources required "offline" is concentrated in full-order operations such as computing exact finite element solutions or assembling the terms of the various affine decompositions. The speed-up obtained by the TF-RBM when exploring the parameter domain is lost due to such overheads. Moreover, the SCM-based RBM is very efficient when a fixed training set is used throughout the greedy process. This is because the expensive part of the computation of the SCM-based error bound, namely the optimisation of the lower bound of the coercivity constant, is performed only once for each of the training points *at the start of the greedy process.* (Hence, one does not need to recompute the lower bound for the coercivity constant during later greedy iterations.) We have tested the idea of using varying random training sets, which has been shown in recent investigations to allow for a more efficient sampling of the parameter domain [26]. In this case, the TF-RBM can be faster than the SCM-based RBM in the "offline" stage. With 1000 randomly distributed training points, we have observed that the construction costs of the TF-RBM model are halved compared to that of the SCM-based approach.

Remark 6.1. *It is worth analysing the behaviour of the TF-greedy algorithm when both fields (displacement and stress) are enriched simultaneously at each greedy iteration. For comparison purposes, we show the results of this case in fig. 9 and fig. 10. In particular, fig. 9 shows the maximum relative errors (i.e.,* $\Delta^{\mathrm{CRE,max}}, \varepsilon_u^{\max}$ *and* $\varepsilon_\sigma^{\max}$*) of the proposed TF-greedy and the TF-greedy enriching both fields at* $\mu^\star$ *at each greedy iteration; while fig. 10 presents displacement and stress effectivities of both algorithms at* $\mu^\star$*.*

Generally speaking, the results at the i^{th} *iteration of the proposed TF-greedy algorithm will be compared with that of the* $\left(\frac{i+1}{2}\right)^{th}$ *iteration of the enriching both fields TF-greedy one*[‡]*. From fig. 9(a) and fig. 9(b), we observe that the former algorithm gives smaller CRE values than that of the latter algorithm with the same total number of displacement and stress RB basis functions. For example, the* 9^{th}*,* 19^{th} *and* 29^{th} *iterations of fig. 9(a) will all give smaller CRE errors than the* 5^{th}*,* 10^{th} *and* 15^{th} *iterations of fig. 9(b) do. Moreover, fig. 10(b) shows that when enriching both fields at every iteration, the stress field will contributes "more" to the CRE than the displacement field does; while fig. 10(a) demonstrates that the proposed algorithm automatically balances out these contributions though the iterative process. However, the gain in terms of accuracy is rather small and may be problem-dependent. If limiting the "offline" cost is of the essence, the second algorithm is probably the one that should be used.*

[‡] i is an odd integer due to the fact that we enrich both fields at the 1st iteration of the TF-greedy algorithm.

6.1.3 Goal-oriented greedy algorithm

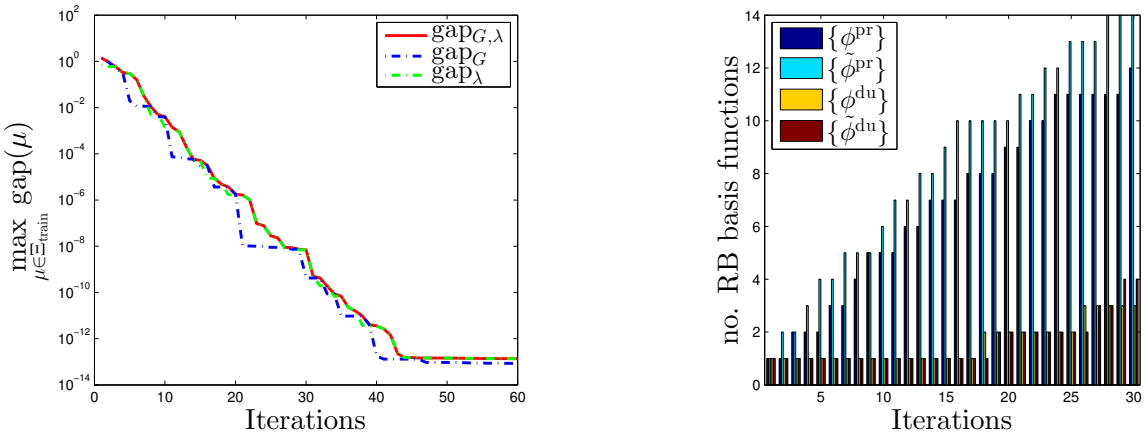

Figure 11: (a) Maximum of $\texttt{gap}_{G,\lambda}$, $\texttt{gap}_G$ and $\texttt{gap}_\lambda$ over Ξ_{train}, and (b) sizes of the sets $\mathcal{Z}^{\text{pr}}$, $\tilde{\mathcal{Z}}^{\text{pr}}$, $\mathcal{Z}^{\text{du}}$ and $\tilde{\mathcal{Z}}^{\text{du}}$ as functions of GO-greedy iterations (only first 30 iterations are shown in fig. 11(b)).

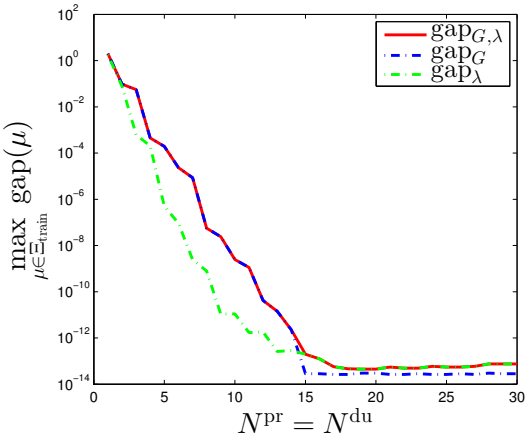

Figure 12: Maximum of $\texttt{gap}_{G,\lambda}$, $\texttt{gap}_G$ and $\texttt{gap}_\lambda$ over Ξ_{train} which are post-processed by primal and dual SCM-greedy algorithms as functions of $N^{\text{pr}} = N^{\text{du}}$.

a) The QoI gaps of the homogenisation problem are defined as (60), i.e.,

$$\texttt{gap}_G \equiv \texttt{gap}(\mu^G) = \frac{2\left|G^{\text{r},+}(\mu^G) - G^{\text{r},-}(\mu^G)\right|}{|G^{\text{r},+}(\mu^G)| + |G^{\text{r},-}(\mu^G)|}, \tag{67a}$$

$$\texttt{gap}_\lambda \equiv \texttt{gap}(\mu^\lambda) = \frac{2\left|\lambda^{\text{r},+}(\mu^\lambda) - \lambda^{\text{r},-}(\mu^\lambda)\right|}{|\lambda^{\text{r},+}(\mu^\lambda)| + |\lambda^{\text{r},-}(\mu^\lambda)|}, \tag{67b}$$

where $G^{\mathrm{r},+}(\mu)$, $G^{\mathrm{r},-}(\mu)$ are defined as in (61), and $\lambda^{\mathrm{r},+}(\mu)$, $\lambda^{\mathrm{r},-}(\mu)$ are defined as in (59) for compliant and noncompliant outputs, respectively. In addition, there is a dual equation associated with $\lambda^{\mathrm{h}}(\mu)$, and no dual equation associated with $G^{\mathrm{h}}(\mu)$ due to this reason.

b) We now implement the proposed goal-oriented greedy sampling strategy (section 5.2). The results are shown in fig. 11. In particular, we present the maximum of gaps $\mathtt{gap}^{\max}_{G,\lambda} = \max_{\mu\in\Xi_{\mathrm{train}}} \{\mathtt{gap}_G, \mathtt{gap}_\lambda\}$ together with $\mathtt{gap}^{\max}_G = \max_{\mu^G\in\Xi_{\mathrm{train}}} \mathtt{gap}_G$ and $\mathtt{gap}^{\max}_\lambda = \max_{\mu^\lambda\in\Xi_{\mathrm{train}}} \mathtt{gap}_\lambda$ in fig. 11(a). Fig. 11(b) shows the sizes of $\mathcal{Z}^{\mathrm{pr}}$, $\tilde{\mathcal{Z}}^{\mathrm{pr}}$, $\mathcal{Z}^{\mathrm{du}}$ and $\tilde{\mathcal{Z}}^{\mathrm{du}}$ as functions of GO-greedy iterations (first 30 iterations), respectively. For reference, we also present the maximum of gaps which are post-processed with $N^{\mathrm{pr}} = N^{\mathrm{du}}$ using primal and dual SCM-greedy algorithms[§] in fig. 12.

It is observed from fig. 11(a) that the proposed GO-greedy strategy converges in a goal-oriented manner: the strategy only enriches necessary RB basis functions (primal/dual displacement/stress) to minimise the QoI gaps. Fig. 11(b) shows that the primal displacement/stress RB basis functions are enriched more frequently than the dual ones. This may be because $\mathcal{Z}^{\mathrm{pr}}$ and $\tilde{\mathcal{Z}}^{\mathrm{pr}}$ help to improve both gaps, i.e., $\{\mathtt{gap}_G, \mathtt{gap}_\lambda\}$; while $\mathcal{Z}^{\mathrm{du}}$ and $\tilde{\mathcal{Z}}^{\mathrm{du}}$ will contribute to the improvement of $\mathtt{gap}_\lambda$ only. This is in fact consistent with and also explains fig. 12: since we use a relatively high N^{du} compared with a N^{pr} ($N^{\mathrm{pr}} = N^{\mathrm{du}}$), $\mathtt{gap}_\lambda$ is thus much smaller than $\mathtt{gap}_G$ with one specific $N^{\mathrm{pr}} = N^{\mathrm{du}}$. Fig. 13 and fig. 14 illustrate the virtual charts of $G(\mu)$ and $\lambda(\mu)$ as functions of the material heterogeneity $\mu^{\mathrm{m}} = \frac{E^{\mathrm{inc}}}{E^{\mathrm{mat}}}$ after first 9 GO-greedy iterations, respectively.

c) We finally report the online computational time of the computation $\mu \to \mathtt{gap}^{\mathrm{X}}(\mu)$, where X=TF-RB or X=SCM-RB in fig. 8(b). (Here, TF-RB implies two-field goal-oriented reduced basis, and SCM-RB means successive constraint method reduced basis.) In particular, by repeating the same procedure as in paragraph c) of section 6.1.2 above, we can obtain the recorded time to compute $\mu^{\mathrm{test}} \to \mathtt{gap}^{\mathrm{TF-RB}}(\mu^{\mathrm{test}})$ (after implementing the proposed GO-greedy algorithm) and $\mu^{\mathrm{test}} \to \mathtt{gap}^{\mathrm{SCM-RB}}(\mu^{\mathrm{test}})$ (after post-processing two SCM-greedy algorithms), respectively. We then plot this recorded time (normalised with respect t_{FEM} to obtain the speed-up) as functions of $\mathtt{gap}^{\mathrm{TF-RB,max}}$ and $\mathtt{gap}^{\mathrm{SCM-RB,max}}$ in fig. 8(b), respectively.

By observation, fig. 8(b) is very consistent with fig. 8(a). We recall from (59) that the computation of $\mathtt{gap}(\mu)$ essentially contains $\Delta^{\mathrm{X}}(\mu)$, $\Delta^{\mathrm{X}}_z(\mu)$ and $R\left(z^{\mathrm{r},0}(\mu)\right)$ where X=CRE or X=SCM. Therefore, the (online) computational time of $\mathtt{gap}(\mu)$ will be a little more than two times of that of $\Delta^{\mathrm{X}}(\mu)$; and this fact is reflected clearly in fig. 8. In conclusion, as similar to the case Δ^{X} above, the online computational time of the proposed GO-greedy strategy is $O(10)$ times smaller than that of the (post-processing) SCM-greedy approach.

6.2 Two-parameter case

6.2.1 Reference problem

We now consider the 2D SVE represented in figure fig. 15. The domain is a unit square $\Omega = [0,1]\times[0,1]$ which is now composed of three distinct material phases: the circular inclusions characterised by Young's modulus E^{inc}_1, the ellipsoid inclusions characterised by Young's modulus E^{inc}_2 and the surrounding matrix characterised by Young's modulus E^{mat}. All phases are assumed to have elastic and isotropic behaviour.

The SVE boundary value problem is parametrised by the elastic contrasts $\mu_1 = \frac{E^{\mathrm{inc}}_1}{E^{\mathrm{mat}}}$, $\mu_2 = \frac{E^{\mathrm{inc}}_2}{E^{\mathrm{mat}}}$ and the load parameters μ_3, μ_4 and μ_5. The load parameters are the parameters that described the Dirichlet boundary conditions in section 6.1.1 (μ_2, μ_3 and μ_4 in eq. (62)).

[§]We choose the specific configuration ($N^{\mathrm{pr}} = N^{\mathrm{du}}$) since this configuration is the most commonly used for noncompliant outputs [22, 28]. However, in [22], the authors already identified and discussed the possibility of balancing the errors in the primal and dual variables by adapting the ratio between N^{pr} and N^{du}.

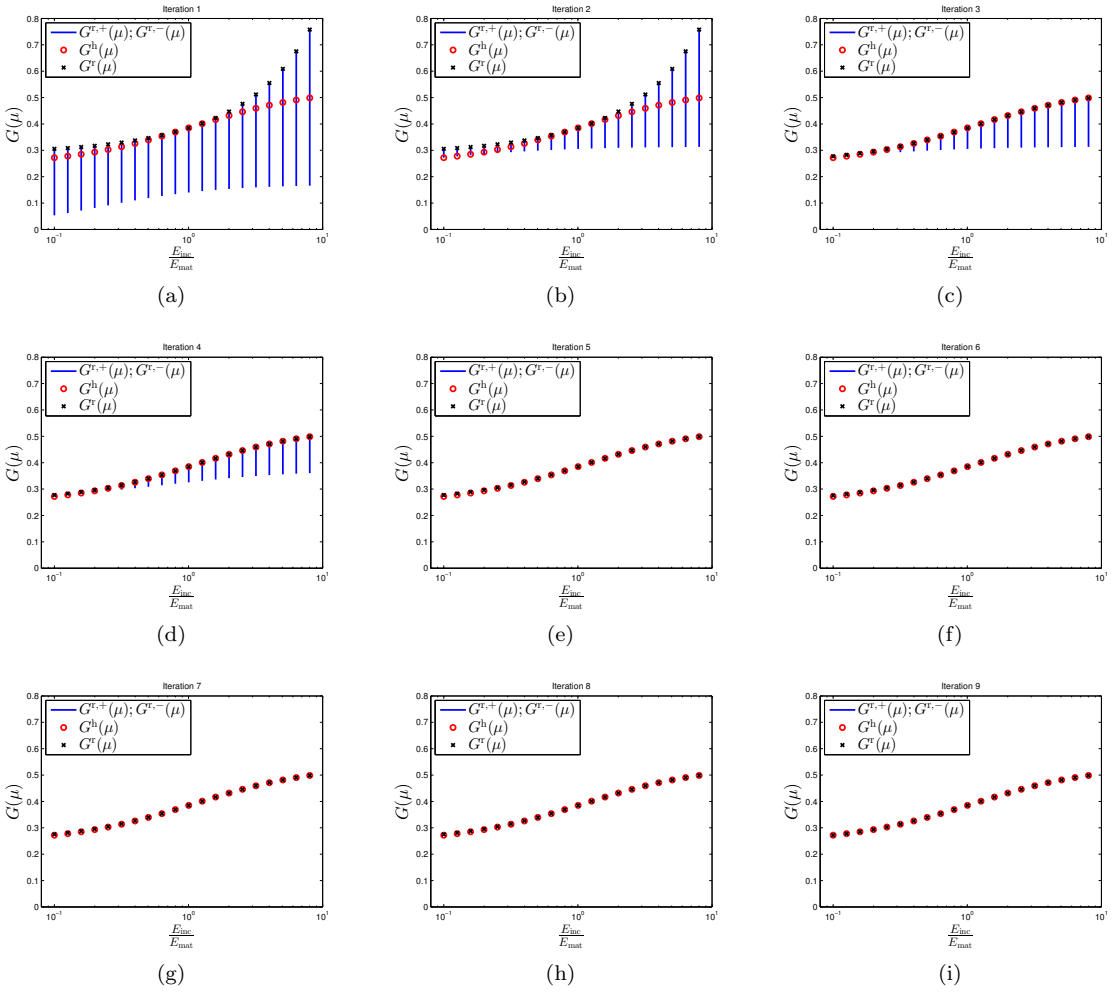

Figure 13: Virtual charts of $G(\mu)$ with respect to the variations of material heterogeneity after first 9 GO-greedy iterations.

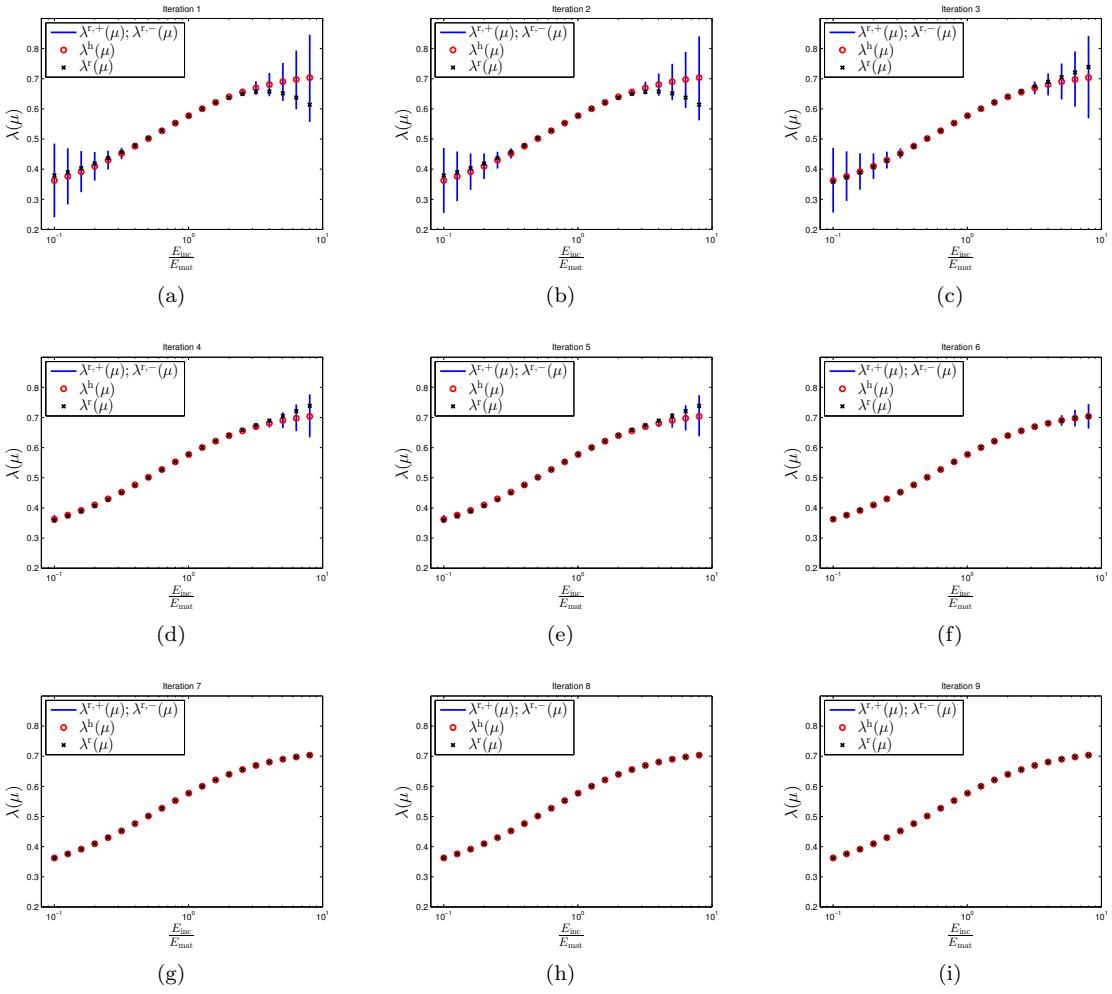

Figure 14: Virtual charts of $\lambda(\mu)$ with respect to the variations of material heterogeneity after first 9 GO-greedy iterations.

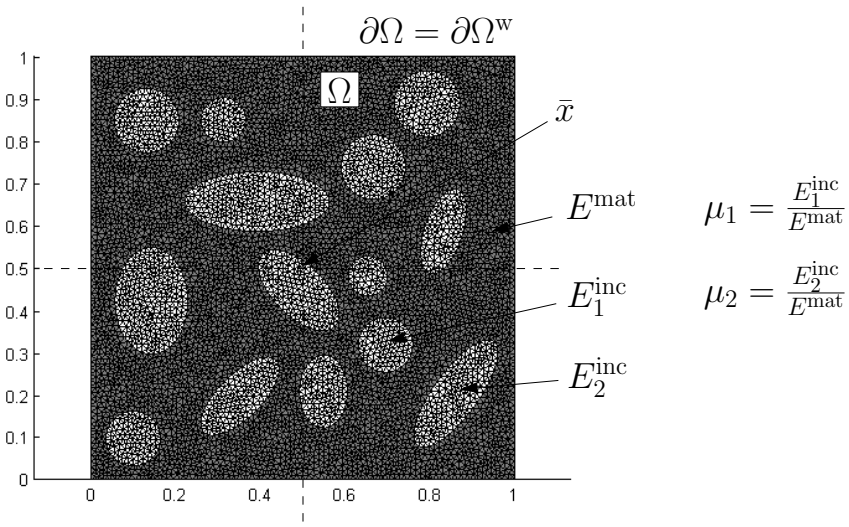

Figure 15: The finite element discretisation of the parametrised SVE.

The Hooke tensor field now admits the following affine representation:

$$D(x,\mu) = D^{\mathrm{mat}} + (\mu_1 - 1)H_1^{\mathrm{inc}}(x)D^{\mathrm{mat}} + (\mu_2 - 1)H_2^{\mathrm{inc}}(x)D^{\mathrm{mat}}, \qquad \forall \mu \in \mathcal{D}, x \in \Omega. \tag{68}$$

In the above equation, the functions $H_1^{\mathrm{inc}}(x)$ and $H_2^{\mathrm{inc}}(x)$ are indicator functions of the circular and ellipsoid inclusions. Namely, the function is equal to 1 for a point located in a corresponding inclusion (circular or ellipsoid) and 0 elsewhere. The elasticity tensor of the matrix phase D^{mat} is defined by eq. (2), with $E^{\mathrm{mat}} = 1$ and $\nu^{\mathrm{mat}} = 0.3$. The affine representation of the compliance tensor over the parameter domain becomes

$$C(x,\mu) = C^{\mathrm{mat}} + \left(\frac{1}{\mu_1} - 1\right) H_1^{\mathrm{inc}}(x)C^{\mathrm{mat}} + \left(\frac{1}{\mu_2} - 1\right) H_2^{\mathrm{inc}}(x)C^{\mathrm{mat}}, \qquad \forall \mu \in \mathcal{D}, x \in \Omega, \tag{69}$$

where C^{mat} is the compliance tensor of the matrix phase.

As in the previous example, setting $\mu \equiv \mu^G = (\mu_1, \mu_2, 0, 0, \frac{1}{2})$, $\Sigma_G = \begin{pmatrix} 0 & \frac{1}{2} \\ \frac{1}{2} & 0 \end{pmatrix}$ will deliver $G^{\mathrm{h}}(\mu)$; while setting $\mu \equiv \mu^\lambda = \left(\mu_1, \mu_2, 1, 0, \frac{1}{\sqrt{2}}\right)$, $\Sigma_\lambda = \begin{pmatrix} 1 & -\frac{1}{\sqrt{2}} \\ -\frac{1}{\sqrt{2}} & 0 \end{pmatrix}$ will deliver $\lambda^{\mathrm{h}}(\mu)$. The two parameters of this problem are allowed to vary as $\mu_1 = \frac{E_1^{\mathrm{inc}}}{E^{\mathrm{mat}}} \in [0.1, 10]$ and $\mu_2 = \frac{E_2^{\mathrm{inc}}}{E^{\mathrm{mat}}} \in [0.1, 10]$. The finite element mesh consists of 7618 nodes and 14963 linear triangular elements as shown in fig. 15. The FE space to approximate the 2D homogenisation problem is of dimension $\mathcal{N} = 14694$, the reference parameter is chosen as $\mu_0 = (1, 1, 0, 0, 0)$; $Q_a = 3$, $n_{\mathrm{w}} = 3$, $n_{\mathrm{c}} = 2$, and $\tilde{n}_{\mathrm{p}} = 0$ as there is no body force nor surface traction (However, for the dual problem, we will have $\tilde{n}_{\mathrm{p}} \neq 0$ as a body force arises from the definition of the primal output $\ell^\lambda(v)$). The FE stress field is illustrated in figure fig. 16 with $\mu^{\mathrm{test}} \equiv \mu^\lambda = (5, 0.2, 1, 0, \frac{1}{\sqrt{2}})$.

We now define the training sample set Ξ_{train}. The parameter range $\mathcal{D} \equiv [0.1, 10] \times [0.1, 10]$ is divided by a logarithmically equidistant distribution along two axes (μ_1 and μ_2) with 625 (=25 × 25) sample "points" (μ_1, μ_2). Each point (μ_1, μ_2) of interest will provide two outputs μ^G and μ^λ. Hence, the training sample set Ξ_{train} contains a total of 1250 sample parameter values that correspond to 625 pairs (μ^G, μ^λ).

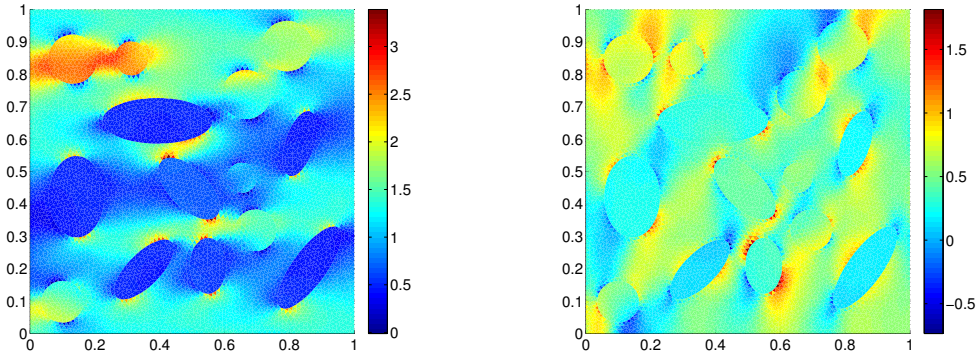

(a) (b)

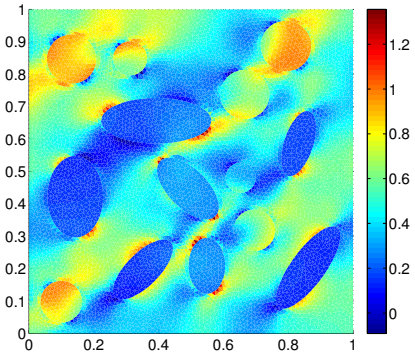

(c)

Figure 16: FE stress field σ_{xx} (a), σ_{yy} (b), and σ_{xy} (c), with $\mu^{\text{test}} \equiv \mu^{\lambda} = \left(5, 0.2, 1, 0, \frac{1}{\sqrt{2}}\right)$.

6.2.2 Performance of the TF-RBM

We directly show the performance of the Goal-oriented TF-RBM for this two-parameter problem. The results are presented in figure fig. 17. The maximum of the gaps (defined as in eq. (67)) $\mathtt{gap}^{\max}_{G,\lambda} = \max_{\mu \in \Xi_{\text{train}}} \{\mathtt{gap}_G, \mathtt{gap}_\lambda\}$, together with $\mathtt{gap}^{\max}_G = \max_{\mu^G \in \Xi_{\text{train}}} \mathtt{gap}_G$ and $\mathtt{gap}^{\max}_\lambda = \max_{\mu^\lambda \in \Xi_{\text{train}}} \mathtt{gap}_\lambda$, is displayed in figure fig. 17(a). Fig. 17(b) shows the sizes of $\mathcal{Z}^{\text{pr}}$, $\tilde{\mathcal{Z}}^{\text{pr}}$, $\mathcal{Z}^{\text{du}}$ and $\tilde{\mathcal{Z}}^{\text{du}}$ as functions of GO-greedy iterations, respectively.

It is observed that the proposed algorithm converges as expected: the algorithm only enriches necessary RB basis functions (primal/dual displacement/stress) to minimise the QoI gaps. We also see from fig. 17(b) that the primal displacement/stress RB basis functions are enriched more than the dual ones with the same reason as explained in paragraph b) of section 6.1.3. Finally, fig. 18 and fig. 19 illustrate the virtual charts of $G(\mu)$ and $\lambda(\mu)$ as functions of the material heterogeneity $\mu_1 = \frac{E_1^{\text{inc}}}{E^{\text{mat}}}$ and $\mu_2 = \frac{E_2^{\text{inc}}}{E^{\text{mat}}}$ after first 36 GO-greedy iterations, respectively.

The convergence rate of the Greedy algorithm (fig. fig. 17(a)) is roughly four times lower than in the single parameter case. This is not due to a deficiency of the proposed Greedy algorithm but to an increase of the Kolmogorov N-Width for this particular parametrised homogenisation problem.

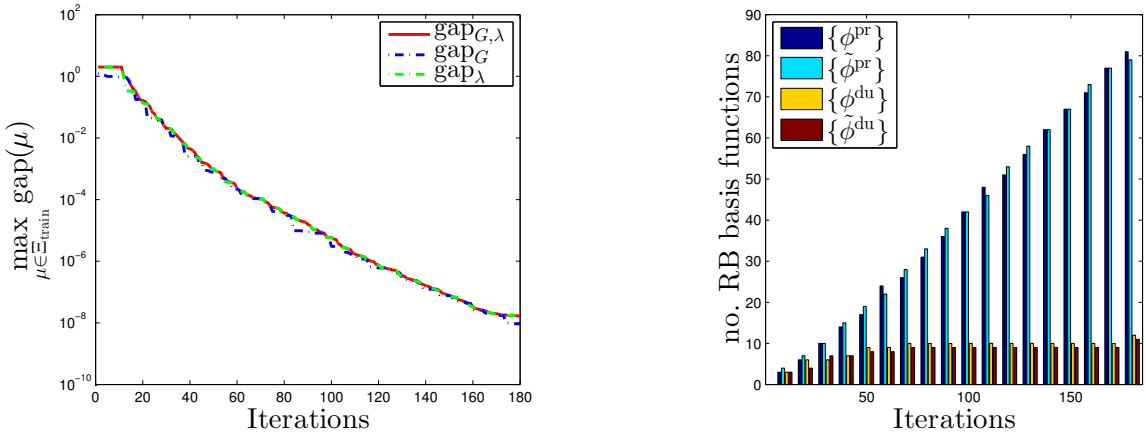

(a) (b)

Figure 17: (a) Maximum of $\texttt{gap}_{G,\lambda}$, $\texttt{gap}_{G}$ and $\texttt{gap}_{\lambda}$ over Ξ_{train}, and (b) sizes of the sets $\mathcal{Z}^{\text{pr}}$, $\tilde{\mathcal{Z}}^{\text{pr}}$, $\mathcal{Z}^{\text{du}}$ and $\tilde{\mathcal{Z}}^{\text{du}}$ as functions of GO-greedy iterations.

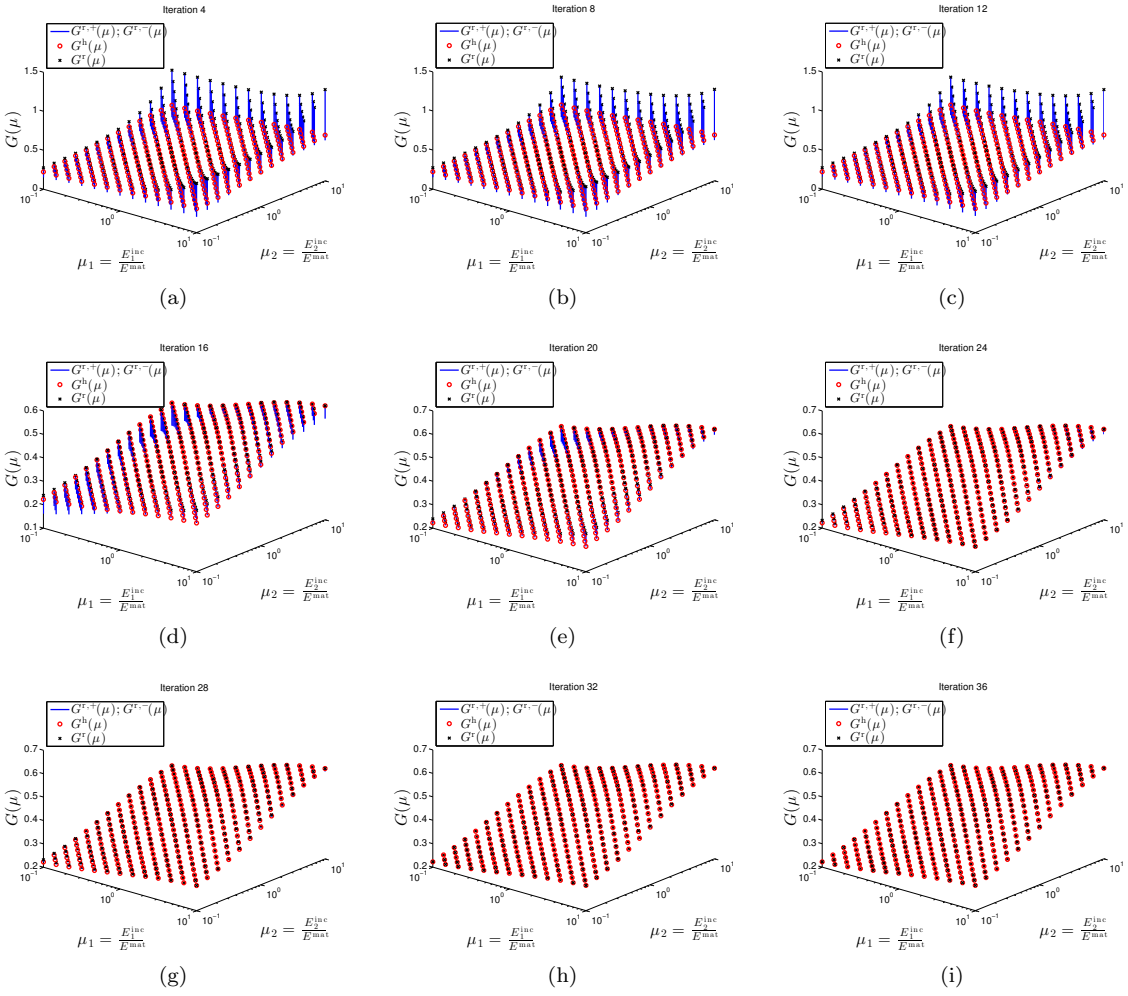

Figure 18: Virtual charts of $G(\mu)$ with respect to the variations of material heterogeneity after first 36 GO-greedy iterations.

7 Conclusion

A new reduced basis framework has been proposed for the metamodelling of parametrised elasticity problems. The first novel idea is to use the Constitutive Relation Error as an indication of accuracy of the reduced order model, in order to (i) construct the projection spaces based on a greedy sampling of the parameter domain and (ii) certify the final reduced order model. The method requires the construction of separate reduced order models for the primal (displacement) and flux (stress) fields. The greedy sampling algorithm is designed to jointly construct optimum projection subspaces for these two fields. We have shown that the numerical efficiency of the resulting reduced order model is up to one order of magnitude higher than state-of-the-art existing methodologies. We have also shown that the construction of this model is considerably simplified due to the fact that the reduced order model and the relevant measures of accuracy are trained together, in a single greedy loop.

The second key idea is to extend this concept to the context of goal-oriented sampling. In this case, the greedy algorithm is aimed at the minimisation of the error in quantity of interest. We have shown that this concept, coupled with the CRE-driven adaptivity, leads to the construction of a metamodel that is "tuning-free", in the sense that the user needs only to specify the desired accuracy for the quantities of interest. There is no other calibration parameter in the proposed algorithm. We have shown that this goal-oriented algorithm permits to construct reduced order models that are directly certified in terms of input/output maps, and extremely efficient in terms of computational expense.

Acknowledgements

We are sincerely grateful for the financial support of the European Research Council Starting Independent Research Grant (ERC grant agreement no. 279578): "Towards real time multiscale simulation of cutting in non-linear materials with applications to surgical simulation and computer guided surgery". The second author also acknowledges the financial support of EPSRC under grant EP/J01947X/1: "Towards rationalised computational expense for simulating fracture over multiple scales (RationalMSFrac)".

References

[1] D. Ryckelynck, F. Chinesta, E. Cueto, and A. Ammar, "On the a priori model reduction: overview and recent developments," *Archives of Computational Methods in Engineering, State of the Art Reviews*, vol. 13, no. 1, pp. 91–128, 2006.

[2] P. Ladevèze, J. Passieux, and D. Néron, "The LaTIn multiscale computational method and the Proper Generalized Decomposition," *Computer Methods in Applied Mechanics and Engineering*, vol. 199(21), pp. 1287–1296, 2009.

[3] F. Chinesta, A. Ammar, and E. Cueto, "Recent Advances and New Challenges in the Use of the Proper Generalized Decomposition for Solving Multidimensional Models," *Archives of Computational Methods in Engineering - State of the Art Reviews*, vol. 17, no. 4, pp. 327–350, 2010.

[4] M. Chevreuil and A. Nouy, "Model order reduction based on proper generalized decomposition for the propagation of uncertainties in structural dynamics," *International Journal for Numerical Methods in Engineering*, vol. 89, no. 2, pp. 241–268, 2012.

[5] D. Amsallem and C. Farhat, "An Interpolation Method for Adapting Reduced-Order Models and Application to Aeroelasticity," *AIAA Journal*, vol. 46, no. 7, pp. 1803–1813, 2008.

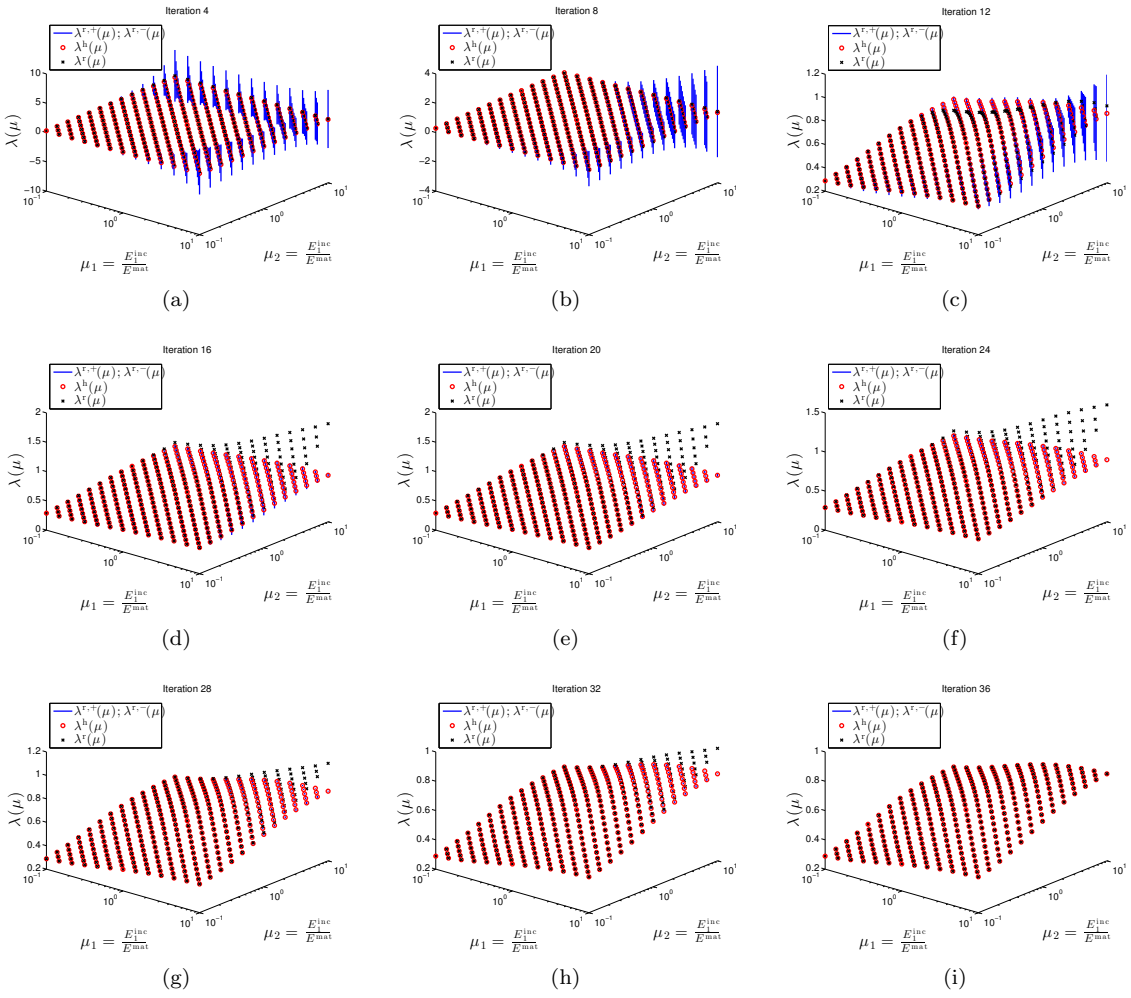

Figure 19: Virtual charts of $\lambda(\mu)$ with respect to the variations of material heterogeneity after first 36 GO-greedy iterations.

[6] M. Xiao, P. Breitkopf, R. Filomeno Coelho, C. Knopf-Lenoir, M. Sidorkiewicz, and P. Villon, "Model reduction by CPOD and Kriging," *Structural and Multidisciplinary Optimization*, vol. 41, pp. 555–574, 2010.

[7] K. Kunisch and S. Volkwein, "Galerkin Proper Orthogonal Decomposition Methods for a General Equation in Fluid Dynamics," *SIAM Journal on Numerical Analysis*, vol. 40, no. 2, pp. 492–515, 2003.

[8] M. Meyer and H. Matthies, "Efficient model reduction in non-linear dynamics using the Karhunen-Loeve expansion and dual-weighted-residual methods," *Computational Mechanics*, vol. 31, no. 1, pp. 179–191, 2003.

[9] A. Radermacher and S. Reese, "A comparison of projection-based model reduction concepts in the context of nonlinear biomechanics," *Archive of Applied Mechanics*, vol. 83, no. 8, pp. 1193–1213, 2013.

[10] K. Karhunen, *Über lineare Methoden in der Wahrscheinlichkeitsrechnung*, vol. 37. Universitat Helsinki, 1947.

[11] L. Sirovich, "Turbulence and the dynamics of coherent structures. part i: Coherent structures," *Quarterly of applied mathematics*, vol. 45, no. 3, pp. 561–571, 1987.

[12] G. Berkooz, P. Holmes, and J. L. Lumley, "The proper orthogonal decomposition in the analysis of turbulent flows," *Annual review of fluid mechanics*, vol. 25, no. 1, pp. 539–575, 1993.

[13] D. Amsallem and U. Hetmaniuk, "Error estimates for galerkin reduced-order models of the semi-discrete wave equation," *ESAIM: Mathematical Modelling and Numerical Analysis*, vol. 48, no. 01, 2014.

[14] P. Kerfriden, J.-J. Ródenas, and S.-A. Bordas, "Certification of projection-based reduced order modelling in computational homogenisation by the constitutive relation error," *International Journal for Numerical Methods in Engineering*, vol. 97, no. 6, pp. 395–422, 2014.

[15] D. Ryckelynck, "Hyper-reduction of mechanical models involving internal variables," *International Journal for Numerical Methods in Engineering*, vol. 77(1), pp. 75 – 89, 2008.

[16] K. Carlberg, C. Bou-Mosleh, and C. Farhat, "Efficient non-linear model reduction via a least-squares Petrov–Galerkin projection and compressive tensor approximations," *International Journal for Numerical Methods in Engineering*, vol. 86, no. 2, pp. 155–181, 2011.

[17] P. Constantine and Q. Wang, "Residual minimizing model interpolation for parameterized nonlinear dynamical systems," *SIAM Journal on Scientific Computing*, vol. 34, no. 4, pp. A2118–A2144, 2012.

[18] P. Kerfriden, J.-C. Passieux, and S. P.-A. Bordas, "Local/global model order reduction strategy for the simulation of quasi-brittle fracture," *International Journal for Numerical Methods in Engineering*, vol. 89, no. 2, pp. 154–179, 2012.

[19] P. Kerfriden, O. Goury, T. Rabczuk, and S.-A. Bordas, "A partitioned model order reduction approach to rationalise computational expenses in nonlinear fracture mechanics," *Computer Methods in Applied Mechanics and Engineering*, vol. 200, no. 5, pp. 850–866, 2012.

[20] F. Fritzen and M. Leuschner, "Reduced basis hybrid computational homogenization based on a mixed incremental formulation," *Computer Methods in Applied Mechanics and Engineering*, vol. 260, pp. 143–154, 2013.

[21] C. Prud'homme, D. V. Rovas, K. Veroy, L. Machiels, Y. Maday, A. T. Patera, and G. Turinici, "Reliable Real-Time Solution of Parametrized Partial Differential Equations: Reduced-Basis Output Bound Methods," *Journal of Fluids Engineering*, vol. 124, no. 1, pp. 70–80, 2002.

[22] G. Rozza, D. Huynh, and A. T. Patera, "Reduced basis approximation and a posteriori error estimation for affinely parametrized elliptic coercive partial differential equations," *Archives of Computational Methods in Engineering*, vol. 15, no. 3, pp. 229–275, 2008.

[23] B. Haasdonk and M. Ohlberger, "Reduced basis method for finite volume approximations of parametrized linear evolution equations," *ESAIM: Mathematical Modelling and Numerical Analysis*, vol. 42, no. 02, pp. 277–302, 2008.

[24] K. C. Hoang, P. Kerfriden, and S. Bordas, "An efficient goal-oriented sampling strategy using reduced basis method for linear elastodynamic problems," *Accepted to publish in Numerical Methods for Partial Differential Equations*, 2014.

[25] D. Amsallem and U. Hetmaniuk, "A posteriori error estimators for linear reduced-order models using krylov-based integrators," *International Journal for Numerical Methods in Engineering*, vol. 102, no. 5, pp. 1238–1261, 2014.

[26] A. Paul-Dubois-Taine and D. Amsallem, "An adaptive and efficient greedy procedure for the optimal training of parametric reduced-order models," *International Journal for Numerical Methods in Engineering*, vol. 102, no. 5, pp. 1262–1292, 2014.

[27] T. Bui-Thanh, K. Willcox, O. Ghattas, and B. van Bloemen Waanders, "Goal-oriented, model-constrained optimization for reduction of large-scale systems," *Journal of Computational Physics*, vol. 224, no. 2, pp. 880–896, 2007.

[28] A. Quarteroni, G. Rozza, and A. Manzoni, "Certified reduced basis approximation for parametrized partial differential equations and applications," *Journal of Mathematics in Industry*, vol. 1, no. 1, pp. 1–49, 2011.

[29] D. B. P. Huynh, G. Rozza, S. Sen, and A. T. Patera, "A successive constraint linear optimization method for lower bounds of parametric coercivity and inf–sup stability constants," *Comptes Rendus Mathematique*, vol. 345, no. 8, pp. 473–478, 2007.

[30] D. Huynh, D. Knezevic, Y. Chen, J. S. Hesthaven, and A. Patera, "A natural-norm successive constraint method for inf-sup lower bounds," *Computer Methods in Applied Mechanics and Engineering*, vol. 199, no. 29, pp. 1963–1975, 2010.

[31] P. Ladevèze and J.-P. Pelle, *Mastering calculations in linear and non linear mechanics*. Springer Verlag, New York, 2004.

[32] K. Willcox and J. Peraire, "Balanced Model Reduction via the Proper Orthogonal Decomposition," *AIAA JOURNAL*, vol. 40, no. 11, 2002.

[33] A. Janon, M. Nodet, and C. Prieur, "Goal-oriented error estimation for reduced basis method, with application to certified sensitivity analysis," *arXiv preprint arXiv:1303.6618*, 2013.

[34] P. Ladevèze and L. Chamoin, "On the verification of model reduction methods based on the proper generalized decomposition," *Computer Methods in Applied Mechanics and Engineering*, vol. 200, no. 23, pp. 2032–2047, 2011.

[35] D. Ryckelynck, L. Gallimard, and S. Jules, "Estimation of the validity domain of hyper-reduction approximations in generalized standard elastoviscoplasticity," *Advanced Modeling and Simulation in Advanced Modeling and Simulation in Engineering Sciences*, vol. 2, no. 6, 2015.

[36] M. D. Gunzburger, J. S. Peterson, and J. N. Shadid, "Reduced-order modeling of time-dependent PDEs with multiple parameters in the boundary data," *Computer Methods in Applied Mechanics and Engineering*, vol. 196, no. 4, pp. 1030–1047, 2007.

[37] K. Hoang, B. Khoo, G. Liu, N. C. Nguyen, and A. T. Patera, "Rapid identification of material properties of the interface tissue in dental implant systems using reduced basis method," *Inverse Problems in Science and Engineering*, vol. 21, no. 8, pp. 1310–1334, 2013.

[38] Y. Saad, *Iterative methods for sparse linear systems*. Siam, 2003.

[39] J. T. Oden and S. Prudhomme, "Goal-oriented error estimation and adaptivity for the finite element method," *Computers & Mathematics with Applications*, vol. 41, no. 5, pp. 735–756, 2001.

[40] R. Becker and R. Rannacher, "An optimal control approach to a posteriori error estimation in finite element methods," *Acta Numerica*, vol. 10, no. 1-102, 2003.

[41] P. Ladevèze, "Upper error bounds on calculated outputs of interest for linear and nonlinear structural problems," *Comptes Rendus Mécanique*, vol. 334, no. 7, pp. 399–407, 2006.

[42] E. Stein and M. Rüter, "Finite Element Methods for Elasticity with Error-controlled Discretization and Model Adaptivity," *Encyclopedia of Computational Mechanics*, 2007.

[43] P. Dıez, N. Parés, and A. Huerta, "Error estimation and quality control," *Encyclopedia of Aerospace Engineering*, 2010.

[44] O. González-Estrada, E. Nadal, J. J. Ródenas, P. Kerfriden, S.-A. Bordas, and F. J. Fuenmayor, "Mesh adaptivity driven by goal-oriented locally equilibrated superconvergent patch recovery," *Computational Mechanics*, vol. 53, no. 5, pp. 957–976, 2014.

[45] S. Nemat-Nasser and M. Hori, *Micromechanics: overall properties of heterogeneous materials*, vol. 2. Elsevier Amsterdam, 1999.

[46] T. I. Zohdi and P. Wriggers, *An introduction to computational micromechanics*, vol. 20. Springer, 2008.

[47] M. Tschopp, "Mathworks website: Synthetic microstructure generator." http://www.mathworks.co.uk/matlabcentral/fileexchange/25389-synthetic-microstructure-generator, Nov. 2009.

[48] M. Tschopp, G. Wilks, and J. Spowart, "Multi-scale characterization of orthotropic microstructures," *Modelling and Simulation in Materials Science and Engineering*, vol. 16, no. 6, p. 065009, 2008.

[49] A. T. Patera. http://augustine.mit.edu/methodology/methodology_rbMIT_SystemPackage.htm.

[50] MathWorks. http://www.mathworks.com/help/optim/ug/linprog.html.

[51] TOMLAB. software. http://tomopt.com/tomlab/.

[52] NAG. toolbox for Matlab. http://www.nag.com/numeric/MB/start.asp.

[53] Y. Yue and K. Meerbergen, "Accelerating optimization of parametric linear systems by model order reduction," *SIAM Journal on Optimization*, vol. 23, no. 2, pp. 1344–1370, 2013.

[54] M. J. Zahr, D. Amsallem, and C. Farhat, "Construction of parametrically-robust CFD-based reduced-order models for PDE-constrained optimization," *AIAA Paper*, vol. 2845, pp. 26–29, 2013.

[55] T. Cui, Y. M. Marzouk, and K. E. Willcox, "Data-driven model reduction for the bayesian solution of inverse problems," *International Journal for Numerical Methods in Engineering*, 2014.

[56] G. Rozza, "Reduced basis approximation and error bounds for potential flows in parametrized geometries," *Communication in Computational Physics*, vol. 9, pp. 1–48, 2011.

A Proof of Prager-Synge equality

The proof is repeated for the sake of clarity but can be found in [14] and is essentially an extension of the technique used to estimate discretisation errors in the context of finite element approximations [31]. We start by expanding the distance between the reduced basis stress field $\sigma^{\mathrm{r}}(\mu)$ and the surrogate stress field $\hat{\sigma}(\mu)$ by using the following identity

$$\|\sigma^{\mathrm{r}}(\mu) - \hat{\sigma}(\mu)\|^2_{C(\mu)} = \left\|\left(\sigma^{\mathrm{r}}(\mu) - \sigma^{\mathrm{h}}(\mu)\right) + \left(\sigma^{\mathrm{h}}(\mu) - \hat{\sigma}(\mu)\right)\right\|^2_{C(\mu)}, \tag{70}$$

where $\sigma^{\mathrm{h}}(\mu) = D(\mu) : \epsilon\left(u^{\mathrm{h}}(\mu)\right)$ is the truth finite element stress field. Then, by using the constitutive relation (2) and the definition of energy norm given previously, (70) can be expanded as

$$\begin{aligned}\|\sigma^{\mathrm{r}}(\mu) - \hat{\sigma}(\mu)\|^2_{C(\mu)} = \left\|u^{\mathrm{r}}(\mu) - u^{\mathrm{h}}(\mu)\right\|^2_{D(\mu)} + \left\|\sigma^{\mathrm{h}}(\mu) - \hat{\sigma}(\mu)\right\|^2_{C(\mu)} \\ + 2\int_\Omega \left(\sigma^{\mathrm{h}}(\mu) - \hat{\sigma}(\mu)\right) : \left(\epsilon\left(u^{\mathrm{r}}(\mu)\right) - \epsilon\left(u^{\mathrm{h}}(\mu)\right)\right) d\Omega.\end{aligned} \tag{71}$$

We recall that both the finite element stress field $\sigma^{\mathrm{h}}(\mu)$ and the surrogate stress field $\hat{\sigma}(\mu)$ are equilibrated in the finite element sense (i.e, verify (29)). Thus, the following identity holds

$$\int_\Omega \left(\sigma^{\mathrm{h}}(\mu) - \hat{\sigma}(\mu)\right) : \epsilon(v)\, d\Omega = 0, \qquad \forall v \in \mathcal{U}^{\mathrm{h},0}(\Omega),\ \mu \in \mathcal{D}, \tag{72}$$

together with (14) and (17), we obtain that the last term in (71) vanishes, which, using the definitions introduced in the Proposition 4.1, concludes the proof.

B Offline-Online computational procedures for $\Delta^{\mathrm{CRE}}(\mu)$

We first expand (50) and noting the definition of $\|\cdot\|_{C(\mu)}$ (Proposition 4.1) as follows[¶]

$$\begin{aligned}\Delta^{\mathrm{CRE}}_{N,\tilde{N}}(\mu)^2 := \|\sigma^{\mathrm{r}}(\mu) - \hat{\sigma}(\mu)\|^2_{C(\mu)} &= \int_\Omega (\sigma^{\mathrm{r}}(\mu) - \hat{\sigma}(\mu)) : C(\mu) : (\sigma^{\mathrm{r}}(\mu) - \hat{\sigma}(\mu))\, d\Omega \\ &= \int_\Omega \sigma^{\mathrm{r}}(\mu) : C(\mu) : \sigma^{\mathrm{r}}(\mu)\, d\Omega + \int_\Omega \hat{\sigma}(\mu) : C(\mu) : \hat{\sigma}(\mu)\, d\Omega - 2\int_\Omega \sigma^{\mathrm{r}}(\mu) : C(\mu) : \hat{\sigma}(\mu)\, d\Omega \\ &= \mathbf{RR}(\mu) + \mathbf{HH}(\mu) - 2\,\mathbf{RH}(\mu).\end{aligned} \tag{73}$$

Now, we expand the expressions for $\sigma^{\mathrm{r}}(\mu)$ by using (2), (17) and (16)

[¶] We use symbol $\Delta^{\mathrm{CRE}}_{N,\tilde{N}}(\mu)$, which implies that this error measure depends on N – the number of RB displacement basis functions and $\tilde{N}$ – the number of RB stress basis functions.

$$\begin{aligned}\sigma^{\mathrm{r}}(\mu) &= D(\mu) : \epsilon\left(u^{\mathrm{r},0}(\mu) + u^{\mathrm{h,p}}(\mu)\right) = D(\mu) : \epsilon\left(\sum_{i=1}^{N} \alpha_i(\mu)\,\phi_i + \sum_{j=1}^{n_{\mathrm{w}}} \gamma_j^{\mathrm{w}}(\mu)\psi_j\right) \\ &= D(\mu) : \epsilon\left(\sum_{i=1}^{N} \alpha_i(\mu)\,\phi_i\right) + D(\mu) : \epsilon\left(\sum_{j=1}^{n_{\mathrm{w}}} \gamma_j^{\mathrm{w}}(\mu)\psi_j\right) = \square + \triangle,\end{aligned} \tag{74}$$

and $\hat{\sigma}(\mu)$ by using (40), (37)

$$\hat{\sigma}(\mu) = \sigma^{\mathrm{r},0}(\mu) + \sigma^{\mathrm{h,p}}(\mu) = \sum_{i=1}^{\tilde{N}} \tilde{\alpha}_i(\mu)\,\tilde{\phi}_i + \sum_{j=1}^{\tilde{n}_{\mathrm{p}}} \tilde{\gamma}_j^{\mathrm{p}}(\mu)\,\sigma_j^{\mathrm{p}} = \blacksquare + \blacktriangle. \tag{75}$$

1. Let us first consider the term $\mathbf{RR}(\mu)$ in (73) (using (74))

$$\begin{aligned}\mathbf{RR}(\mu) &= \int_\Omega \sigma^{\mathrm{r}}(\mu) : C(\mu) : \sigma^{\mathrm{r}}(\mu)\, d\Omega = \int_\Omega (\square + \triangle) : C(\mu) : (\square + \triangle)\; d\Omega \\ &= \int_\Omega \square : C(\mu) : \square\, d\Omega + 2\int_\Omega \square : C(\mu) : \triangle\, d\Omega + \int_\Omega \triangle : C(\mu) : \triangle\, d\Omega \\ &= \mathbf{RRss}(\mu) + 2\,\mathbf{RRst}(\mu) + \mathbf{RRtt}(\mu).\end{aligned} \tag{76}$$

The term $\mathbf{RRss}(\mu)$ can be computed as follows:

$$\begin{aligned}\mathbf{RRss}(\mu) &= \int_\Omega \left(D(\mu) : \epsilon\left(\sum_{i=1}^{N} \alpha_i(\mu)\,\phi_i\right)\right) : C(\mu) : \left(D(\mu) : \epsilon\left(\sum_{j=1}^{N} \alpha_j(\mu)\,\phi_j\right)\right)\; d\Omega \\ &= \int_\Omega \epsilon\left(\sum_{i=1}^{N} \alpha_i(\mu)\,\phi_i\right) : D(\mu) : \epsilon\left(\sum_{j=1}^{N} \alpha_j(\mu)\,\phi_j\right)\; d\Omega, \quad (\text{as } D(\mu) : C(\mu) = \mathbb{I}) \\ &= \sum_{i,j=1}^{N} \alpha_i(\mu)\left(\int_\Omega \epsilon(\phi_i) : D(\mu) : \epsilon(\phi_j)\, d\Omega\right)\; \alpha_j(\mu) \\ &= \sum_{i,j=1}^{N} \alpha_i(\mu)\; a\left(\phi_i, \phi_j; \mu\right)\; \alpha_j(\mu), \quad (\text{from (5a)}) \\ &= \sum_{i,j=1}^{N} \alpha_i(\mu)\left(\sum_{q=1}^{Q_a} \Theta_a^q(\mu)\,\boldsymbol{a^q(\phi_i, \phi_j)}\right) \alpha_j(\mu), \quad (\text{from (7a)}).\end{aligned} \tag{77}$$

We observe from the last line of (77) that the term $a^q(\phi_i, \phi_j)$ (in bold typeface) can be pre-computed and stored in the Offline stage; and then in the Online stage $\mathbf{RRss}(\mu)$ can be estimated rapidly with the computational cost independent of $\mathcal{N}$ by assembling all remaining terms. Applying the same trick to other terms, we obtain the following results (note that all the offline terms will be in bold typeface):

$$\mathbf{RRst}(\mu) = \sum_{i=1}^{N}\sum_{j=1}^{n_{\mathrm{w}}} \alpha_i(\mu)\left(\sum_{q=1}^{Q_a} \Theta_a^q(\mu)\,\boldsymbol{a^q(\phi_i, \psi_j)}\right) \gamma_j^{\mathrm{w}}(\mu), \tag{78}$$

and

$$\mathbf{RRtt}(\mu) = \sum_{i,j=1}^{n_{\mathrm{w}}} \gamma_i^{\mathrm{w}}(\mu) \left(\sum_{q=1}^{Q_a} \Theta_a^q(\mu)\, \boldsymbol{a^q(\psi_i, \psi_j)} \right) \gamma_j^{\mathrm{w}}(\mu). \tag{79}$$

2. Similarly, the term $\mathbf{HH}(\mu)$ in (73) can be written as (using (75))

$$\begin{aligned} \mathbf{HH}(\mu) &= \int_\Omega \hat{\sigma}(\mu) : C(\mu) : \hat{\sigma}(\mu)\, d\Omega = \int_\Omega (\blacksquare + \blacktriangle) : C(\mu) : (\blacksquare + \blacktriangle)\; d\Omega \\ &= \int_\Omega \blacksquare : C(\mu) : \blacksquare\, d\Omega + 2 \int_\Omega \blacksquare : C(\mu) : \blacktriangle\, d\Omega + \int_\Omega \blacktriangle : C(\mu) : \blacktriangle\, d\Omega \\ &= \mathbf{HHss}(\mu) + 2\,\mathbf{HHst}(\mu) + \mathbf{HHtt}(\mu). \end{aligned} \tag{80}$$

Using the same method as above: substituting the expressions for ■ and ▲ (from (75)), expanding and assembling the μ-independent terms, we finally obtain

$$\begin{aligned} \mathbf{HHss}(\mu) &= \sum_{i,j=1}^{\tilde{N}} \tilde{\alpha}_i(\mu) \left(\sum_{q=1}^{n_{\mathrm{c}}} \gamma_q^{\mathrm{c}}(\mu) \int_{\boldsymbol{\Omega}} \boldsymbol{\tilde{\phi}_i : \bar{C}_q : \tilde{\phi}_j\, d\Omega} \right) \tilde{\alpha}_j(\mu), \\ \mathbf{HHst}(\mu) &= \sum_{i=1}^{\tilde{N}} \sum_{j=1}^{\tilde{n}_{\mathrm{p}}} \tilde{\alpha}_i(\mu) \left(\sum_{q=1}^{n_{\mathrm{c}}} \gamma_q^{\mathrm{c}}(\mu) \int_{\boldsymbol{\Omega}} \boldsymbol{\tilde{\phi}_i : \bar{C}_q : \sigma_j^{\mathrm{p}}\, d\Omega} \right) \tilde{\gamma}_j^{\mathrm{p}}(\mu), \\ \mathbf{HHtt}(\mu) &= \sum_{i,j=1}^{\tilde{n}_{\mathrm{p}}} \tilde{\gamma}_i^{\mathrm{p}}(\mu) \left(\sum_{q=1}^{n_{\mathrm{c}}} \gamma_q^{\mathrm{c}}(\mu) \int_{\boldsymbol{\Omega}} \boldsymbol{\sigma_i^{\mathrm{p}} : \bar{C}_q : \sigma_j^{\mathrm{p}}\, d\Omega} \right) \tilde{\gamma}_j^{\mathrm{p}}(\mu). \end{aligned} \tag{81}$$

3. Finally, for the term $\mathbf{RH}(\mu)$ in (73), we also have

$$\begin{aligned} \mathbf{RH}(\mu) &= \int_\Omega \sigma^{\mathrm{r}}(\mu) : C(\mu) : \hat{\sigma}(\mu)\, d\Omega = \int_\Omega (\square + \triangle) : C(\mu) : (\blacksquare + \blacktriangle)\; d\Omega \\ &= \int_\Omega \square : C(\mu) : \blacksquare\, d\Omega + \int_\Omega \square : C(\mu) : \blacktriangle\, d\Omega + \int_\Omega \triangle : C(\mu) : \blacksquare\, d\Omega + \int_\Omega \triangle : C(\mu) : \blacktriangle\, d\Omega \\ &= \mathbf{RHss}(\mu) + \mathbf{RHst}(\mu) + \mathbf{RHts}(\mu) + \mathbf{RHtt}(\mu), \end{aligned} \tag{82}$$

where

$$\begin{aligned} \mathbf{RHss}(\mu) &= \sum_{i=1}^{N} \sum_{j=1}^{\tilde{N}} \alpha_i(\mu) \left(\int_{\boldsymbol{\Omega}} \boldsymbol{\epsilon(\phi_i) : \tilde{\phi}_j\, d\Omega} \right) \tilde{\alpha}_j(\mu), \\ \mathbf{RHst}(\mu) &= \sum_{i=1}^{N} \sum_{j=1}^{\tilde{n}_{\mathrm{p}}} \alpha_i(\mu) \left(\int_{\boldsymbol{\Omega}} \boldsymbol{\epsilon(\phi_i) : \sigma_j^{\mathrm{p}}\, d\Omega} \right) \tilde{\gamma}_j^{\mathrm{p}}(\mu), \\ \mathbf{RHts}(\mu) &= \sum_{i=1}^{n_{\mathrm{w}}} \sum_{j=1}^{\tilde{N}} \gamma_i^{\mathrm{w}}(\mu) \left(\int_{\boldsymbol{\Omega}} \boldsymbol{\epsilon(\psi_i) : \tilde{\phi}_j\, d\Omega} \right) \tilde{\alpha}_j(\mu), \\ \mathbf{RHtt}(\mu) &= \sum_{i=1}^{n_{\mathrm{w}}} \sum_{j=1}^{\tilde{n}_{\mathrm{p}}} \gamma_i^{\mathrm{w}}(\mu) \left(\int_{\boldsymbol{\Omega}} \boldsymbol{\epsilon(\psi_i) : \sigma_j^{\mathrm{p}}\, d\Omega} \right) \tilde{\gamma}_j^{\mathrm{p}}(\mu). \end{aligned} \tag{83}$$

C Residual-based error bound and SCM

The technique to derive this bound is well-established and has been described in many papers (see for instance [22, 28, 56]). Hence the proof and detailed computation will not be shown here, we only recall the basic components and then formulate this error bound.

In order to define properly this error bound, we shall introduce two different inner products and norms for members of $\mathcal{U}^{\mathrm{h},0}(\Omega)$, inherited from $\mathcal{U}^{\mathrm{Ad},0}(\Omega)$ (section 2.1). First, an energy inner product and energy norm are defined respectively as[‖]

$$(u, v)_\mu = a(u, v; \mu), \qquad \forall u, v \in \mathcal{U}^{\mathrm{Ad},0}(\Omega), \tag{84a}$$

$$\|v\|_\mu = (v, v)_\mu^{1/2}, \qquad \forall v \in \mathcal{U}^{\mathrm{Ad},0}(\Omega). \tag{84b}$$

Second, the X-inner product and norm, are defined as follows: for given $\mu_0 \in \mathcal{D}$ and (non-negative) real τ,

$$(u, v)_X = (u, v)_{\mu_0} + \tau (u, v)_{L^2(\Omega)}, \qquad \forall u, v \in \mathcal{U}^{\mathrm{Ad},0}(\Omega), \tag{85a}$$

$$\|v\|_X = (v, v)_X^{1/2}, \qquad \forall v \in \mathcal{U}^{\mathrm{Ad},0}(\Omega), \tag{85b}$$

where μ_0 here is the same as that in section 3.1.2 and section 3.2.2; and the L^2-norm is defined as $(u, v)_{L^2(\Omega)} = \int_\Omega u\, v\, d\Omega$.

C.1 Basic components

There are two basic components which constitute the SCM/residual-based error bound: the dual norm of the residual and the lower bound of the FE coercivity constant. In order to obtain the former, we start from the error residual relationship. The residual $R(v; \mu)$ which is associated with (18) is defined as in equation (58). Together with (12) and the bilinearity of a, the error residual relationship for the RB error $e^0(\mu) = u^{\mathrm{h},0}(\mu) - u^{\mathrm{r},0}(\mu) \in \mathcal{U}^{\mathrm{h},0}(\Omega)$ can be established as follows

$$a\left(e^0(\mu), v; \mu\right) = R(v; \mu), \qquad \forall v \in \mathcal{U}^{\mathrm{h},0}(\Omega). \tag{86}$$

We then introduce the Riesz representation of $R(v; \mu)$: $\hat{e}^0(\mu) \in \mathcal{U}^{\mathrm{h},0}(\Omega)$ satisfies

$$\left(\hat{e}^0(\mu), v\right)_X = R(v; \mu), \qquad \forall v \in \mathcal{U}^{\mathrm{h},0}(\Omega). \tag{87}$$

Thus we can write (86) as

$$a\left(e^0(\mu), v; \mu\right) = \left(\hat{e}^0(\mu), v; \mu\right)_X, \qquad \forall v \in \mathcal{U}^{\mathrm{h},0}(\Omega), \tag{88}$$

and it follows that the dual norm of the residual can be computed through the Riesz representation [56, 22]:

$$\|R(\cdot; \mu)\|_{(\mathcal{U}^{\mathrm{h},0}(\Omega))'} = \sup_{v \in \mathcal{U}^{\mathrm{h},0}(\Omega)} \frac{R(v; \mu)}{\|v\|_X} = \|\hat{e}^0(\mu)\|_X. \tag{89}$$

The second basic component is a parametric lower bound function $\alpha_{\mathrm{LB}}^{\mathcal{N}}(\mu)$ for $\alpha^{\mathcal{N}}(\mu)$ – the FE coercivity constant defined as

$$\alpha^{\mathcal{N}}(\mu) = \inf_{v \in \mathcal{U}^{\mathrm{h},0}(\Omega)} \frac{a(v, v; \mu)}{\|v\|_X^2}. \tag{90}$$

Hence, we have

[‖] This energy norm was denoted by $\|v\|_{D(\mu)}$ in Proposition 4.1.

$$0 < \alpha_{\rm LB}^{\mathcal{N}}(\mu) \leq \alpha^{\mathcal{N}}(\mu), \qquad \forall \mu \in \mathcal{D}, \tag{91}$$

where the online computational time to evaluate $\mu \to \alpha_{\rm LB}^{\mathcal{N}}(\mu)$ has to be independent of $\mathcal{N}$. The computation of $\alpha_{\rm LB}^{\mathcal{N}}(\mu)$ is given by an efficient algorithm so-called Successive Constraint Method (SCM), which is analysed in [29, 30]. The SCM algorithm also comprises of Offline-Online computational procedures: an expensive $\mathcal{N}$–dependent Offline stage and a cheap $\mathcal{N}$–independent Online stage. Specifically, in the Online stage a small optimisation problem needs to be solved with the cost independent of $\mathcal{N}$ for any given parameter μ.

C.2 Error bound

The SCM error estimator for the field variable in the energy norm is defined as

$$\Delta^{\rm SCM}(\mu) = \frac{\|\hat{e}^0(\mu)\|_X}{\sqrt{\alpha_{\rm LB}^{\mathcal{N}}(\mu)}}. \tag{92}$$

We also introduce the effectivity associated with this error estimator as

$$\eta^{\rm SCM}(\mu) = \frac{\Delta^{\rm SCM}(\mu)}{\|u^{\rm h,0}(\mu) - u^{\rm r,0}(\mu)\|_\mu}. \tag{93}$$

Following the proof as in [22, 28], we obtain that for any $N = 1, \ldots, N_{\max}$, the effectivity satisfies

$$1 \leq \eta^{\rm SCM}(\mu), \qquad \forall \mu \in \mathcal{D}. \tag{94}$$

The "online computation" of $\Delta^{\rm SCM}(\mu)$ in (92) is efficient: its computational cost is completely independent of $\mathcal{N}$ [28, 22]. In addition, we also note from equations (14), (17) that the RB error for the field variable will be $e^{\rm r}(\mu) = u^{\rm h}(\mu) - u^{\rm r}(\mu) = u^{\rm h,0}(\mu) - u^{\rm r,0}(\mu) = e^0(\mu)$. Therefore, error estimation for $e^0(\mu)$ is completely equivalent to that for $e^{\rm r}(\mu)$, providing that the lifting procedure is performed exactly.